Summary of major revisions

We have carefully considered all the comments and made point-to-point modifications in the revised manuscript.

Firstly, we have more precisely described the datasets as “the first data-driven energy-conservation datasets of global land-surface radiation and heat fluxes”.

Secondly, following the reviewers’ suggestions, we have additionally incorporated 44 test sites to validate and compare the performance of the CoSEB-based datasets with mainstream products (Section 4.2) and with the ERA5-Land datasets (Figs. S6 and S7).

Thirdly, we have (1) added a new table (Table S3) summarizing the mean accuracy of the training datasets of the renewed CoSEB model to evaluate potential overfitting; (2) briefly described the optimization of hyperparameters for the renewed CoSEB model (Section 3); and (3) added a new table (Table S4) presenting the importance scores of different feature variables for estimating daily surface radiation and heat fluxes.

Fourthly, we have included new experiments to (1) illustrate the relationship between the energy (radiation) imbalance ratio derived from RF-based uncoordinated models and three critical input variables (Fig. S1); (2) investigate the impact of lagged effects of input variables on model performance (Fig. S4); (3) demonstrate the effects of incorporating additional radiation components in the renewed CoSEB model (Fig. S5) compared with the original version by Wang et al. (2025).

Lastly, in Section 5, we have discussed the selection of 19 input feature variables, the uncertainty introduced by the downscaling of ERA5-Land datasets, the consistent spatial patterns between CoSEB-based datasets and CESM Large Ensemble Project (Fig. S8) while noting that a more detailed analysis of their spatial-temporal patterns and variability could be conducted in future work.

Accordingly, the texts, figures, and tables have been updated throughout the manuscript. We believe our manuscript has been greatly improved by following the reviewers’ comments and suggestions.

Responses to the Comments and Suggestions

Reviewer #1:

This paper presents an energy conservation datasets of global land surface radiation and heat fluxes from 2000 to 2020. The dataset is generated by the model of Coordinated estimates of land Surface Energy Balance components (CoSEB), with a combination of GLASS and MODIS remote sensing data, ERA5-Land reanalysis datasets, topographic data, CO2 concentration data, and observations at 258 eddy covariance sites worldwide from the AmeriFlux, FLUXNET, EuroFlux, OzFlux, ChinaFLUX and TPDC. The primary merit of this new model is energy-conservation. Although the dataset might be useful, this dataset is not the first energy conservation datasets of global land surface radiation and heat fluxes as claimed by the authors. Therefore, major revisions are required before the paper is accepted.

Ans: Thank you very much for your valuable comments and suggestions. We sincerely appreciate your recognition of the dataset and the CoSEB model's merit in ensuring energy conservation. We would like to clarify that our initial statement, which described the datasets as "the first energy-conservation datasets of global land surface radiation and heat fluxes," may not have been entirely accurate. After careful consideration, we have revised the manuscript to more precisely describe the datasets as "the first data-driven energy-conservation datasets of global land-surface radiation and heat fluxes". Besides, we have carefully considered all the comments and suggestions from you and another reviewer and made corresponding modifications and clarifications in the revised manuscript. More detailed information of our revisions can be found in the item-by-item response below.

Specific comments:

1. The authors claim that "This study presents the first energy conservation datasets of global land surface radiation and heat fluxes", but reanalysis datasets, such as ERA5 which is used as inputs of this new dataset, also provide energy conservation surface fluxes for these energy fluxes. Maybe the authors want to say that this is the first remote sensing-based dataset? But the ERA5 radiative fluxes, which are not remote sensing-based, are used to generate surface fluxes in this paper, so this dataset is neither the first remote sensing-based dataset.

Ans: We sincerely thank the reviewer for this insightful comment. We acknowledge that reanalysis datasets, such as ERA5-Land, can in principle calculate these fluxes based on surface energy conservation. However, these reanalysis datasets rarely include all eight flux components directly. For example, ERA5-Land does not explicitly provide upward shortwave radiation, upward longwave radiation, net radiation or soil heat flux. Additionally, we would also like to clarify that the CoSEB-based datasets were developed by integrating both remote sensing products (e.g., PTC from MOD44B, LAI and FVC from GLASS, DEM, slope, and aspect from GMTED2010) and meteorological reanalysis data as inputs. It should be noted that widely used surface radiation and heat flux products, commonly referred to as remote sensing-based datasets, generally require meteorological reanalysis data as inputs, e.g., the MOD16 ET product (Mu et al., 2011), SSEBop ET product (Senay et al., 2020), and GLASS radiation products (Wang et al., 2015; Xu et al., 2022), rather than relying solely on remote sensing data. Therefore, although our CoSEB-based datasets incorporate meteorological data from ERA5-Land in addition to remote sensing data, we believe it appropriate to refer to them as remote sensing-based datasets.

After careful consideration, we have revised the manuscript to more precisely describe the datasets as "the first data-driven energy-conservation datasets of global land-surface radiation and heat fluxes". We have revised this in the new manuscript as follows:

Abstract:

"This study presents the first data-driven energy-conservation datasets of global land surface radiation and heat fluxes from 2000 to 2020 ... The developed CoSEB-based datasets are strikingly advantageous in that [1] they are the first data-driven global datasets that satisfy both surface radiation balance (SWI_N - SW_{OUT} + LW_{IN} - LW_{OUT} = Rn) and heat balance (LE + H + G = Rn) among the eight fluxes,…"

5 Discussion

"The main advantages of our CoSEB-based datasets of land surface radiation and heat fluxes lie in that [1] they are the first data-driven global datasets that satisfy both surface radiation balance (SWI_N - SW_{OUT} + LW_{IN} - LW_{OUT} = Rn) and heat balance (LE + H + G = Rn) among the eight fluxes, as demonstrated by both the RIR and EIR of 0, …"

"Despite these uncertainties, it is worth emphasizing that our work was the first attempt to innovatively develop data-driven energy-conservation datasets of global land surface radiation and heat fluxes with high accuracies."

7 Summary and Conclusion

"This study for the first time developed data-driven energy-conservation datasets of global land surface radiation and heat fluxes…"

"The CoSEB-based datasets of land surface radiation and heat fluxes are the first data-driven global datasets that satisfy both surface radiation balance (SWI_N - SW_{OUT} + LW_{IN} - LW_{OUT} = Rn) and heat balance (LE + H + G = Rn) among the eight fluxes."

2. The merit of this new dataset is still unclear to me. According to Lines 171-180, ERA5 downward solar radiation and net thermal radiation at the surface is used in this paper, but why not simply use ERA5 fluxes if someone need to surface fluxes? The new dataset might be more accurate than ERA5 in places where ground-based observations are used to generate the new dataset, but the ground sites are sparce. To solve this problem, the authors should compare in-situ measurements with both the new data and ERA5 data in independent sites (i. e., sites that are not used in the generation of the new dataset).

Ans: We sincerely appreciate the reviewer's insightful comment and suggestion. We would like to clarify that the ERA5-Land reanalysis datasets do not explicitly provide upward shortwave radiation, upward longwave radiation, net radiation, or soil heat flux, although these components can theoretically be computed using surface radiation and heat balance principles. The purpose of our work was to innovatively provide energy-conservation surface radiation and heat fluxes based on data-driven technique. This is motivated by the fact that existing data-driven products (e.g., FLUXCOM and GLASS) estimate each energy component separately, leading to obvious energy imbalance among these components (Wang et al., 2025).

To further address the reviewer's concern, we have compared estimates from CoSEB-based datasets and ERA5-Land datasets with in-situ observations from 44 sites (collected from recently published JapanFlux and updated AmeriFlux, see the sites for "test" in Table S1), which are independent from the 258 sites that are used for model construction and datasets generation. As demonstrated by the comparison results (see Figs. S6 and S7), the CoSEB-based datasets exhibit higher accuracy than the ERA5-Land datasets in estimating surface energy fluxes, especially in estimating SW_{OUT}, H and G. We have discussed this in the third paragraph of Section 5 in the revised manuscript with the following sentences:

"Furthermore, the CoSEB-based datasets outperformed the ERA5-Land reanalysis datasets in estimating surface energy fluxes (where SW_{OUT}, LW_{OUT}, Rn and G for the ERA-Land were inferred from surface radiation balance and heat balance), particularly for SW_{OUT}, H and G, with RMSE reductions of 0.13-8.15 W/m^2 when validated against in situ observations at the 44 test sites (Figs. S6 and S7 in the Supplementary Material)."

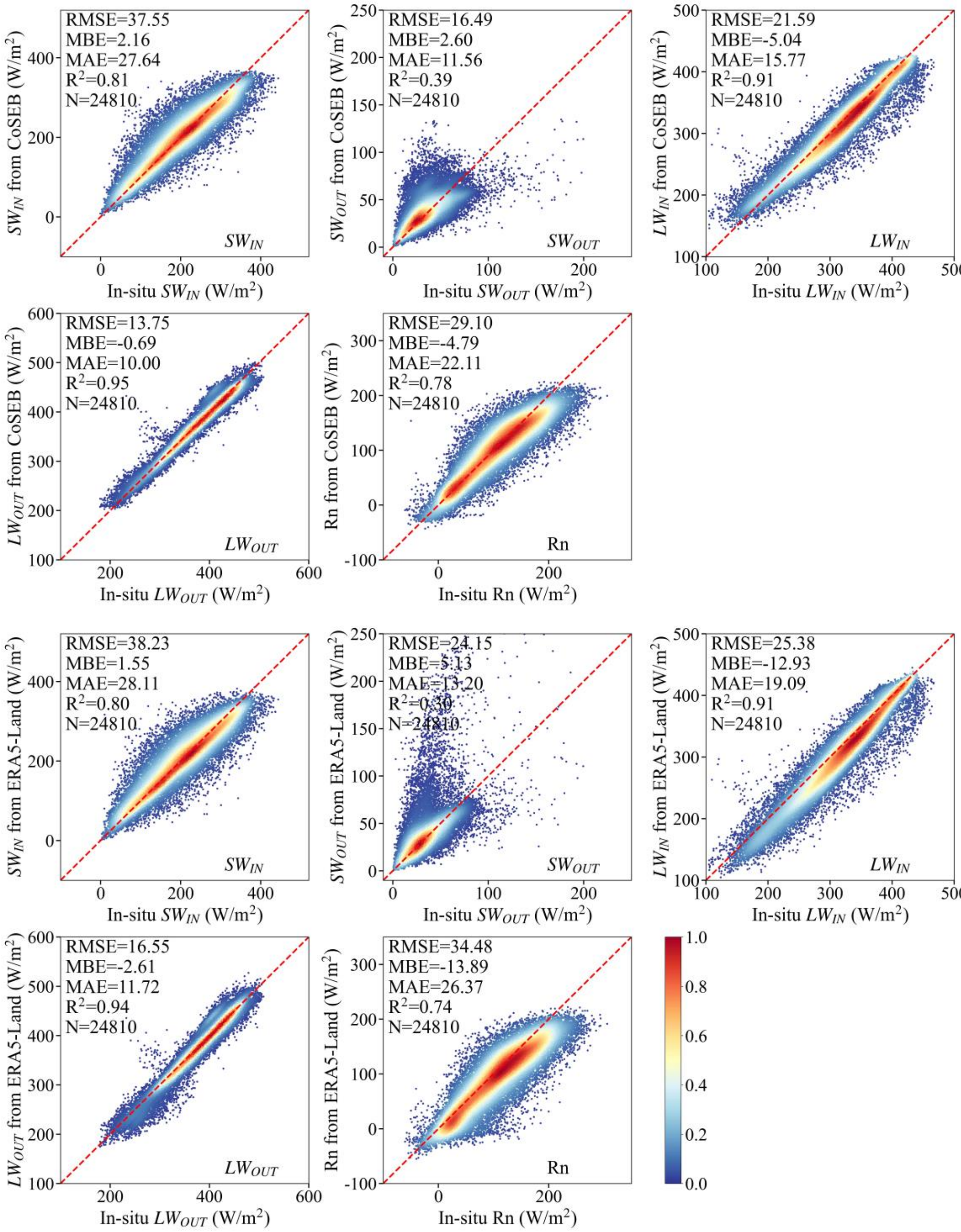

Fig. S6 Comparison of the daily downward shortwave radiation (*SW_{IN}*), upward shortwave radiation (*SW_{OUT}*), downward longwave radiation (*LW_{IN}*), upward longwave radiation (*LW_{OUT}*) and net radiation (Rn) from the CoSEB-based datasets (upper 5 panels) and ERA5-Land (lower 5 panels) with the in-situ observed *SW_{IN}*, *SW_{OUT}*, *LW_{IN}* and *LW_{OUT}* at 44 test sites. The colorbar represents the normalized density of data points.

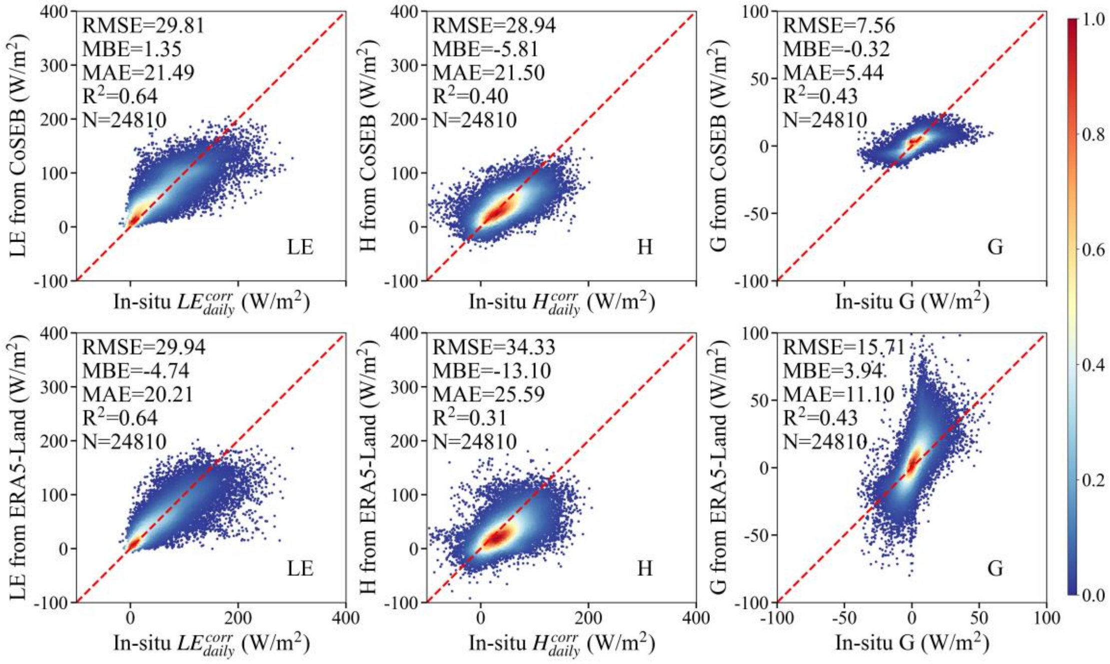

Fig. S7 Comparison of the daily latent heat flux (LE), sensible heat flux (H) and soil heat flux (G) from the CoSEB-based datasets (first row) and ERA5-Land (second row)with the in-situ energy imbalance-corrected LE (LE_{daily}^{corr}) and H (H_{daily}^{corr}), as well as observed G at 44 test sites. The colorbar represents the normalized density of data points.

3. The abstract is not well formatted. An abstract usually provides a brief and comprehensive summary, so trivial details in brackets [including downward shortwave radiation (SWIN), downward longwave radiation (LWIN), upward shortwave 15 radiation (SWOUT), upward longwave radiation (LWOUT) and net radiation (Rn)], [including latent heat flux (LE), soil heat flux (G) and sensible heat flux (H)], and (SWIN - SWOUT + LWIN - LWOUT = Rn) might be deleted. Internet links https://doi.org/10.11888/Terre.tpdc.302559 and citations (Tang et al., 2025a) should be removed from the abstract. On the other hand, the authors should briefly describe how these data sources are used to generate the new dataset.

Ans: We appreciate the reviewer's suggestion. We would like to clarify that the latter part of the Abstract describes the accuracy of each of the eight surface radiation and heat flux components, as well as the overall surface radiation balance and energy balance among them. Therefore, to ensure consistency and readability, we chose to retain the introduction of all eight fluxes and their corresponding abbreviations at the beginning of the Abstract. However, the two equations, (SW_{IN} - SW_{OUT} + LW_{IN} - LW_{OUT} = Rn) and (LE + H + G = Rn), were deleted in the Abstract, as suggested by the reviewer. Furthermore, the links and citations of the datasets are mandatorily required by the journal and editors in the Abstract, and therefore cannot be removed. Besides, following the reviewer's suggestion, we have briefly explained how multiple data sources were integrated to generate the CoSEB-based datasets in the revised manuscript as follows:

“This study presents the first data-driven energy-conservation datasets of global land surface radiation and heat fluxes from 2000 to 2020, generated by our model of Coordinated estimates of land Surface Energy Balance components (CoSEB). The model integrates GLASS and MODIS remote sensing data, ERA5-Land reanalysis datasets, topographic data, CO_2 concentration data as independent variables and in situ radiation and heat flux observations at 258 eddy covariance sites worldwide as dependent variables within a multivariate random forest technique to effectively learn the physics of energy conservation.”

Reviewer #2:

Review of Energy-conservation datasets of global land surface radiation and heat fluxes from 2000-2020 generated by CoSEB

Summary and recommendation- In this paper, the authors apply a model of Coordinated estimates of land surface energy balance components (CoSEB) to generate estimates of surface radiation and heat fluxes from 2000 to 2020. An advantage of the CoSEB based approach is that estimates of radiation and heat are in "harmony" as opposed to generating independent estimates of each. The authors compare their estimates against observations from eddy covariance sites, other individual estimates and other individual observations. The paper is generally well written, and the results are presented clearly. However, I had several questions about the CoSEB framework itself and also the validations applied here in the manuscript. Hence I recommend major revisions. I have presented major comments and specific comments below.

Ans: Thank you very much for your thoughtful and constructive comments. We sincerely appreciate your recognition of the CoSEB model and the datasets, particularly the advantage of generating global surface radiation and heat fluxes that adhere to energy conservation. We have carefully considered all the comments and suggestions from you and another reviewer, especially your concerns regarding the CoSEB framework and the validation of the datasets, and have made corresponding modifications and clarifications in the revised manuscript. More detailed information of our revisions can be found in the item-by-item response as below.

Major comments-

1. **Explanation of updates to the CoSEB framework-** While reading the manuscript I realized that it is not only a paper that applies the existing CoSEB framework that is already published but also updates this framework to estimate to estimate radiation (previously this model estimated only land surface energy components and not short wave and long wave radiation). Therefore, authors need to discuss the effect of the addition of additional predicted variables on the equations and the results of the random forest. In particular, can the authors discuss which of the predictors were found to be the most important and also discuss how this differed with their previous publication? Also, can authors discuss generic details such as how many splits were generated by the random forest before and after the updates. Authors should also discuss the directionality of effects of different predictor variables based on the revised random forest.

Ans: We thank the reviewer for these insightful comments and questions. Indeed, the renewed CoSEB model extends beyond the original version (Wang et al., 2025) by jointly estimating both radiation components (SW_{IN}, SW_{OUT}, LW_{IN}, LW_{OUT} and Rn) and heat fluxes (LE, H, G), thereby ensuring that both radiation and energy balance are simultaneously satisfied.

(1) To illustrate the effect of including additional radiation components (SW_{IN}, SW_{OUT}, LW_{IN} and LW_{OUT}) in the renewed CoSEB model compared with the original

version by Wang et al. (2025), we have tested the performance of a reconstructed model that estimated only Rn, LE, H and G using the same independent variables and samples as those in the renewed CoSEB model. The results (Fig. S5 in the supplementary material) showed no significant differences from those produced by the renewed CoSEB model, indicating that the expansion of radiation components did not compromise the model's overall performance. We have discussed this in the second paragraph of Section 5 with the following sentences:

"Furthermore, to better illustrate the effect of including additional radiation components (SW_{IN}, SW_{OUT}, LW_{IN} and LW_{OUT}) in the renewed CoSEB model compared with the original version by Wang et al. (2025), we have tested the performance of a reconstructed model that estimated only Rn, LE, H and G using the same independent variables and samples as those in the renewed CoSEB model. The results (Fig. S5 in the supplementary material) showed no significant differences in accuracy compared with those of the renewed CoSEB model, indicating the expansion of radiation components did not compromise model performance."

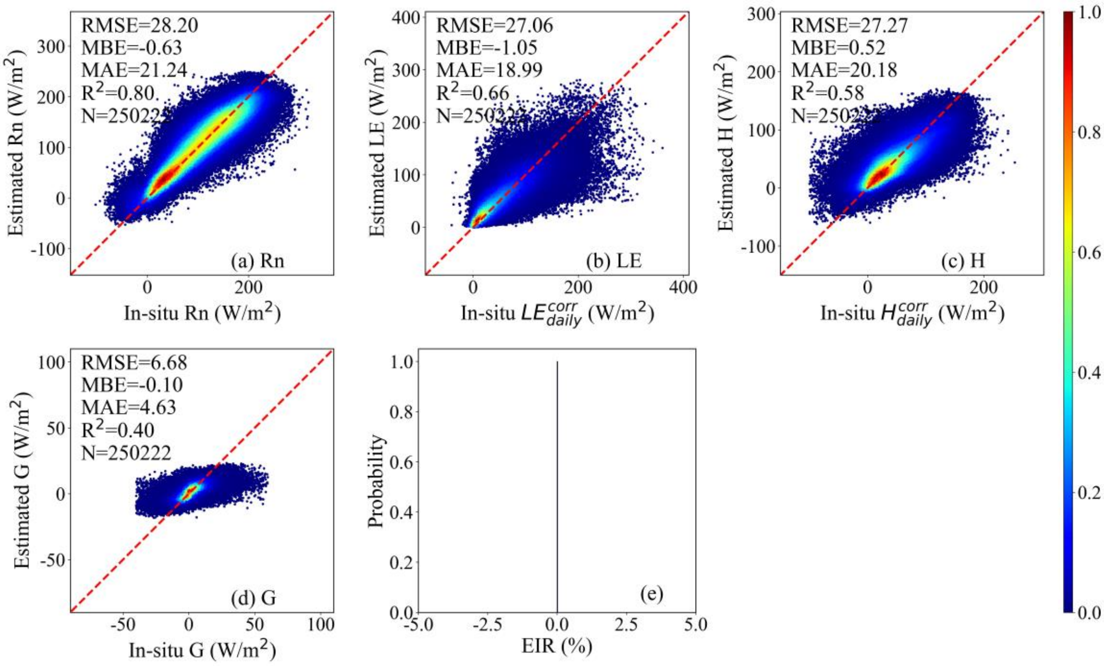

Fig. S5 Scatter density plots of the site-based 10-fold cross-validation of daily net radiation (Rn), soil heat flux (G), latent heat flux (LE) and sensible heat flux (H) derived by a reconstructed model within the CoSEB framework against in-situ observed Rn, G, and energy imbalance-corrected LE (LE^{corr}_{daily}) and H (H^{corr}_{daily}), where the model was designed to estimate only four of the eight flux components. The EIR in the subfigure (e) represents the energy imbalance ratio, which are defined as 100% × (Rn - G - LE - H)/Rn. The colorbar represents the normalized density of data points.

(2) Regarding your concern about the importance of the feature variables to the renewed CoSEB model, we have added a new table (Table S4 in the Supplementary Material) to show the importance scores of different feature variables using the built-

in method of the random forests. The results showed that solar radiation reaching the surface of the earth is the most important variable, which is consistent with the results from our previous study (Wang et al., 2025). We have discussed this in the second paragraph of Section 5 with the following sentences:

"The importance scores of the 19 different feature variables are exhibited in Table S4 in the Supplementary Material, and downward solar radiation, the primary source of the energy at the earth surface, is the most important input variable, consistent with the results from our previous study (Wang et al., 2025)."

Table S4 Importance scores of the 19 different feature variables in the construction of the renewed CoSEB model for estimating daily downward shortwave and longwave radiation (SW_{IN} and LW_{IN}), upward shortwave and longwave radiation (SW_{OUT} and LW_{OUT}), net radiation (Rn), latent heat flux (LE), sensible heat flux (H) and soil heat flux (G).

Types	Features Variables	Abbreviation	Importance Score	Cumulative Percentage (%)
Climate/meteorology	solar radiation reaching the surface of the earth	SW_{IN}^{ERA5}	0.5724	57.24
Climate/meteorology	2 m air temperature	T_a	0.2338	80.62
Vegetation and soil	Fractional tree cover	*FVC*	0.0292	83.54
Climate/meteorology	net thermal radiation at the surface	LW_{net}	0.0241	85.95
Vegetation and soil	Leaf area index	*LAI*	0.0241	88.36
Vegetation and soil	Percent tree cover	*PTC*	0.0177	90.13
Vegetation and soil	soil temperature in surface layer	T_{S1}	0.0107	91.20
Climate/meteorology	surface air pressure	*PA*	0.0097	92.17
Topography	Surface slope	*Slope*	0.0093	93.10
Climate/meteorology	precipitation	P_r	0.0091	94.01
Others	inverse relative distance from the Earth to the Sun	*dr*	0.0089	94.9
Others	latitude	*Lat*	0.0075	96.65
Climate/meteorology	Relative air humidity	*RH*	0.0074	96.39
Topography	Digital elevation model	*DEM*	0.0072	97.11
Vegetation and soil	soil volumetric moisture content in surface layer	*SM1*	0.007	97.81
Others	longitude	*Lon*	0.0067	98.48
Climate/meteorology	Carbon dioxide concentration	CO_2	0.0056	99.04
Topography	Surface aspect	*Aspect*	0.005	99.54
Climate/meteorology	Wind speed	*WS*	0.0046	100

(3) We have added a brief description of the optimization of hyperparameters for the renewed CoSEB model using the random search method and grid search method. Specifically, the number of decision trees, the max depth, min samples split, and min samples leaf of the MRF are set to 281, 21, 8, and 8, respectively, compared to 295, 20, 12, and 8 in our previous study of Wang et al. (2025). The corresponding details have been added at the beginning of the third paragraph of Section 3 in the revised manuscript with the following sentences:

"To enhance model generalization, the renewed CoSEB model was reoptimized using random and grid search methods, resulting in different hyperparameters of 281 decision trees, a maximum depth of 21, and minimum samples split and leaf of 8 from those of Wang et al. (2025)."

(4) We would like to emphasize that the main focus of this study was to develop the data-driven energy-conservation global datasets using multiple input variables that have certain influences on surface radiation and heat fluxes, rather than to explore the directionality of effects of each input variable on surface radiation and heat fluxes. Since directionality analysis does not alter model parameters, affect

model construction, or impact the generation of the CoSEB-based datasets, in almost no articles (Jung et al., 2019; Mu et al., 2011; Ryu et al., 2018; Xu et al., 2022) focusing on models and algorithms for surface radiation fluxes and heat fluxes have we seen anyone conduct directionality analysis; therefore, conducting directionality analysis is not necessary within the scope of our study.

2. Multi-collinearity amongst predictor variables- Authors should also discuss how multi-collinearity is handled amongst predictor variables given the large number of predictors. As far as I understand, random forests do not explicitly deal with multi collinearity unlike a PCA based approach for example. This can affect variable importance significantly. I would suggest authors explore this in detail.

Ans: We thank the reviewer for this comment. While random forests do not explicitly eliminate multi-collinearity among input variables, they randomly select subsets of input features at each split (Breiman, 2001) and are generally considered robust in terms of performance even when multi-collinearity exists among some inputs (Drobnič et al., 2020). Besides, in selecting the input variables, prior knowledge derived from previous studies was employed to identify factors that exert significant influence on surface radiation and heat flux while maintaining relative inter-independence. This practice is widely adopted in data-driven models for estimating land surface water, energy, and carbon fluxes (Bai et al., 2024; Elghawi et al., 2023; Han et al., 2023; O. & Orth, 2021), and few studies specifically perform multicollinearity analysis before modeling. Although some of the selected variables may exhibit a certain degree of multi-collinearity, each carries unique characteristic information, making it inappropriate to consider only a single dominant variable during model construction. Moreover, we acknowledge that variable importance should be interpreted with caution, since the importances may not be accurate in the presence of multicollinearity. However, we would also like to clarify that the primary aim of this study was to improve the accuracy of the developed datasets rather than to interpret the individual contributions of each input variable. We have discussed this in second paragraph of Section 5 with the following sentence:

"In selecting the 19 input variables to accommodate the additional target variables, prior knowledge derived from previous studies was employed to identify factors that exert significant influence on surface radiation and heat flux while maintaining relative inter-independence as much as possible (Jung et al., 2019; Mohan et al., 2020; Wang et al., 2021; Xian et al., 2024). This practice is commonly adopted in data-driven models for estimating land surface water, energy, and carbon fluxes (Bai et al., 2024; Elghawi et al., 2023; Han et al., 2023; O. & Orth, 2021). The importance scores of the 19 different feature variables are exhibited in Table S4 in the Supplementary Material, and downward solar radiation, the primary source of the energy at the earth surface, is the most important input variable, consistent with the results from our previous study (Wang et al., 2025). Although some of the selected variables may exhibit a certain degree of multi-collinearity, each contributes unique and physically meaningful information, supporting the inclusion of all variables in model construction. Note that the variable importance, derived from the built-in method of the random forests and potentially affected by multicollinearity among the input variables, is presented only as a reference. Retaining all 19 feature variables ensures the model's flexibility and generalization capability, enabling future incorporation of additional representative ground-based observations for further training and improvement."

3. Effect of autocorrelation- Given the temporal nature of several predictor variables, can authors confirm that autocorrelation does not exist or is minimized in their framework? What tests were performed to check for this? In particular I would recommend authors add lagged variables to the model to make sure that this is not the case. I believe several models constructed for earth system variables tend to ignore aspects such as autocorrelation and therefore this is an important point to address.

Ans: Thanks for your question and suggestion. We agree that several predictor variables may exhibit autocorrelation. To investigate the impact of lagged effects of input variables on model performance, we specifically conducted an experiment by including lagged air temperature (i.e., the air temperature of the previous day, because air temperature, identified alongside downward solar radiation as one of the two most influential variables in the model based on the importance scores in Supplementary Table S4, exhibits a more pronounced lagged effect than solar radiation) as additional predictor. The results (Fig. S4 in the Supplementary Material) showed no noticeable improvement in model accuracy, suggesting that lagged effects were negligible in the CoSEB framework for estimates of daily surface radiation and heat fluxes. We speculate that lagged effects may have a more pronounced influence on flux estimates at higher temporal resolutions (e.g., half-hourly), but this is beyond the scope of the present study. We have discussed this in the second paragraph of Section 5 with the following sentence:

"Besides, to investigate the impact of lagged effects of input variables on model performance, experiments were also conducted by adding lagged variables (e.g., the air temperature of the previous day) to the 19 input features. The results (Fig. S4 in the Supplementary Material) showed almost no improvement in model accuracy, suggesting that lagged effects on model performance were negligible within the CoSEB framework for estimates of daily surface radiation and heat fluxes."

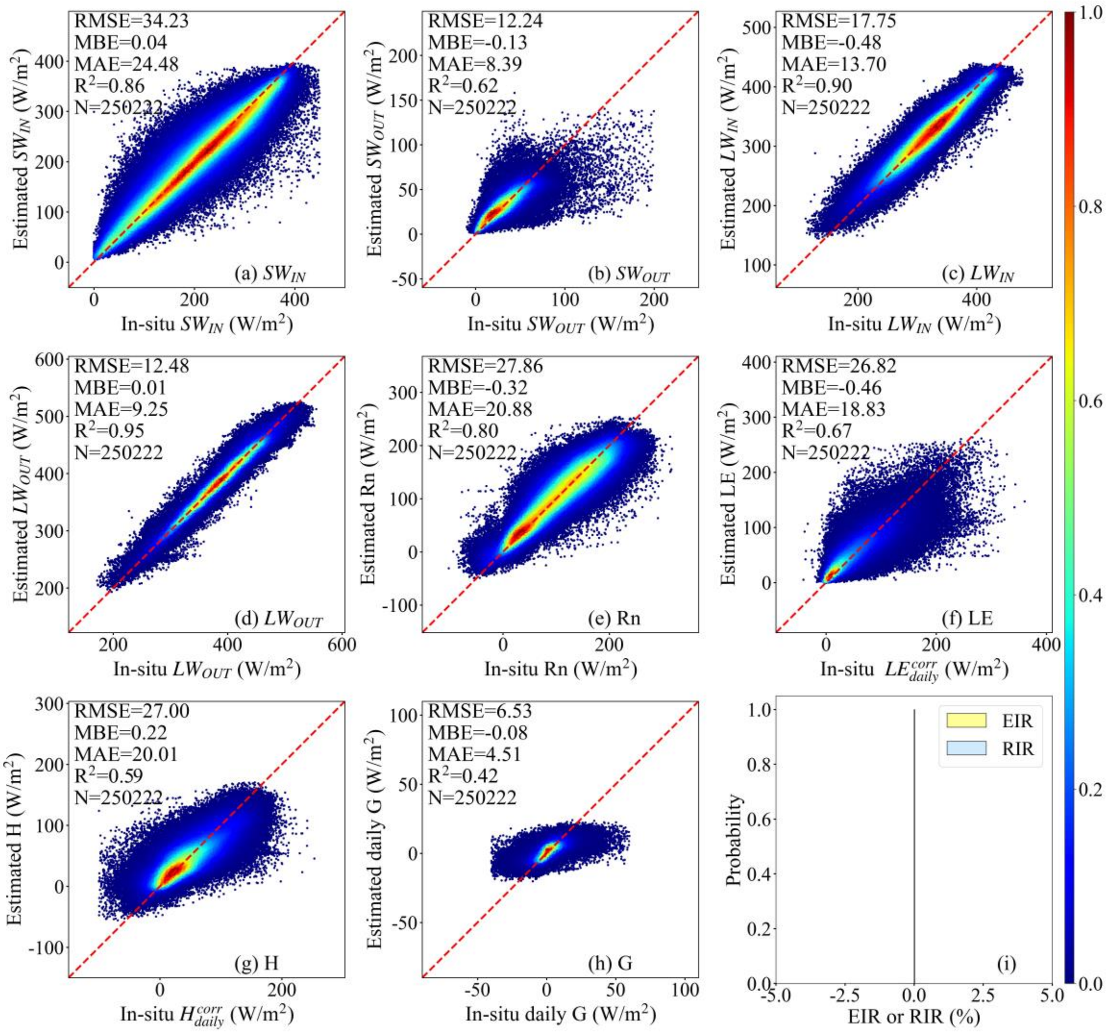

Fig. S4 Scatter density plots of the site-based 10-fold cross-validation of daily downward shortwave and longwave radiation (*SW_{IN}* and *LW_{IN}*), upward shortwave and longwave radiation (*SW_{OUT}* and *LW_{OUT}*), net radiation (Rn), soil heat flux (G), latent heat flux (LE) and sensible heat flux (H) derived by a reconstructed model within the CoSEB framework against in situ observed *SW_{IN}*, *LW_{IN}*, *SW_{OUT}*, *LW_{OUT}*, Rn, G, and energy imbalance-corrected LE (LE_{daily}^{corr}) and H (H_{daily}^{corr}), where the air temperature of the previous day was additionally added to the 19 input feature variables of the model as the lagged variable. The EIR and RIR in the subfigure (i) represent the energy imbalance ratio and radiation imbalance ratio, which are defined as 100% × (Rn - G - LE - H)/Rn and 100% × (*SW_{IN}* – *SW_{OUT}* + *LW_{IN}* - *LW_{OUT}*)/Rn, respectively. The colorbar represents the normalized density of data points.

4. Effect of downscaling ERA5- Land datasets- The authors note on lines 195-197 that the ERA 5 land datasets used here have been downscaled from a resolution of ~9 kms to ~500m. This is a significant level of downscaling performed using a rather simple cubic convolution method. There are several variables related to the land cover (such as the LAI for example) that are used as predictor variables in the author’s framework. Can the authors address the uncertainty caused by

such large downscaling between scales on their results? On the one hand, based on the results, it seems that the model has produced reliable results compared to observations and other datasets even after such large downscaling. Is it that the land cover related variables do not play an important role in the predictions?

Ans: Thanks for your comment and question. We would like to clarify that the ERA5-Land datasets used in this study mainly include meteorological reanalysis variables (e.g., solar radiation, pressure of the atmosphere, wind speed and relative air humidity), which were downscaled from their original ~9 km spatial resolution to 500 m. In contrast, the land cover-related vegetation variables, including LAI, FVC, and PTC, were directly obtained from remote sensing products such as MODIS and GLASS (see Section 2.2), which already have an original spatial resolution of ~500 m and therefore did not require spatial downscaling.

Besides, we acknowledge that downscaling ERA5-Land datasets from ~9 km to ~500 m using a cubic convolution method may introduce certain uncertainties. However, this resampling was necessary to match the footprint of the site-based measurements of turbulent heat fluxes, which is a common practice in the generation of remote sensing products (Mu et al., 2011; Ryu et al., 2018; Senay et al., 2020; Zhang et al., 2019; Zheng et al., 2022). Moreover, the machine learning framework of the CoSEB model can partially mitigate such uncertainties introduced by the downscaling during training by learning complex relationships among multiple inputs and in situ observed energy components. This is reflected in the good agreement of the CoSEB-based estimates with both in-situ observations and other mainstream products. Our previous studies (Wang et al., 2025, the last paragraph of Section 5.1) also have demonstrated that the differences in meteorological reanalysis data caused by spatial downscaling have a relatively small impact on the estimates by the machine-learning-based CoSEB model.

Furthermore, it is also important to note that this does not imply that land-cover-related variables do not play an important role in the estimations. As shown by the variable importance scores presented in the newly added Table S4 in the Supplementary Material, vegetation and surface-related parameters such as FVC and LAI have high importance scores. These variables can partially compensate for the spatial heterogeneity and localized variations not captured by the coarse-resolution ERA5-Land datasets, thereby enhancing the performance of the model.

We have discussed this in the last paragraph of Section 5 with the following sentence:

"Another potential source of uncertainty arises from differences in meteorological reanalysis data caused by spatial downscaling, which, as demonstrated in our previous study (Wang et al., 2025, the last paragraph of Section 5.1), has a relatively small impact on model estimates by the machine-learning-based CoSEB model combined with finer-resolution surface-related variables that partially compensate for the spatial heterogeneity and localized variations not captured by the coarse-resolution datasets."

5. In sample vs out of sample testing- While the authors present significant

comparisons with observations and other datasets to validate their model (e.g. Figure 3, Figure 4 and Figure 5), it seems the authors have not checked for overfitting of their approach by splitting the dataset into a training vs testing dataset. This is especially important since as mentioned in Major comment 1., the CoSEB framework itself has been updated. Authors should address this in detail. In fact, looking at Figure 3, it seems that the R squared values for G and H are on the lower side. I am curious as to what the values look like when out of sample testing is conducted?

Ans: We appreciate the reviewer's insightful comments and questions. We would like to clarify that the out-of-sample testing of the updated CoSEB model has already been evaluated using site-based 10-fold cross-validation. In this approach, all sites were divided into ten folds, where the samples from each fold of sites in turn served as validation datasets while the remaining folds were used for training. This ensures that the validation datasets are spatially independent from the training datasets, effectively serving as out-of-sample testing. The results shown in Figure 3, corresponding to the site-based 10-fold cross-validation, showed that the R^2 values for H and G are 0.59 and 0.42, respectively. We have already described the site-based 10-fold cross-validation in the third paragraph of Section 3 with the following sentence:

"Site-based 10-fold cross-validation was employed to evaluate the transferability and generalization of the CoSEB model by randomly dividing all sites into ten folds, where the samples from each fold of sites in turn served as validation datasets while the remaining folds were used as training datasets, ensuring that the validation was conducted on sites spatially independent from the training data."

Furthermore, to evaluate potential overfitting, the mean RMSE and R^2 values along with their standard deviations across the ten folds of the site-based cross-validation have been presented in Table S3 of the Supplementary Material. Comparisons between the training results (Table S3) and validation results (Fig. 3) indicate that, although the CoSEB model performs better on the training datasets than on the validation datasets, the overall performance remains stable. This stability, particularly given that the validation is conducted on spatially independent sites, demonstrates that the model is not affected by overfitting. We have illustrated this in the first paragraph of Section 4.1.1 with the following sentence:

"Comparisons with the corresponding training results (Table S3 in the Supplementary Material) indicated that although the CoSEB model performed better on the training datasets, its overall performance remained stable, suggesting that the CoSEB model was not affected by overfitting."

Table S3 The mean root mean square error (RMSE) and coefficient of determination (R^2) along with their standard deviations across the ten folds of the site-based cross-validation for the renewed CoSEB model.

	RMSE (W/m^2)	R^2
SW_{IN}	28.56±0.09	0.91±0.001
SW_{OUT}	9.83±0.10	0.79±0.003
LW_{IN}	12.41±0.08	0.95±0.001
LW_{OUT}	8.52±0.07	0.97±0.001
Rn	22.49±0.08	0.85±0.001
LE	19.75±0.15	0.82±0.003
H	19.36±0.12	0.76±0.003
G	5.39±0.04	0.60±0.004

Specific comments-

1. Abstract lines 31-36- The RMSEs presented here do not make any sense at this point since the reader has no sense of scale of values to expect. I recommend authors report the R squared values here instead. Also make sure to report whether the R squared is based on pooled data or just the testing data (See Major comment 5)

Ans: We appreciate the reviewer's constructive suggestion. We would like to clarify that RMSE remains a key metric for evaluating the accuracy of the model and datasets, particularly for energy flux estimations (Bisht & Bras, 2011; Comini De Andrade et al., 2024; Kalma et al., 2008; Ryu et al., 2008; Zhang et al., 2019), as it directly quantifies prediction errors in physical units (W/m^2), making it an indicator of significant interest to both model developers and product users. However, R^2 indeed is another important metric, indicating the degree to which the model predictions align with the reference truth. Therefore, in the revised Abstract, we have reported both RMSE and R^2 values for the CoSEB-based datasets. In addition, we have clarified that the reported RMSE and R^2 values of the CoSEB-based datasets are derived from validation at independent test datasets across 44 sites (see Section 2.1). The revised sentences are as follows:

"(1) the RMSEs (R^2) for daily estimates of SW_{IN}, SW_{OUT}, LW_{IN}, LW_{OUT}, Rn, LE, H and G from the CoSEB-based datasets at 44 independent test sites were 37.52 W/m^2 (0.81), 14.20 W/m^2 (0.42), 22.47 W/m^2 (0.90), 13.78 W/m^2 (0.95), 29.66 W/m^2 (0.77), 30.87 W/m^2 (0.60), 29.75 W/m^2 (0.44) and 5.69 W/m^2 (0.44), respectively,"

2. Introduction lines 74-75- Can the authors differentiate the citations between those for physical vs those for statistical methods.

Ans: Thanks for your valuable suggestion. We have clearly differentiated the citations between those for physical vs those for statistical methods in the revised manuscript as follows:

"In past decades, numerous RS-based products/datasets of global surface radiation and heat fluxes have significantly advanced, which were generally generated by physical (Li et al., 2023; Mu et al., 2011; Yu et al., 2022) or statistical methods (Jiao et al., 2023; Jung et al., 2019; Peng et al., 2020)."

3. Introduction line 92- “impending” is an awkward word here. I would just say “It was imperative”.

Ans: We appreciate the reviewer’s suggestion. We have revised this sentence to “It was imperative to develop global datasets of land surface radiation and heat fluxes characterized by high accuracies, radiation balance as well as heat balance, to better meet the requirements in practical applications of various fields.” in the new manuscript.

4. Data lines 131-132- Why could a simple interpolation not be applied for missing half hourly data? Is the data extremely sensitive to time? Some clarification is needed here.

Ans: Thank you for your comments and questions. The half-hourly surface radiation and heat fluxes are sensitive to short-term temporal variations caused by rapid changes in meteorological conditions, but their intraday dynamics are often nonlinear, particularly due to the intermittent effects of cloud cover. Therefore, applying simple interpolation methods (e.g. linear interpolation) could introduce considerable uncertainties. To ensure data quality, we only retained directly observed values (data quality flag=0) and good-quality gap-filled data (data quality flag=1) provided by the official gap-filling algorithms, and then computed daily averages only when more than 80% of half-hourly observations were available, as already described in the first paragraph of Section 2.1 with the following sentence:

“(3) the half-hourly ground-based observations with quality-control flag of 2 or 3 (bad quality) were removed but quality-control flag of 0 and 1 (good quality) were maintained; (4) a daily average of the half-hour observations was calculated for each day with greater than 80% good-quality data, further reducing the 472 sites to 355 sites;”

Besides, we have already discussed the uncertainties caused by the daily averages of surface radiation and heat fluxes in the last paragraph of Section 5 with the following sentence:

“Specifically, daily averages of surface radiation and heat fluxes for each day were obtained for analysis from good-quality half-hourly observations when the fraction of these good-quality half-hourly observations was greater than 80% in a day, due to the lack of consensus on the method for aggregating gapped half-hourly observations to daily data (Tang et al., 2024a; Yao et al., 2017; Zheng et al., 2022).”

Following your suggestion, we have also further clarified the simple temporal interpolation in the last paragraph of Section 5 with the following sentence:

“Simple temporal interpolation of half-hourly in situ observations, which could therefore introduce substantial uncertainties, was not applied, because surface radiation and heat fluxes are sensitive to short-term variations in meteorological conditions and their intraday dynamics are often complex.”

5. Data lines 138-139- Can the authors clarify why this criteria was applied for screening outliers?

Ans: Thank you for your valuable question. We would like to clarify that the energy balance ratio (EBR) of 0.2-1.8 and the 1st-99th quantiles of the daily evaporation fraction was both applied to remove physically implausible measurements, such as cases where the available surface energy (Rn − G) is close to zero while LE and H remain comparatively large, where the threshold of 0.2-1.8 was adopted following our previous study (Wang et al., 2025), which has demonstrated that nearly all available data fall within this range and that the accuracy of the CoSEB model showed no significant differences when applying different EBR thresholds, while the percentile-based screening was employed following common practice in flux and remote sensing studies (Bartkowiak et al., 2024; Ghorbanpour et al., 2022; Wang et al., 2023). We have clarified this in the first paragraph of Section 2.1 with the following sentence:

"(5) the aggregated daily LE and H were corrected for energy imbalance using the Bowen ratio method when the daily energy balance closure [defined as $(LE+H)/(Rn-G)$] varied between 0.2 and 1.8 following Wang et al. (2025) to exclude physically implausible measurements; (6) extreme outliers in the daily evaporative fraction were further removed by excluding values outside the 1st–99th percentile range, a common practice in flux and remote sensing studies (Bartkowiak et al., 2024; Wang et al., 2023), further reducing the 355 sites to 337 sites."

6. Mainstream datasets/products for inter comparison- I was curious as to why the authors so not compare their estimates with heat and radiation estimates from popular earth system modelling systems such as CESM and CTSM (https://www.cesm.ucar.edu/). In fact, if the authors approach can produce estimates similar to earth system models, this would be a huge benefit to the community (since these models are laborious to run)

Ans: Thanks for your comment. The outputs of Earth system models generally have coarse spatial resolutions (e.g., the CESM Large Ensemble Project has a spatial resolution of ~1°). Due to the surface heterogeneity, these model outputs cannot be directly validated using radiation and heat flux observations from ground sites with limited spatial representativeness. This is the main reason why both we and others usually do not compare the outputs of Earth system models with remote sensing-based datasets.

Although we believe that comparing the outputs of Earth system models with remote sensing-based datasets (including our CoSEB-based datasets and others' PML_V2, MOD16A2, FLUXCOM, BESSV2.0, GLASS) and validating them against ground-based observations is not appropriate, following the reviewer's suggestion, we compared the global spatial distributions of mean annual estimates from CoSEB-based datasets with the outputs from the CESM Large Ensemble project. The results (see Section 4.3 and Fig. S8) show that, overall, the global spatial patterns of the estimated SW_{IN}, LW_{IN}, LW_{OUT}, Rn, LE and H are consistent, though numerical differences exist. Considering the scope and length of the current manuscript, a more detailed analysis of the spatial-temporal distribution patterns, trends, and variability between Earth system model outputs and remote sensing-based datasets could be conducted in future work. We have discussed this in the third paragraph of Section 5 with the following sentences:

"Preliminary analysis indicates that the CoSEB-based datasets exhibit spatial patterns consistent with those of mainstream RS-based datasets and Earth system model outputs (see Fig. S8 in the supplementary material). More detailed analysis about their similarities and differences can be further conducted in future work."

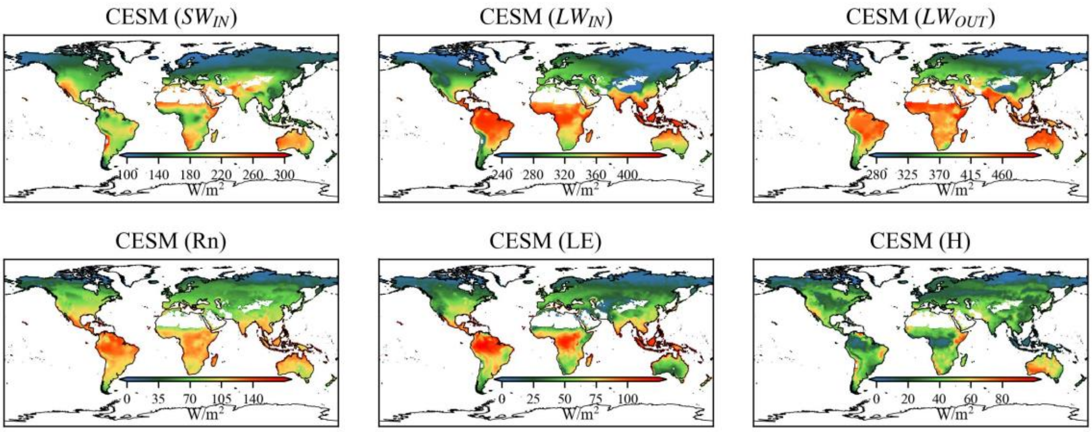

Fig. S8 Spatial patterns of global mean annual downward shortwave radiation (SW_{IN}), downward longwave radiation (LW_{IN}), upward longwave radiation (LW_{OUT}), net radiation (Rn), latent heat flux (LE) and sensible heat flux from 2001 to 2018 by Community Earth System Model (CESM) Large Ensemble project, where LW_{OUT} and Rn were inferred from surface radiation balance and heat balance.

7. Methods lines 243-244- Once again the usage of RMSEs here does not make much sense. Can the authors just report the R squared values instead.

Ans: We appreciate the reviewer's suggestion. We would like to clarify that RMSE remains an essential metric for evaluating the accuracy of the model and datasets, particularly for energy flux estimations (Bisht & Bras, 2011; Comini De Andrade et al., 2024; Kalma et al., 2008; Ryu et al., 2008; Zhang et al., 2019), as it directly quantifies prediction errors in physical units (W/m^2), making it an indicator of significant interest to both model developers and product users. Nevertheless, R^2 indeed is another important metric, indicating the degree to which the model predictions align with the reference truth. After careful consideration, we have additionally reported R^2 values in the revised manuscript to more comprehensively demonstrate the model performance. The revised sentence is as follows:

"The CoSEB model was demonstrated to be able to produce high-accuracy estimates of land surface energy components, with the RMSE of <17 W/m^2 and R^2 of > 0.83 for estimating 4-day Rn, LE and H, and the RMSE of <5 W/m^2 and R^2 of 0.55 for estimating 4-day G."

8. Methods lines 269-270- Just to confirm, the RF based uncoordinated models are models where only individual variables are estimated rather than the simultaneous calculation of several variables? This should be clarified.

Ans: Thanks for your valuable question. Your understanding is correct. We have more clearly clarified this in the third paragraph of Section 3 of the revised manuscript with the following sentence:

"Furthermore, to benchmark the coordinated estimates from the renewed CoSEB model, eight RF-based uncoordinated models were constructed, each separately estimating one of SW_{IN}, SW_{OUT}, LW_{IN}, LW_{OUT}, Rn, LE, H or G using the same inputs as those in the renewed CoSEB model."

9. Results Lines 306-309- I was curious looking at Figure 4 whether there were correlations or relationships between the EIR or RIR values and any of the other predictor variables? Is the shape of that distribution affected by any particular variables?

Ans: Thanks for your question. We would like to clarify that our CoSEB model showed no energy imbalance, with the RIR and EIR of 0, as shown in Figure 3. The distributions of RIR and EIR in Figure 4 were derived from RF-based uncoordinated models, which were used only for comparison with our CoSEB model and were not the focus of our study.

However, considering your concern about whether the distributions of the RIR and EIR values are affected by specific predictor variables, we further conducted a binned statistical analysis, where the three most critical input variables identified in Table S4 (i.e. SW_{IN}^{ERA5}, T_a *and FVC*) were divided into equal-width bins, and for each bin the mean and standard deviation for positive and negative RIR conditions were calculated. Besides, the Pearson correlation coefficients (r) between RIR (EIR) and each input variable were computed to quantify their overall relationships. The results showed that lower levels of solar radiation, air temperature, or FVC are associated with larger RIR (EIR), while the predominance of low values of these three variables tends to result in decreased kurtosis correspondingly, implying flatter and broader probability shapes of RIR and EIR. We have also briefly illustrated this in the end of the second paragraph of Section 4.1.1 with the following sentence:

"Furthermore, the RIR as well as EIR tended to be higher under lower solar radiation, air temperature, or FVC, with more frequent low values of these three variables leading to a broader and less peaked distribution of RIR and EIR (see Fig. S1 in the Supplementary Material)."

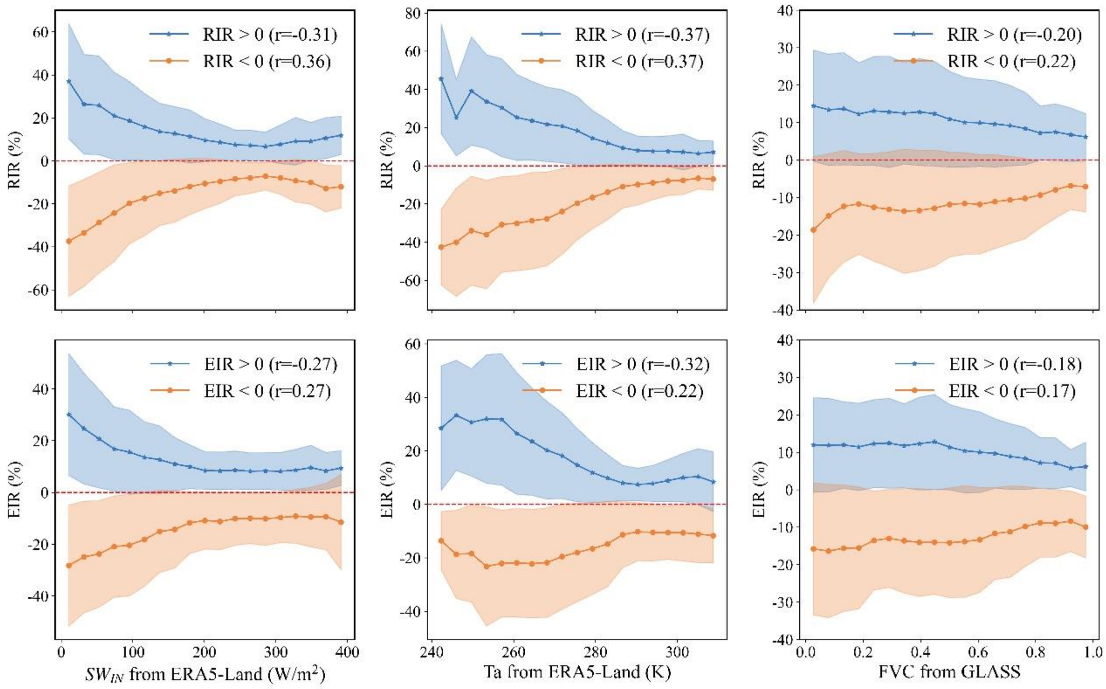

Fig. S1 Relationships between radiation imbalance ratio [RIR, 100% × ($SW_{IN} - SW_{OUT} + LW_{IN} - LW_{OUT}$)/Rn] and energy imbalance ratio [EIR, 100% × (Rn - G - LE - H)/Rn] derived from RF-based uncoordinated models and three critical input variables identified in Table S4, including solar radiation reaching the surface of the earth from ERA5-Land (SW_{IN}^{ERA5}, the first column), 2 m air temperature from ERA5-Land (T_a, the second column) and fraction vegetation cover from GLASS (*FVC*, the third column). The mean and standard deviation were calculated within equal-width bins of SW_{IN}^{ERA5}, T_a, and FVC under positive and negative EIR (RIR) conditions, where the solid lines represent the mean values, and the shaded area represents the corresponding variation of standard deviations. The r values in legends indicate the Pearson correlation coefficients.

10. Results Lines 311-312- Can the authors clarify the differences between site-based validation vs sample-based validation?

Ans: We appreciate the reviewer's insightful comment. Sample-based 10-fold cross-validation refers to randomly splitting all available samples from all sites into ten folds, with each fold in turn serving as the validation dataset while the remaining folds are used for training. This approach allows samples from the same site to appear in both the training and validation datasets. In contrast, site-based 10-fold cross-validation was performed by randomly dividing all sites into ten folds, with the samples from each fold of sites used for validation in turn. This strategy ensures that the validation datasets are spatially independent from the training datasets, thereby providing a more rigorous assessment of the model's spatial generalization capability. We have already described the site-based 10-fold cross-validation in the third paragraph of Section 3 with the following sentences:

"Site-based 10-fold cross-validation was employed to evaluate the transferability and generalization of the CoSEB model by randomly dividing all sites into ten folds, where the samples from each fold of sites in turn served as validation datasets while the remaining folds were used as training datasets, ensuring that the validation was conducted on sites spatially independent from the training data."

Furthermore, after careful consideration, site-based 10-fold cross-validation was deemed to be more suitable for assessing the performance of the model than sample-based 10-fold cross-validation, as the validation datasets in site-based cross-validation are spatially independent from the training datasets. To make the main focus of the manuscript clearer and more concise, we retained only the site-based 10-fold cross-validation and removed the sample-based 10-fold cross-validation in the revised manuscript.

11. Results lines 381-382- Once again, the RMSE values don't make a lot of sense here. Authors should report the R squared values instead.

Ans: We appreciate the reviewer's suggestion. We would like to clarify that RMSE remains an essential metric for evaluating the accuracy of the model and datasets, particularly for energy flux estimations (Bisht & Bras, 2011; Comini De Andrade et al., 2024; Kalma et al., 2008; Ryu et al., 2008; Zhang et al., 2019), as it directly quantifies prediction errors in physical units (W/m^2), making it an indicator of significant interest to both model developers and product users. However, R^2 indeed is another important metric, indicating the degree to which the model predictions align with the reference truth. After careful consideration, we have additionally incorporated the R^2 values into the revised manuscript. The revised sentence is as follows:

"Results indicated that the CoSEB-based datasets could provide good estimates of SW_{OUT}, H and G, with the RMSEs (R^2) of 14.20 W/m^2 (0.42), 29.75 W/m^2 (0.44) and 5.69 W/m^2 (0.44) at daily scale, respectively, and the RMSE (R^2) of 12.19 W/m^2 (0.39) and 4.60 W/m^2 (0.47) for 8-day SW_{OUT} and G, respectively."

12. Section 4.2- When discussing the differences between the CoSEB model estimates vs other estimates, can authors also describe why the differences occur? A detailed discussion is not warranted here. Rather, I was interested in the author's perspective as to why the author's approach produces some differences over existing approaches.

Ans: Thanks for your constructive comments. The possible reasons for the differences between estimates from the CoSEB-based datasets and the mainstream products/datasets are complex and may arise from differences in both methodological frameworks and input datasets. Specifically, the discrepancies may result from the simplification of physical processes and the uncertainties in parameterization within the physics-based products (e.g., MOD16A1, BESSV2.0, PML_V2, and ETMonitor). In contrast, the differences between the CoSEB-based datasets and other machine-learning-based products (e.g., BESS-Rad, GLASS, and FLUXCOM) may be attributed to the limited sample sizes of training data, the

incomplete consideration of influencing factors (e.g., CO_2 concentration, surface aspect), and the lack of physical constraints among energy balance components in existing machine-learning frameworks. We have briefly discussed this in the last paragraph of Section 4.2 of the revised manuscript with the following sentence:
"The differences between the estimates from the CoSEB-based datasets and mainstream datasets are likely multifactorial, arising from the simplification and parameterization uncertainties in physics-based models, as well as the lack of physical constraints, limited training samples, and incomplete consideration of influencing factors in other machine-learning-based models."

Reference:

Bai, Y., Mallick, K., Hu, T., Zhang, S., Yang, S. and Ahmadi, A.: Integrating machine learning with thermal-driven analytical energy balance model improved terrestrial evapotranspiration estimation through enhanced surface conductance, Remote Sens. Environ., 311, 114308. 10.1016/j.rse.2024.114308, 2024.

Bartkowiak, P., Ventura, B., Jacob, A. and Castelli, M.: A Copernicus-based evapotranspiration dataset at 100 m spatial resolution over four Mediterranean basins, Earth Syst. Sci. Data, 16, 4709-4734. 10.5194/essd-16-4709-2024, 2024.

Bisht, G. and Bras, R. L.: Estimation of Net Radiation From the Moderate Resolution Imaging Spectroradiometer Over the Continental United States, IEEE Trans. Geosci. Remote Sensing, 49, 2448-2462. 10.1109/tgrs.2010.2096227, 2011.

BREIMAN, L.: Random forests, Mach. Learn., 45, 5-32. 2001.

Comini de Andrade, B., Laipelt, L., Fleischmann, A., Huntington, J., Morton, C., Melton, F., Erickson, T., Roberti, D. R., de Arruda Souza, V., Biudes, M., Gomes Machado, N., Antonio Costa dos Santos, C., Cosio, E. G. and Ruhoff, A.: geeSEBAL-MODIS: Continental-scale evapotranspiration based on the surface energy balance for South America, ISPRS-J. Photogramm. Remote Sens., 207, 141-163. 10.1016/j.isprsjprs.2023.12.001, 2024.

Drobnič, F., Kos, A. and Pustišek, M.: On the Interpretability of Machine Learning Models and Experimental Feature Selection in Case of Multicollinear Data, Electronics, 9. 10.3390/electronics9050761, 2020.

ElGhawi, R., Kraft, B., Reimers, C., Reichstein, M., Körner, M., Gentine, P. and Winkler, A. J.: Hybrid modeling of evapotranspiration: inferring stomatal and aerodynamic resistances using combined physics-based and machine learning, Environ. Res. Lett., 18, 034039. 10.1088/1748-9326/acbbe0, 2023.

Ghorbanpour, A. K., Kisekka, I., Afshar, A., Hessels, T., Taraghi, M., Hessari, B., Tourian, M. J. and Duan, Z.: Crop Water Productivity Mapping and Benchmarking Using Remote Sensing and Google Earth Engine Cloud Computing, Remote Sens., 14. 10.3390/rs14194934, 2022.

Han, Q., Zeng, Y., Zhang, L., Wang, C., Prikaziuk, E., Niu, Z. and Su, B.: Global long term daily 1 km surface soil moisture dataset with physics informed machine learning, Sci. Data, 10, 101. 10.1038/s41597-023-02011-7, 2023.

Jung, M., Koirala, S., Weber, U., Ichii, K., Gans, F., Camps-Valls, G., Papale, D., Schwalm, C.,

Tramontana, G. and Reichstein, M.: The FLUXCOM ensemble of global land-atmosphere energy fluxes, Sci. Data, 6, 74. 10.1038/s41597-019-0076-8, 2019.
Kalma, J. D., McVicar, T. R. and McCabe, M. F.: Estimating Land Surface Evaporation: A Review of Methods Using Remotely Sensed Surface Temperature Data, Surveys in Geophysics, 29, 421-469. 10.1007/s10712-008-9037-z, 2008.
Mu, Q., Zhao, M. and Running, S. W.: Improvements to a MODIS global terrestrial evapotranspiration algorithm, Remote Sens. Environ., 115, 1781-1800. 10.1016/j.rse.2011.02.019, 2011.
O., S. and Orth, R.: Global soil moisture data derived through machine learning trained with in-situ measurements, Sci. Data, 8. 10.1038/s41597-021-00964-1, 2021.
Ryu, Y., Jiang, C., Kobayashi, H. and Detto, M.: MODIS-derived global land products of shortwave radiation and diffuse and total photosynthetically active radiation at 5 km resolution from 2000, Remote Sens. Environ., 204, 812-825. 10.1016/j.rse.2017.09.021, 2018.
Ryu, Y., Kang, S., Moon, S.-K. and Kim, J.: Evaluation of land surface radiation balance derived from moderate resolution imaging spectroradiometer (MODIS) over complex terrain and heterogeneous landscape on clear sky days, Agric. For. Meteorol., 148, 1538-1552. 10.1016/j.agrformet.2008.05.008, 2008.
Senay, G. B., Kagone, S. and Velpuri, N. M.: Operational Global Actual Evapotranspiration: Development, Evaluation and Dissemination, Sensors (Basel), 20. 10.3390/s20071915, 2020.
Wang, D., Liang, S., He, T. and Shi, Q.: Estimation of Daily Surface Shortwave Net Radiation From the Combined MODIS Data, IEEE Trans. Geosci. Remote Sensing, 53, 5519-5529. 10.1109/tgrs.2015.2424716, 2015.
Wang, J., Tang, R., Liu, M., Jiang, Y., Huang, L. and Li, Z.-L.: Coordinated estimates of 4-day 500 m global land surface energy balance components, Remote Sens. Environ., 326, 114795. 10.1016/j.rse.2025.114795, 2025.
Wang, Y., Hu, J., Li, R., Song, B. and Hailemariam, M.: Remote sensing of daily evapotranspiration and gross primary productivity of four forest ecosystems in East Asia using satellite multi-channel passive microwave measurements, Agric. For. Meteorol., 339, 109595. 10.1016/j.agrformet.2023.109595, 2023.
Xu, J., Liang, S., Ma, H. and He, T.: Generating 5 km resolution 1981–2018 daily global land surface longwave radiation products from AVHRR shortwave and longwave observations using densely connected convolutional neural networks, Remote Sens. Environ., 280, 113223. 10.1016/j.rse.2022.113223, 2022.
Zhang, Y., Kong, D., Gan, R., Chiew, F. H. S., McVicar, T. R., Zhang, Q. and Yang, Y.: Coupled estimation of 500 m and 8-day resolution global evapotranspiration and gross primary production in 2002–2017, Remote Sens. Environ., 222, 165-182. 10.1016/j.rse.2018.12.031, 2019.
Zheng, C., Jia, L. and Hu, G.: Global land surface evapotranspiration monitoring by ETMonitor model driven by multi-source satellite earth observations, J. Hydrol., 613, 128444. 10.1016/j.jhydrol.2022.128444, 2022.

Energy-conservation datasets of global land surface radiation and heat fluxes from 2000-2020 generated by CoSEB

Junrui Wang[a, b], Ronglin Tang[a, b, *], Meng Liu[c], Zhao-Liang Li[a, b, c]

[a] State Key Laboratory of Resources and Environment Information System, Institute of Geographic Sciences and Natural Resources Research, Chinese Academy of Sciences, Beijing 100101, China

[b] University of Chinese Academy of Sciences, Beijing 100049, China

[c] State Key Laboratory of Efficient Utilization of Arable Land in China, Institute of Agricultural Resources and Regional Planning, Chinese Academy of Agricultural Sciences, Beijing 100081, China

* Authors to whom correspondence should be addressed: tangrl@lreis.ac.cn

Abstract

Accurately estimating global land surface radiation [including downward shortwave radiation (SW_{IN}), downward longwave radiation (LW_{IN}), upward shortwave radiation (SW_{OUT}), upward longwave radiation (LW_{OUT}) and net radiation (Rn)] and heat fluxes [including latent heat flux (LE), soil heat flux (G) and sensible heat flux (H)] is essential for quantifying the exchange of radiation, heat and water between the land and atmosphere under global climate change. This study presents the first data-driven energy-conservation datasets of global land surface radiation and heat fluxes from 2000 to 2020, generated by our model of Coordinated estimates of land Surface Energy Balance components (CoSEB). The model~~that~~ integrates GLASS and MODIS remote sensing data, ERA5-Land reanalysis datasets, topographic data, CO_2 concentration data as independent variables and in situ radiation and heat flux observations at 258 eddy covariance sites worldwide as dependent variables within a multivariate random forest technique to effectively learn the physics of energy conservation~~was renewed with a combination of GLASS and MODIS remote sensing data, ERA5-Land reanalysis datasets, topographic data, CO_2 concentration data, and observations at 258 eddy~~

~~covariance sites worldwide from the AmeriFlux, FLUXNET, EuroFlux, OzFlux, ChinaFLUX and TPDC~~. The developed CoSEB-based datasets are strikingly advantageous in that [1] they are the first ~~RS-based~~data-driven global datasets that satisfy both surface radiation balance~~ ($SW_{IN} - SW_{OUT} + LW_{IN} - LW_{OUT}$ = Rn)~~ and heat balance~~ (LE + H + G = Rn)~~ among the eight fluxes, as demonstrated by both the radiation imbalance ratio [RIR, defined as 100% × ($SW_{IN} - SW_{OUT} + LW_{IN} - LW_{OUT}$)/Rn] and energy imbalance ratio [EIR, defined as 100% × (Rn - G - LE - H)/Rn] of 0, [2] the radiation and heat fluxes are characterized by high accuracies, where (1) the RMSEs (R^2) for daily estimates of SW_{IN}, SW_{OUT}, LW_{IN}, LW_{OUT}, Rn, LE, H and G from the CoSEB-based datasets at 44 independent test sites were ~~28.51~~37.52 W/m^2 (0.81), 1~~0.39~~4.20 W/m^2 (0.42), ~~14.29~~22.47 W/m^2 (0.90), 1~~0.62~~3.78 W/m^2 (0.95), 2~~2.40~~9.66 W/m^2 (0.77), ~~24.38~~30.87 W/m^2 (0.60), 2~~2.67~~9.75 W/m^2 (0.44) and ~~6.77~~5.69 W/m^2 (0.44), respectively~~, as well as for 8-day estimates were 12.81 W/m^2, 7.08 W/m^2, 9.22 W/m^2, 8.34 W/m^2, 13.38 W/m^2, 19.99 W/m^2, 17.44 W/m^2 and 4.25 W/m^2, respectively~~, (2) the CoSEB-based datasets, in comparison to the mainstream products/datasets (i.e. GLASS, BESS-Rad, BESSV2.0, FLUXCOM, MOD16A2, PML_V2 and ETMonitor) that generally separately estimated subsets of the eight flux components, better agreed with the in situ observations. Our developed datasets hold significant potential for application across diverse fields such as agriculture, forestry, hydrology, meteorology, ecology, and environmental science, which can facilitate comprehensive studies on the variability, impacts, responses, adaptation strategies, and mitigation measures of global and regional land surface radiation and heat fluxes under the influences of climate change and human activities. The CoSEB-based datasets are open access and available through the National Tibetan Plateau Data Center (TPDC) at https://doi.org/10.11888/Terre.tpdc.302559 (Tang et al., 2025a) and through the Science Data Bank (ScienceDB) at https://doi.org/10.57760/sciencedb.27228 (Tang et al., 2025b).

Key words: Surface energy balance; Surface radiation balance; Shortwave/Longwave

radiation; Net radiation; Sensible/Latent heat flux; Evapotranspiration; CoSEB

1 Introduction

Land surface radiation balance and heat balance play important roles in Earth's climate system, representing the physical processes by which the surface-atmosphere absorbs and redistributes radiation and heat fluxes (Berbery et al., 1999; Betts et al., 1996; Mueller et al., 2009; Sellers et al., 1997; Xu et al., 2022a), and facilitating the exchange of water, energy, carbon, and other agents essential to climatic and ecological systems and human society (Jia et al., 2013; Wang et al., 2012; Wild, 2009; Wild et al., 2012; Xia et al., 2006). Accurately monitoring the spatial and temporal variations of global land surface radiation [including downward shortwave radiation (SW_{IN}), downward longwave radiation (LW_{IN}), upward shortwave radiation (SW_{OUT}), upward longwave radiation (LW_{OUT}) and net radiation (Rn)] and heat fluxes [including latent heat flux (LE), soil heat flux (G) and sensible heat flux (H)] is indispensable for quantifying the exchange of radiation, heat and water between the land and atmosphere under global climate change (Ersi et al., 2024; Liang et al., 2019; Rios & Ramamurthy, 2022; Tang et al., 2024a; Wang et al., 2021), and for studying solar energy utilization (Tang et al., 2024b; Zhang et al., 2017), hydrological cycle (Huang et al., 2015; Wild & Liepert, 2010), ecosystem productivity (Nemani et al., 2003), agricultural management (De Wit et al., 2005) and ecological protection (Tang et al., 2023). Remote sensing (RS) technology, with its high spatial-temporal resolution and applicability over large areas, is considered to be the most effective and economical means for obtaining global land surface radiation and heat fluxes (Liu et al., 2016; Van Der Tol, 2012; Zhang et al., 2010).

In past decades, numerous RS-based products/datasets of global surface radiation and heat fluxes have significantly advanced, which were generally generated by physical (Li et al., 2023; Mu et al., 2011; Yu et al., 2022) or statistical methods (Jiao et al., 2023; Jung et al., 2019; Peng et al., 2020). However, two key limitations still exist in these products. Firstly, most available products provide only a single component of land surface radiation or heat fluxes, e.g. ETMonitor (Zheng et al., 2022) and MOD16A2 (Mu et al., 2011) only estimating LE, leading to the failure to satisfy surface radiation balance and heat balance when the single radiation or heat flux is utilized in conjunction with products containing other radiation and heat components (Wang et al., 2025), and further posing significant uncertainties to understand the interactions and redistributions of surface radiation and energy in the Earth-atmosphere system. Secondly, a few products, e.g., FLUXCOM (Jung et al., 2019) and GLASS (Jiang et al., 2015; Zhang et al., 2014), generated datasets for multiple components of surface radiation and heat fluxes by using ~~independent~~ separate estimates from the uncoordinated models, which make them difficult to abide by surface radiation and heat conservation. These energy-imbalanced and radiation-imbalanced estimates among multiple components from previous products/datasets severely limit their in-depth applications in analyzing the spatial and temporal trends, simulating the physical processes of radiation, heat and water cycles as well as revealing the attributions and mechanisms in Earth-surface system under global climate change. It was ~~impending and~~ imperative to develop global datasets of land surface radiation and heat fluxes characterized by high accuracies, radiation balance as well as heat balance, to better meet the requirements in practical applications of various fields.

Our proposed data-driven model/framework of Coordinated estimates of land Surface Energy Balance components (CoSEB) (Wang et al., 2025), which effectively learns the underlying physical interrelations (i.e., surface energy conservation law) among multiple targeted variables, provides an unprecedented opportunity to develop global datasets of land surface radiation and heat fluxes that can not only simultaneously provide high-accuracy estimates of these components but also adhere to surface radiation- and heat-conservation laws.

The objectives of this study are twofold: (1) to develop high-accuracy datasets of global land surface radiation and heat fluxes, which comply with the principles of radiation balance and heat balance, using our CoSEB model renewed based on in situ observations, remote sensing data and reanalysis datasets; (2) to validate the datasets/model estimates against data from in situ observations, mainstream products as well as estimates from uncoordinated random forest (RF) techniques. Section 2 introduces the data resources used in this study. Section 3 briefly describes the method we used to estimate global surface radiation and heat fluxes. Section 4 presents the evaluation of the datasets/model estimates generated by our renewed CoSEB model. Section 5 discusses the superiority, potential applications and uncertainties of the developed datasets. Data availability is given in Section 6, and a summary and conclusion is provided in Section 7.

2 Data

2.1 Ground-based observations

In this study, the in situ observations of land surface radiation and heat fluxes at ~~258~~ 302 eddy covariance (EC) sites from the networks of AmeriFlux (~~145~~ 174 sites, 2000–2020, https://AmeriFlux.lbl.gov/Data/, last access: 6 August 2024), EuroFlux (72 sites, 2000-2020, http://www.europe-fluxdata.eu/, last access: 6 August 2024), OzFlux (5 sites, 2007-2012, https://data.ozflux.org.au/, last access: 6 August 2024), FLUXNET (108 sites, 2000–2014, https://FLUXNET.org/Data/download-Data/, last access: 6 August 2024), JapanFlux (15 sites, 2001-2020, https://ads.nipr.ac.jp/japan-flux2024/, last access: 10 October 2025), ChinaFLUX (5 sites, 2005-2020, http://www.chinaflux.org/, last access: 6 August 2024) and National Tibetan Plateau/Third Pole Environment Data Center (TPDC, 13 sites, 2012–2020, https://Data.tpdc.ac.cn/en/Data, last access: 6 August 2024) were used (Fig. 1), where 37, 48 and 5 sites in FLUXNET were also shared in AmeriFlux, EuroFlux and OzFlux, respectively. These ~~258~~ 302 sites were filtered out from all collected ~~1008~~ 1098 sites by following the quality-assurance and quality-control steps, including: (1) any site with a missing component of any of the SW_{IN}, SW_{OUT}, LW_{IN}, LW_{OUT}, LE, H and G was excluded, reducing the ~~1008~~ 1098 sites to ~~388~~ 472 sites for further analysis; (2) any half-hour period with missing data for any of these components was excluded; (3) the half-hourly ground-based observations with quality-control flag of 2 or 3 (bad quality) were removed but quality-control flag of 0 and 1 (good quality) were maintained; (4) a daily average of the half-hour observations was calculated for each day with greater than 80% good-quality data, further reducing the ~~388~~ 472 sites to ~~286~~ 355 sites; (5) the aggregated daily LE and H were corrected for energy imbalance using the Bowen ratio method when the daily energy balance closure [defined as $\left(LE+H\right)/(Rn-G)$] varied between 0.2 and 1.8 following Wang et al. (2025) to exclude physically implausible measurements; (~~5~~6) extreme outliers in the daily evaporative fraction were further removed by excluding values outside the 1st–99th percentile range, a common practice in flux and remote sensing studies (Bartkowiak et al., 2024; Wang et al., 2023), further reducing the 355 sites to 337 sites. ~~outliers were discarded, corresponding to the 1 and 99 quantiles of the daily evaporation fraction, further reducing the 286 sites to 268 sites.~~ Besides, the RS ~~data~~ products/datasets involved in this study collocated at the sites should not be missing, finally reducing the ~~268~~ 337 sites to ~~258~~ 302 sites for analysis. Note that the Rn at these sites used in this study was calculated from the sum of net longwave radiation (LW_{IN} minus LW_{OUT}) and net shortwave radiation (SW_{IN} minus SW_{OUT}), rather than using the observed Rn directly, to ensure surface radiation balance in training datasets.

These ~~258~~ 302 sites used in this study cover a wide range of global climate regimes across 14 land cover types, including (1) evergreen needleleaf forests (ENF, ~~54~~ 55 sites); (2) evergreen broadleaf forests (EBF, ~~11~~ 12 sites); (3) deciduous needleleaf forests (DNF, ~~1~~ 7 sites); (4) deciduous broadleaf forests (DBF, ~~39~~ 40 sites); (5) mixed forests (MF, 8 sites); (6) closed shrublands (CSH, 5 sites); (7) open shrublands (OSH, ~~9~~ 11 sites); (8) woody savannas (WSA, 6 sites); (9) savannas (SAV, 10 sites); (10) grasslands (GRA, ~~54~~ 62 sites); (11) permanent wetlands (WET, ~~16~~ 22 sites); (12) croplands (CRO, ~~43~~ 59 sites); (13) water bodies (WAT, 1 sites); (14) cropland/natural vegetation mosaics (CVM, ~~1~~ 4 sites). Among them, 44 sites (~15% of the total, see Table S1) were isolated to serve as spatially independent sites to test the generated datasets and they did not participate in the development of the model/datasets.

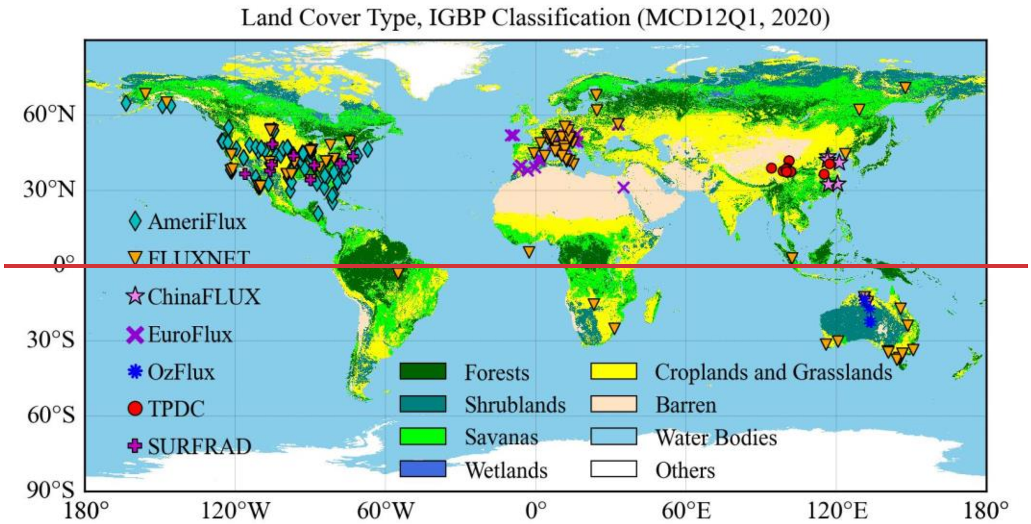

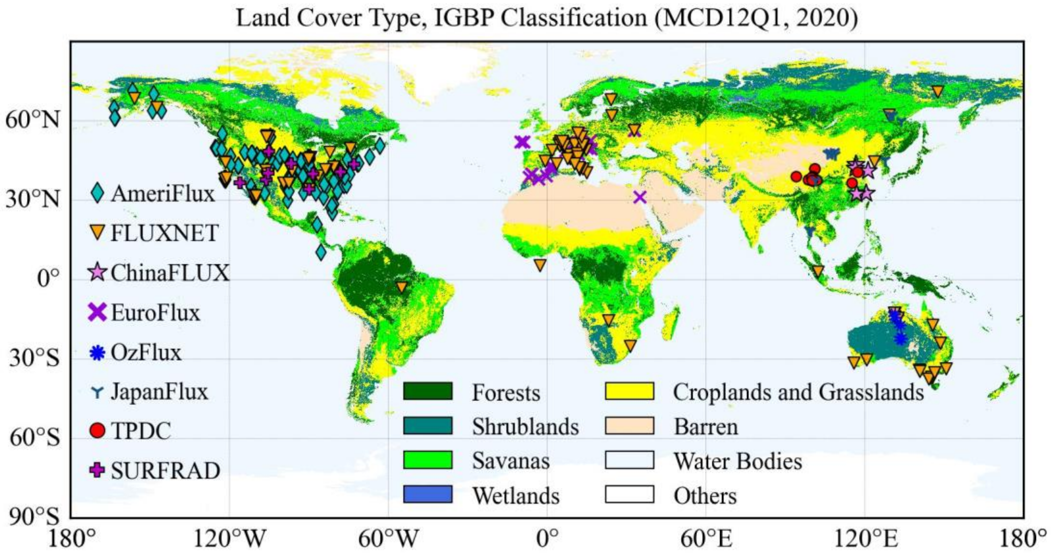

Fig. 1 Spatial distribution of the ~~258~~ 302 eddy covariance sites from AmeriFlux, FLUXNET, EuroFlux, OzFlux, JapanFlux, ChinaFLUX and TPDC, and nine radiation sites from SURFRAD involved for analysis in this study.

Furthermore, ground-based radiation observations from nine sites that are located in large flat agricultural areas covered by crops and grasses from SURFRAD were also introduced to validate land surface radiation estimates. Similar to the preprocessing performed on the observations of the ~~258~~ 302 EC sites, the SW_{IN}, SW_{OUT}, LW_{IN}, LW_{OUT} and Rn from the SURFRAD were also quality-controlled and aggregated to daily data.

Spatial distribution of the ~~258~~ 302 EC sites and nine radiation sites from SURFRAD are shown in Fig. 1, with site details (latitude, longitude, land cover types, digital elevation model and temporal coverage) provided in Supplementary Tables S1 and S2.

~~**Table 1 Summary of mainstream datasets/products for inter-comparison used in this study**~~

~~Products/ datasets~~	~~Reso-lution~~	~~Time coverage~~	~~Variables~~	~~Algorithms~~	~~References~~
~~GLASS~~	~~0.05°/ daily~~	~~2000-2018~~	~~SW_{IN}, LW_{IN}, LW_{OUT}, Rn~~	~~Machine learning, direct estimation algorithm~~	~~Wang et al. (2015); Xu et al. (2022b); Jiang et al. (2015)~~
~~BESS-Rad~~	~~0.05°/ daily~~	~~2000-2020~~	~~SW_{IN}~~	~~BESS process model~~	~~Ryu et al. (2018)~~
~~BESSV2.0~~	~~0.05°/ daily~~	~~2000-2020~~	~~Rn, LE~~	~~BESS process model~~	~~Li et al. (2023)~~
~~FLUXCOM~~	~~0.0833°/ 8-day~~	~~2000-2020~~	~~Rn, LE, H~~	~~Model tree ensembles~~	~~Jung et al. (2019)~~
~~MOD16A2~~	~~500 m/ 8-day~~	~~2000-2020~~	~~Rn, LE~~	~~Modified Penman-Monteith equation~~	~~Mu et al. (2011)~~
~~PML_V2~~	~~500 m/ 8-day~~	~~2002-2020~~	~~LE~~	~~Penman Monteith-Leuning model, Priestly Taylor equation and Gash model~~	~~Zhang et al. (2019)~~
~~ETMonitor~~	~~1 km/ daily~~	~~2000-2020~~	~~LE~~	~~Shuttleworth-Wallace two-source scheme, Gash model and Penman equation~~	~~Zheng et al. (2022)~~

2.2 Climate/meteorology and remote sensing data

To generate global datasets of land surface radiation and heat fluxes from 2000 to 2020, five types of climate/meteorology and remote sensing data were used in this study, including:

(1) ERA5-Land reanalysis datasets (https://cds.climate.copernicus.eu/, last access: 6 August 2024) with the spatial resolution of ~9 km from 1950 (Muñoz-Sabater et al., 2021). Following our previous work (Wang et al., 2025), this study used

variables from the ERA5-Land datasets to drive the model, including near-surface 2 m air temperature (T_a), soil temperature in layer 1 (0-7 cm, T_{S1}), soil volumetric moisture content in layer 1 (0-7 cm, $SM1$ ~~$SM1$~~), solar radiation reaching the surface of the earth (SW_{IN}^{ERA5}), net thermal radiation at the surface (LW_{net}), pressure of the atmosphere (PA ~~PA~~), 10 m wind speed (WS ~~WS~~), precipitation (P_r ~~P_r~~) and the 2 m dewpoint temperature, daily minimum and maximum air temperature [for calculating relative air humidity (RH ~~RH~~)].

(2) GLASS datasets (https://glass.bnu.edu.cn/, last access: 6 August 2024), which provide the 500 m 8-day leaf area index (*LAI*) and fractional vegetation cover (*FVC*) from February 2000 to December 2021.

(3) MOD44B product (https://lpdaac.usgs.gov/, last access: 6 August 2024), which offers yearly 250 m percent tree cover (*PTC*) since 2000, representing the percentage (0~100%) of a pixel covered by tree canopy.

(4) NOAA/GML atmospheric carbon dioxide (CO_2) concentration data, providing monthly global marine surface mean data since 1958 (ftp://aftp.cmdl.noaa.gov/products/trends/co2/co2_mm_gl.txt, last access: 6 August 2024).

(5) GMTED2010 topographic data (https://topotools.cr.usgs.gov/gmted_viewer/gmted2010_global_grids.php, last access: 6 August 2024), providing 500 m digital elevation model (DEM), slope, and aspect.

The ~9 km ERA5-Land datasets were spatially interpolated to 500 m using the cubic convolution method, and the 250 m PTC was resampled to 500 m using the arithmetic averaging method.

2.3 Mainstream datasets/products for inter-comparison

Mainstream RS-based datasets/products of moderate-resolution global land surface radiation and heat fluxes were collected for inter-comparison (Table 1), including (1) the daily 0.05° GLASS SW_{IN}, LW_{IN}, LW_{OUT} and Rn products from 2000 to 2018 (https://glass.bnu.edu.cn/, last access: 6 August 2024), (2) the daily 0.05° Breathing Earth System Simulator Radiation (BESS-Rad) SW_{IN} products from 2000 to 2020 (https://www.environment.snu.ac.kr/bess-rad), (3) the daily 0.05° BESS Version2.0 (BESSV2.0) Rn and LE products from 2000 to 2020 (https://www.environment.snu.ac.kr/bessv2), (4) the 8-day 0.0833° FLUXCOM Rn, LE and H products from 2001 to 2020 (https://fluxcom.org/, last access: 6 August 2024), (5) the daily 1 km ETMonitor LE product from 2000 to 2020 (https://data.casearth.cn/, last access: 6 August 2024), (6) the 8-day 500 m Penman-Monteith-Leuning Version2 (PML_V2, https://www.tpdc.ac.cn/, last access: 6 August 2024) LE product from 2000 to 2020; and (7) the 8-day 500 m MOD16A2 (https://lpdaac.usgs.gov/, last access: 6 August 2024) LE product from 2000 to 2020.

The GLASS SW_{IN} products are derived from a combination of the GLASS broadband albedo product and the surface shortwave net radiation estimates, where the surface shortwave net radiation is estimated using linear regression with MODIS top-of-atmosphere (TOA) spectral reflectance (Wang et al., 2015). The GLASS LW_{IN} and LW_{OUT} products are generated using densely connected convolutional neural networks, incorporating Advanced Very High-Resolution Radiometer (AVHRR) TOA reflectance and ERA5 near-surface meteorological data (Xu et al., 2022b). The GLASS Rn products are estimated from the meteorological variables from MERRA2 and surface variables from GLASS using the multivariate adaptive regression splines model (Jiang et al., 2015). The BESS-Rad and BESSV2.0 estimate SW_{IN} and Rn using a radiative transfer model (i.e., Forest Light Environmental Simulator, FLiES) with an artificial neural network based on MODIS and MERRA2 reanalysis datasets, and using FLiES based on MODIS products and NCEP/NCAR reanalysis data, respectively (Li et al., 2023; Ryu et al., 2018). Moreover, the BESSV2.0 (Li et al., 2023), MOD16A2 (Mu et al., 2011), PML_V2 (Zhang et al., 2019) and ETMonitor (Zheng et al., 2022) generated global LE by physical models, such as Penman-Monteith equation, Priestley-Taylor equation and/or Shuttleworth-Wallace two-source scheme. The FLUXCOM Rn, LE and H datasets are obtained through multiple machine learning methods based on in situ observations from FLUXNET and remote sensing and meteorological data (Jung et al., 2019). For better consistency, RF-based 8-day 0.0833° Rn and Bowen ratio-corrected LE and H for the periods of 2000 to 2020 from the FLUXCOM were used in this study.

Table 1 Summary of mainstream datasets/products for inter-comparison used in this study

Products/ datasets	Reso-lution	Time coverage	Variables	Algorithms	References
GLASS	0.05°/ daily	2000-2018	SW_{IN}, LW_{IN}, LW_{OUT}, Rn	Machine learning, direct estimation algorithm	Wang et al. (2015); Xu et al. (2022b); Jiang et al. (2015)
BESS-Rad	0.05°/ daily	2000-2020	SW_{IN}	BESS process model	Ryu et al. (2018)
BESSV2.0	0.05°/ daily	2000-2020	Rn, LE	BESS process model	Li et al. (2023)
FLUXCOM	0.0833°/ 8-day	2000-2020	Rn, LE, H	Model tree ensembles	Jung et al. (2019)
MOD16A2	500 m/ 8-day	2000-2020	LE	Modified Penman-Monteith equation	Mu et al. (2011)
PML_V2	500 m/ 8-day	2002-2020	LE	Penman Monteith-Leuning model, Priestly Taylor equation and Gash model	Zhang et al. (2019)
ETMonitor	1 km/ daily	2000-2020	LE	Shuttleworth-Wallace two-source scheme, Gash model and Penman equation	Zheng et al. (2022)

3 Methods

The method used to generate global datasets of land surface radiation and heat fluxes is based on the CoSEB model/framework, which was developed by our ~~recently~~

previously published work (Wang et al., 2025), to coordinately estimate global land surface energy balance components (including Rn, LE, H and G) using the multivariate random forest technique, with a combination of MODIS and GLASS products, ERA5-Land reanalysis datasets, and in situ observations at 336 EC sites~~from the FLUXNET, AmeriFlux, ChinaFLUX, EuroFlux, OzFlux and Heihe River Basin flux network~~. The CoSEB model was demonstrated to be able to produce high-accuracy estimates of land surface energy components, with the RMSE of <17 W/m^2 and R^2 of > 0.83 for estimating 4-day Rn, LE and H, and the RMSE of <5 W/m^2 and R^2 of 0.55 for estimating 4-day G. The most praiseworthy superiority of the CoSEB model lies in its ability to balance the land surface energy components, with an energy imbalance ratio [EIR, defined as 100%×(Rn - G - LE - H)/Rn~~$100\%\times(Rn-G-LE-H)/Rn$~~] of 0.

To coordinately estimate land surface radiation and heat fluxes that comply with both radiation balance and heat balance, one of the key procedures in the construction of the CoSEB model was to prepare training datasets that satisfy surface radiation and heat balance. For this purpose, the energy-imbalance corrections on daily in situ observed LE and H were conducted by the most widely applied Bowen ratio method [$H^{corr}=\frac{H}{H+LE}\times(Rn-G)$, $LE^{corr}=\frac{LE}{H+LE}\times(Rn-G)$, where H^{corr} and LE^{corr} represent the sensible heat flux and latent heat flux after energy-imbalance correction, respectively] with the aid of Rn and G observations, and the in situ Rn was calculated from the sum of in situ observed net longwave radiation (LW_{IN} minus LW_{OUT}) and net shortwave radiation (SW_{IN} minus SW_{OUT}). The input variables to renew the CoSEB model include: (1) climate/meteorology: T_a, SW_{IN}^{ERA5}, LW_{net}, WS, PA, P_r, RH, CO_2 concentration; (2) vegetation and soil: *LAI*, *FVC*, *PTC*, T_{S1}~~T_{S1}~~, *SM1*~~–SM1~~; (3) topography data: *DEM*, *Slope* and *Aspect*, in addition to longitude (*Lon*), latitude (*Lat*), and inverse relative distance from the Earth to the Sun (*dr*), in which the *dr* was calculated as $dr=1+0.033\times\cos\left(\frac{2\pi\times DOY}{365}\right)$, where *DOY* represents the day of year.

Considering that the footprint of the site-based measurements of turbulent heat fluxes is generally at a scale of hundreds of meters, to reduce the effect of differences of spatial scales between ground-based measurements (dependent variables) and remotely sensed/reanalysis datasets (independent variables), we renewed the CoSEB model at a spatial scale of 500 m for coordinately estimating global daily land surface radiation and heat fluxes, which can be expressed as follows:

$$\begin{pmatrix} SW_{IN}, SW_{OUT}, LW_{IN}, \\ LW_{OUT}, Rn, LE, H, G \end{pmatrix} = f\begin{pmatrix} Lon, Lat, T_a, T_{S1}, SM1, SW_{IN}^{ERA5}, LW_{net}, PA, WS, P_r, dr \\ RH, LAI, FVC, PTC, DEM, Slope, Aspect, CO_2 \end{pmatrix} \quad (1)$$

To enhance model generalization, the renewed CoSEB model was reoptimized using random and grid search methods, resulting in different hyperparameters of 281 decision trees, a maximum depth of 21, and minimum samples split and leaf of 8 from those of Wang et al. (2025). Site-based 10-fold cross-validation was employed to evaluate the transferability and generalization of the CoSEB model by randomly dividing all sites into ten folds, where the samples from each fold of sites in turn served as validation datasets while the remaining folds were used as training datasets, ensuring that the validation was conducted on sites spatially independent from the training data. ~~For comparison, eight RF-based uncoordinated models for separate estimates of SW_{IN}, SW_{OUT}, LW_{IN}, LW_{OUT}, Rn, LE, H and G were also constructed using the same inputs as those in the renewed CoSEB model. Site-based 10-fold cross-validation was employed to assess the transferability and generalization of the CoSEB model by randomly dividing all sites into ten folds, where each fold in turn serves as validation datasets while the other folds as the training datasets, ensuring the validation of the estimates of the CoSEB was conducted at sites that are spatially independent from those selected for the training datasets.~~ Furthermore, to benchmark the coordinated estimates from the renewed CoSEB model, eight RF-based uncoordinated models were constructed, each separately estimating one of SW_{IN}, SW_{OUT}, LW_{IN}, LW_{OUT}, Rn, LE, H or G using the same inputs as those in the renewed CoSEB model. Fig. 2 illustrates the flowchart for generating global datasets of land surface radiation and heat fluxes by the CoSEB model.

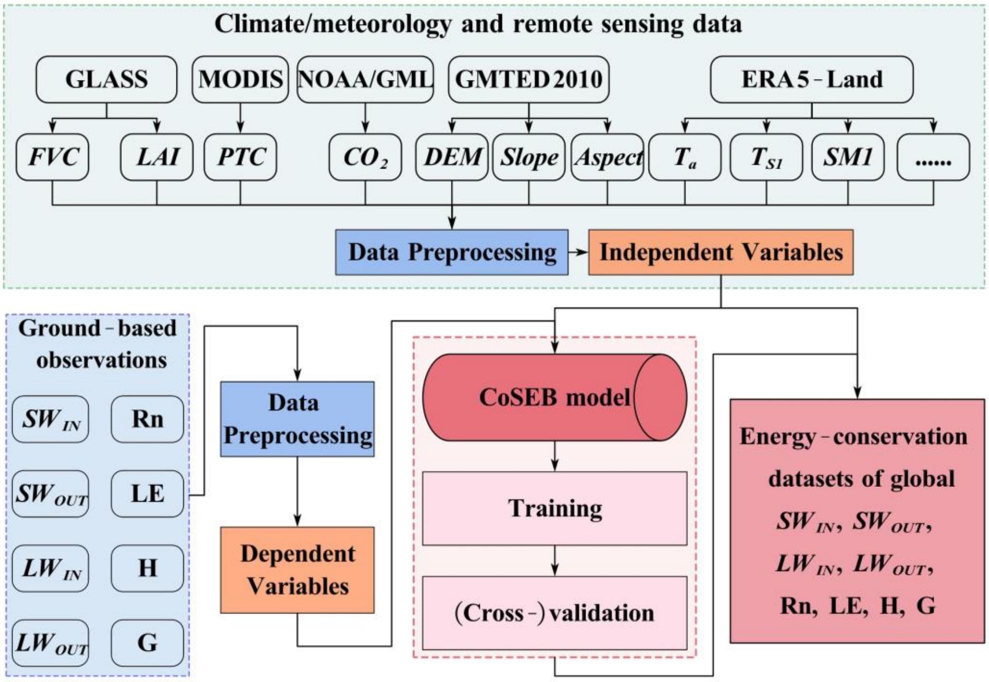

Fig. 2 Flowchart for generating energy-conservation datasets of global land surface radiation [including downward shortwave radiation (SW_{IN}), downward longwave radiation (LW_{IN}), upward shortwave radiation (SW_{OUT}), upward longwave radiation (LW_{OUT}) and net radiation (Rn)] and heat fluxes [including latent heat flux (LE), soil heat flux (G) and sensible heat flux (H)] by the CoSEB model renewed from in situ observations at 258 sites worldwide and collocated remote sensing and reanalysis datasets.

4 Results

4.1 Validation of the CoSEB model

4.1.1 Site-based 10-fold cross-validations at 258 EC sites

Fig. 3 and Fig. 4 present the scatter density plots of the site-based 10-fold cross-validation of daily SW_{IN}, LW_{IN}, SW_{OUT}, LW_{OUT}, Rn, LE, H and G estimated from the renewed CoSEB model and the RF-based uncoordinated models, respectively, by using the validation datasets collected at 258 EC sites worldwide. Results indicated that the estimates from both the CoSEB model and the RF-based uncoordinated models agreed well with the in situ observations, with the coefficient of determination (R^2) varying between 0.80 and 0.95 for SW_{IN}, LW_{IN}, LW_{OUT} and Rn, and between 0.59 and 0.67 for SW_{OUT}, LE and H. The CoSEB model, with the root mean square error (RMSE) of 26.82 to 34.25 W/m^2 and mean absolute error (MAE) of 18.83 to 24.49 W/m^2 for SW_{IN}, Rn, LE and H, the RMSE of 12.24 to 17.75 W/m^2 and the MAE of 8.39 to 13.70 W/m^2 for

SW_{OUT}, LW_{IN} and LW_{OUT}, demonstrated comparable accuracies to the RF-based models, with the RMSE of 27.07 to 33.34 W/m^2 and MAE of 19.29 to 23.64 W/m^2 for SW_{IN}, Rn, LE and H, the RMSE of 12.12 to 16.93 W/m^2 and the MAE of 8.68 to 12.99 W/m^2 for SW_{OUT}, LW_{IN} and LW_{OUT}. In the validation of daily G, both the CoSEB and RF-based models yielded RMSEs below 7 W/m^2. Comparisons with the corresponding training results (Table S3 in the Supplementary Material) indicated that although the CoSEB model performed better on the training datasets, its overall performance remained stable, suggesting that the CoSEB model was not affected by overfitting.

Strikingly, the CoSEB model exhibited large superiority in balancing the surface radiation and heat fluxes, with the radiation imbalance ratio [RIR, defined as 100% × (SW_{IN} – SW_{OUT} + LW_{IN} - LW_{OUT})/Rn ~~$100\%\times\left(SW_{IN}+LW_{IN}-SW_{OUT}-LW_{OUT}-Rn\right)/Rn$~~] and energy imbalance ratio [EIR, defined as 100% × (Rn - G - LE - H)/Rn ~~$100\%\times\left(Rn-G-LE-H\right)/Rn$~~] of 0, while the RF-based uncoordinated models showed substantial imbalances of the surface radiation and heat fluxes, with RIR and EIR that were approximately normally distributed, having absolute mean values of 38.84% and 31.22%, respectively, and reaching as high as 50% in some cases. Furthermore, the RIR as well as EIR tended to be higher under lower solar radiation, air temperature, or FVC, with more frequent low values of these three variables leading to a broader and less peaked distribution of RIR and EIR (see Fig. S1 in the Supplementary Material).

~~It should be pointed out that the performances of both the renewed CoSEB model and the RF-based models could be further improved if the site-based 10-fold cross-validation was replaced with the sample-based 10-fold cross-validation (Figs. S1 and S2 in the Supplementary Material). Specifically, for the CoSEB model, using the sample-based 10-fold cross-validation decreased the RMSE by 0.61 to 3.92 W/m^2 for five radiation components and G, and by 6.25 W/m^2 and 5.50 W/m^2 for LE and H, respectively, in comparison to using the site-based 10-fold cross-validation. Likewise, for the RF-based models, the RMSE decreased by 1.41 to 5.25 W/m^2 for five radiation~~

~~components and G, and by 9.63 W/m² and 7.43 W/m² for LE and H, respectively. The R² of both the CoSEB model and the RF-based models using the sample-based 10-fold cross-validation increased by 0.02 to 0.28 compared to the R² using the site-based 10-fold cross-validation.~~

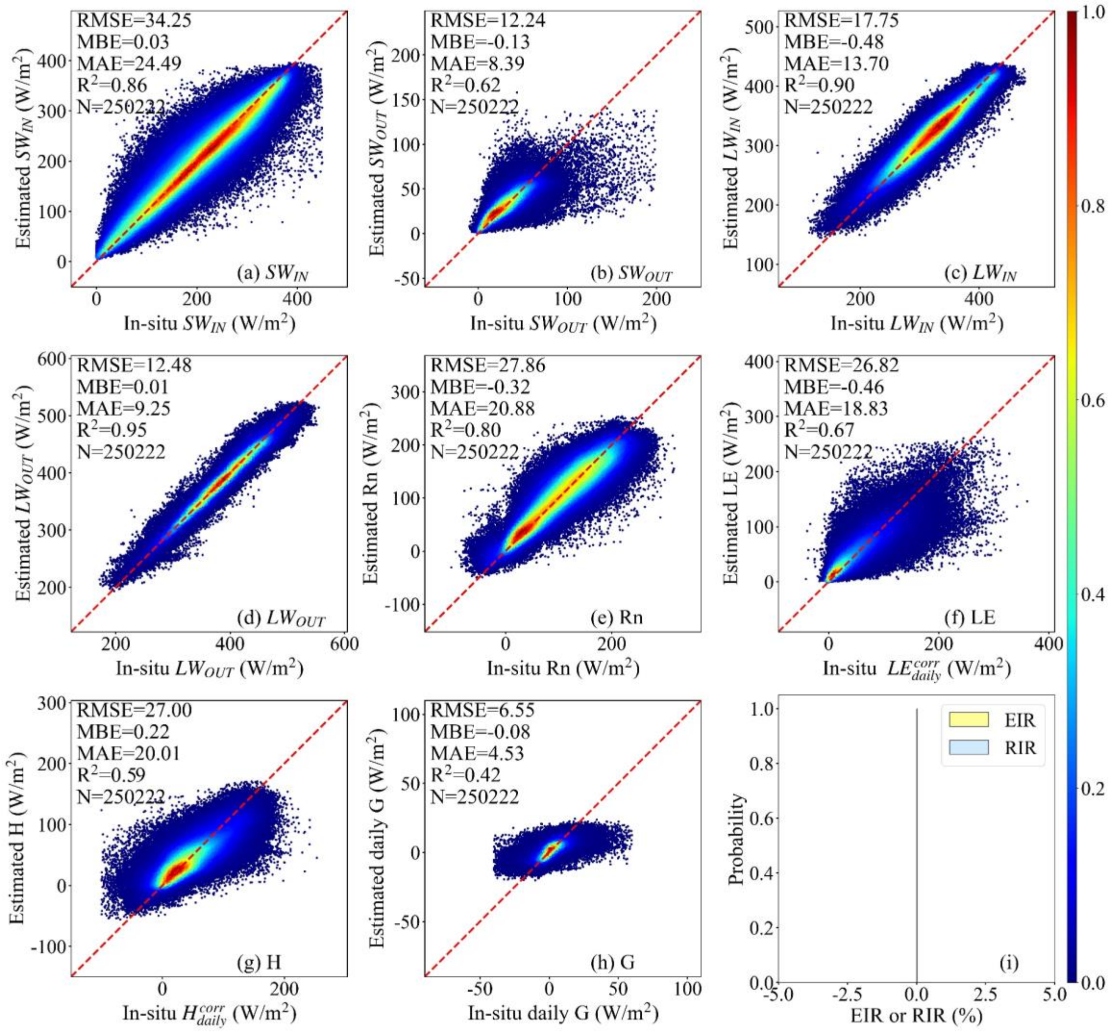

Fig. 3 Scatter density plots of the site-based 10-fold cross-validation of daily downward shortwave and longwave radiation (SW_{IN} and LW_{IN}), upward shortwave and longwave radiation (SW_{OUT} and LW_{OUT}), net radiation (Rn), soil heat flux (G), latent heat flux (LE) and sensible heat flux (H) derived by the CoSEB model against in situ observed SW_{IN}, LW_{IN}, SW_{OUT}, LW_{OUT}, Rn, G, and energy imbalance-corrected LE (LE_{daily}^{corr}) and H (H_{daily}^{corr}). The EIR and RIR in the subfigure (i) represent the energy imbalance ratio and radiation imbalance ratio, which are defined as 100% × (Rn - G - LE - H)/Rn ~~$100\%\times(Rn-G-LE-H)/Rn$~~ and 100% × ($SW_{IN}$ − SW_{OUT} + LW_{IN} - LW_{OUT})/Rn ~~$100\%\times(SW_{IN}+LW_{IN}-SW_{OUT}-LW_{OUT}-Rn)/Rn$~~, respectively. The colorbar represents the normalized density of data points.

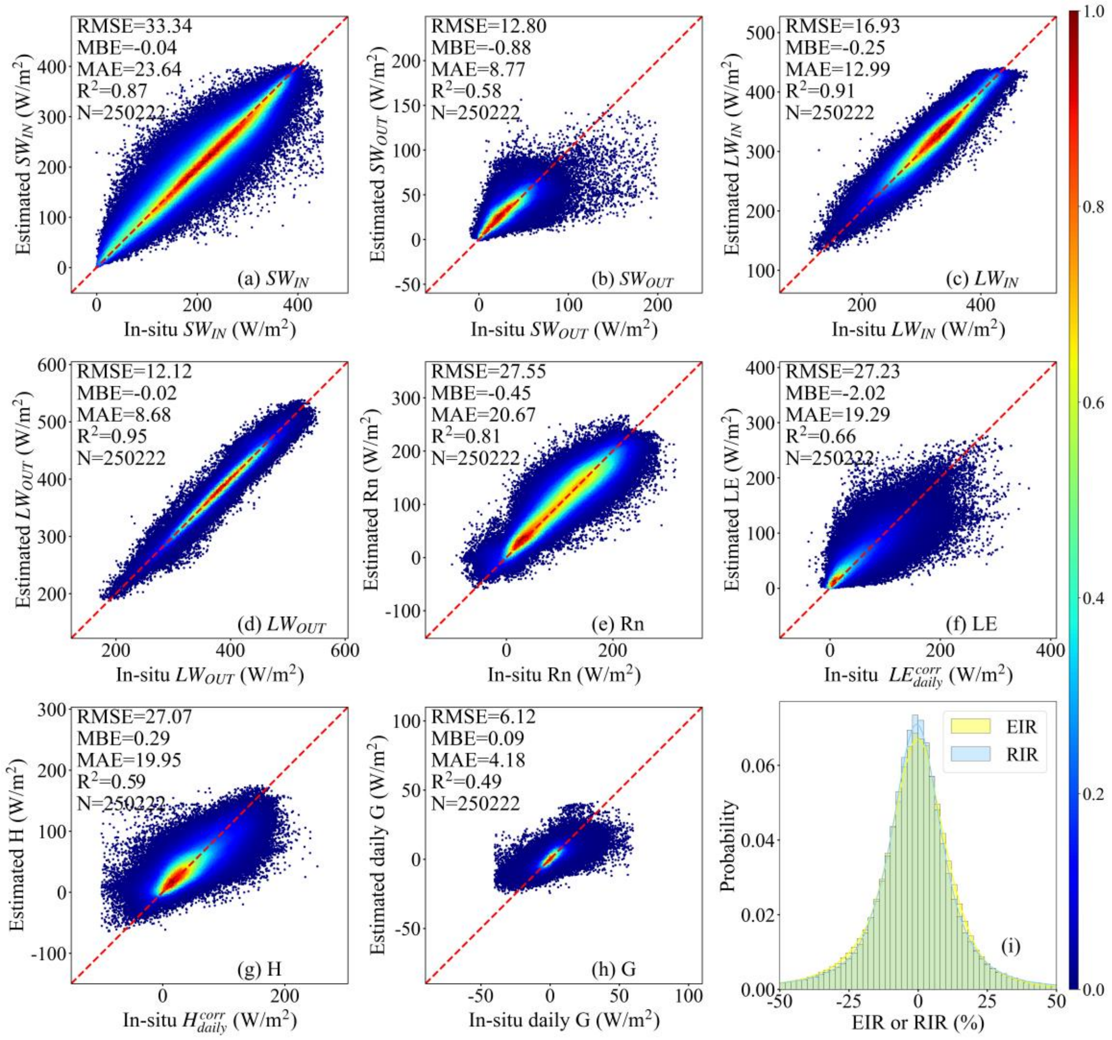

Fig. 4 Same as Fig. 3, but for estimates from RF-based uncoordinated models.

4.1.2 Validation at nine radiation sites from SURFRAD

To further illustrate the generality and transferability of the renewed CoSEB model, the validation of estimates of the five radiation components (including SW_{IN}, SW_{OUT}, LW_{IN}, LW_{OUT}, Rn) derived from both the CoSEB model and RF-based uncoordinated models against observations at nine radiation sites from SURFRAD was performed, as shown in Fig. 5. The results showed that both the CoSEB model and the RF-based models achieved high accuracy in estimating daily SW_{IN}, SW_{OUT}, LW_{IN}, LW_{OUT} and Rn, with the RMSE of ~30 W/m^2 for SW_{IN}, ~14 W/m^2 for SW_{OUT} and LW_{IN}, ~12 W/m^2 for LW_{OUT} and ~24 W/m^2 for Rn, with the R^2 >0.9 for SW_{IN}, LW_{IN} and LW_{OUT}, ~0.65 for SW_{OUT} and ~0.85 for Rn. Compared to the results of the site-based 10-fold cross-validation at 258 EC sites, the performances at nine radiation sites showed slight improvements, with the RMSE decreasing by 0.74 to 4.54 W/m^2 for SW_{IN}, LW_{IN}, LW_{OUT} and Rn in the CoSEB model, but a slight degradation with the RMSE increasing by ~1.05 W/m^2 for SW_{OUT}, suggesting the robust performance of the CoSEB model. Furthermore, the CoSEB model demonstrated a large superiority in maintaining surface radiation balance among the five radiation components, with the RIR of 0, in contrast to the RF-based models, which failed to meet this balance, exhibiting significant RIR exceeding 50%.

4.2 Validation and inter-comparisons of the CoSEB-based datasets

As demonstrated in Section 4.1, the renewed CoSEB model with a spatial scale of 500 m achieved comparable accuracies to the RF-based uncoordinated models but outperformed them in balancing surface radiation and heat fluxes. Evidenced by the validation for its superiority, the renewed CoSEB model was then applied to the spatially aggregated input datasets to generate our developed global daily datasets with a spatial resolution of 0.05°. To further assess the performance of the developed CoSEB-based datasets, in situ observations from another 44 spatially independent test sites (see Section 2.1), which were not involved in model construction and datasets generation, were used for validation. Mainstream products (i.e. GLASS, BESS-Rad, BESSV2.0, FLUXCOM, PML_V2, MOD16A2 and ETMonitor) were also involved for inter-comparison at the 44 test sites.

Note that due to the lack of moderate-resolution global RS-based products/datasets of daily and/or 8-day SW_{OUT}, H and G, the intercomparison between different products/datasets was impossible. Instead, we conducted a validation of these components from the CoSEB-based datasets against in situ observations at 44 test sites, as shown in Figs S2 and S3 in the Supplementary Material. Results indicated that the CoSEB-based datasets could provide good estimates of SW_{OUT}, H and G, with the RMSEs (R^2) of 14.20 W/m^2 (0.42), 29.75 W/m^2 (0.44) and 5.69 W/m^2 (0.44) at daily scale, respectively, and the RMSE (R^2) of 12.19 W/m^2 (0.39) and 4.60 W/m^2 (0.47) for 8-day SW_{OUT} and G, respectively.

412

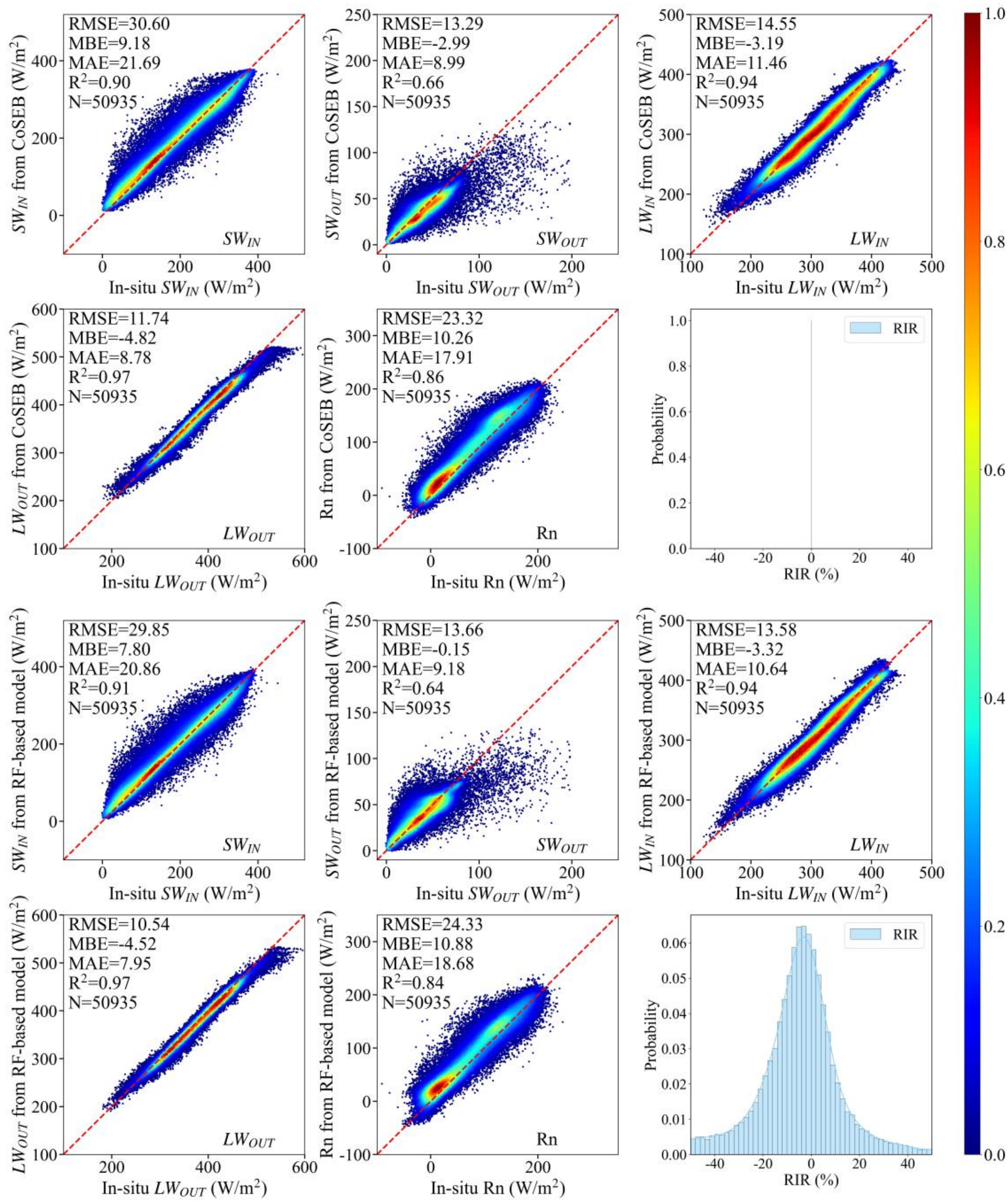

Fig. 5 Scatter density plots of the validation of daily downward shortwave and longwave radiation (SW_{IN} and LW_{IN}), upward shortwave and longwave radiation (SW_{OUT} and LW_{OUT}) and net radiation (Rn) from the renewed CoSEB model (upper two rows) and RF-based uncoordinated models (lower two rows) ~~-based datasets~~ against in situ observations at nine radiation sites from SURFRAD. The RIR represents the radiation imbalance ratio, defined as $100\% \times (SW_{IN} - SW_{OUT} + LW_{IN} - LW_{OUT})/Rn$ ~~$100\% \times (SW_{IN} + LW_{IN} - SW_{OUT} - LW_{OUT} - Rn)/Rn$~~. The colorbar represents the normalized density of data points.

~~**4.2 Validation and inter-comparisons of the CoSEB-based datasets**~~

~~As demonstrated in Section 4.1, the renewed CoSEB model with a spatial scale of~~

~~500 m achieved comparable accuracies to the RF-based uncoordinated models but outperformed them in balancing surface radiation and heat fluxes. Evidenced by the validation for its superiority, the renewed CoSEB model was then applied to the spatially aggregated input datasets to generate our developed global daily datasets with a spatial resolution of 0.05°. To further assess the performance of the developed datasets, in situ observations at 134 sites out of the 258 EC sites were further used to test the performance of the CoSEB-based datasets, where the 134 sites were selected based on the commonly applied criterion (Salazar-Martínez et al., 2022; Tang et al., 2024a) that the fraction of the dominant land cover types (from the 500 m MCD12Q1 product) exceeded 80% within the 0.05° grid, ensuring surface homogeneity and spatial representativeness of the observations. Mainstream products (i.e. GLASS, BESS-Rad, BESSV2.0, FLUXCOM, PML_V2, MOD16A2 and ETMonitor) were also involved for inter-comparison at the 134 EC sites.~~

~~Note that due to the lack of moderate-resolution global RS-based products/datasets of daily and/or 8-day SW_{OUT}, H and G, the intercomparison between different products/datasets was impossible. Instead, we conducted a validation of these components from the CoSEB-based datasets against in situ observations at 134 EC sites, as shown in Figs S3 and S4 in the Supplementary Material. Results indicated that the CoSEB-based datasets could provide good estimates of SW_{OUT}, H and G, with the RMSE of 10.39 W/m^2, 22.67 W/m^2 and 6.77 W/m^2 at daily scale, respectively, and the RMSE of 7.08 W/m^2 and 4.25 W/m^2 for 8-day SW_{OUT} and G, respectively.~~

Fig. 6 and Fig. 7 present the comparison of daily SW_{IN}, LW_{IN} and LW_{OUT}, as well as Rn and LE from the CoSEB-based datasets and mainstream products/datasets (including GLASS, BESS-Rad, BESSV2.0 and ETMonitor), with in situ observations at ~~134~~ 44 ~~EC~~ test sites, respectively. Overall, the estimates from the CoSEB-based datasets exhibited a closer agreement with in situ observations than those from mainstream products/datasets, where the CoSEB-based datasets reduced the RMSE by ~~4.35~~0.01 W/m^2 to ~~11.46~~4.58 W/m^2 and increased the R² by 0.~~04~~01 to 0.~~3~~09 compared to mainstream products. Specifically, the RMSE for the SW_{IN}, LW_{IN}, LW_{OUT} increased from ~~28.51~~37.52 W/m^2, ~~14.29~~22.47 W/m^2 and ~~10.62~~13.78 W/m^2 in the CoSEB-based datasets to 3~~5.44~~7.53 W/m^2 ,~~18.64~~23.37 W/m^2 and ~~15.29~~16.46 W/m^2 in the GLASS, respectively, and for SW_{IN} from ~~28.51~~37.52 W/m^2 in the CoSEB-based datasets to ~~36.23~~40.87 W/m^2 in the BESS-Rad. Likewise, the RMSEs for daily Rn and LE were 2~~2.40~~9.66 W/m^2 and ~~24.38~~30.87 W/m^2 in the CoSEB-based datasets, which were lower than those of ~~29.80~~34.24 W/m^2 and 3~~5.75~~4.36 W/m^2 in BESSV2.0, respectively, as well as those of ~~27.11~~30.60 W/m^2 for Rn in GLASS and 3~~5.84~~3.62 W/m^2 for LE in ETMonitor.

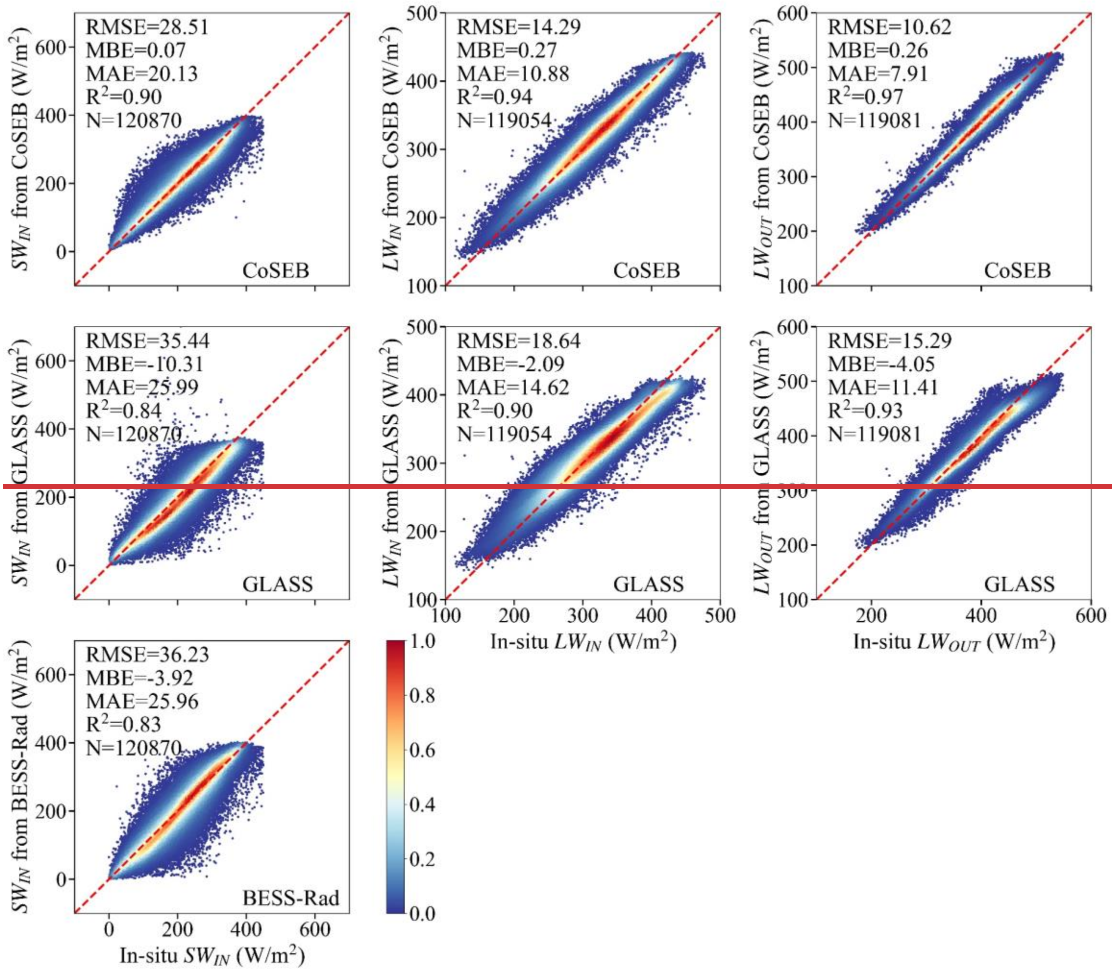

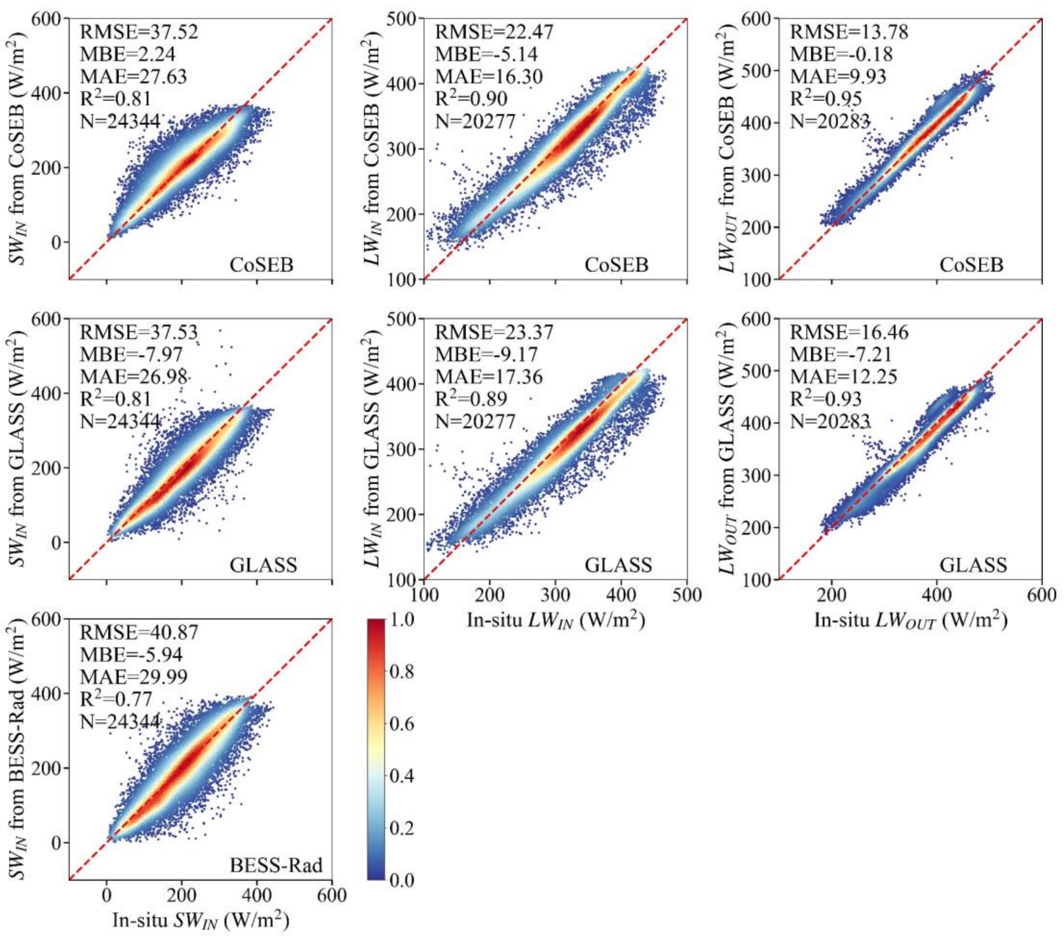

Fig. 6 Comparison of the daily downward shortwave radiation (*SW_{IN}*, the first column), downward longwave radiation (*LW_{IN}*, the second column) and upward longwave radiation (*LW_{OUT}*, the third column) from the CoSEB-based datasets, GLASS and BESS-Rad with the in situ observed *SW_{IN}*, *LW_{IN}* and *LW_{OUT}* at ~~134~~ 44 ~~eddy covariance~~test sites. The colorbar represents the normalized density of data points.

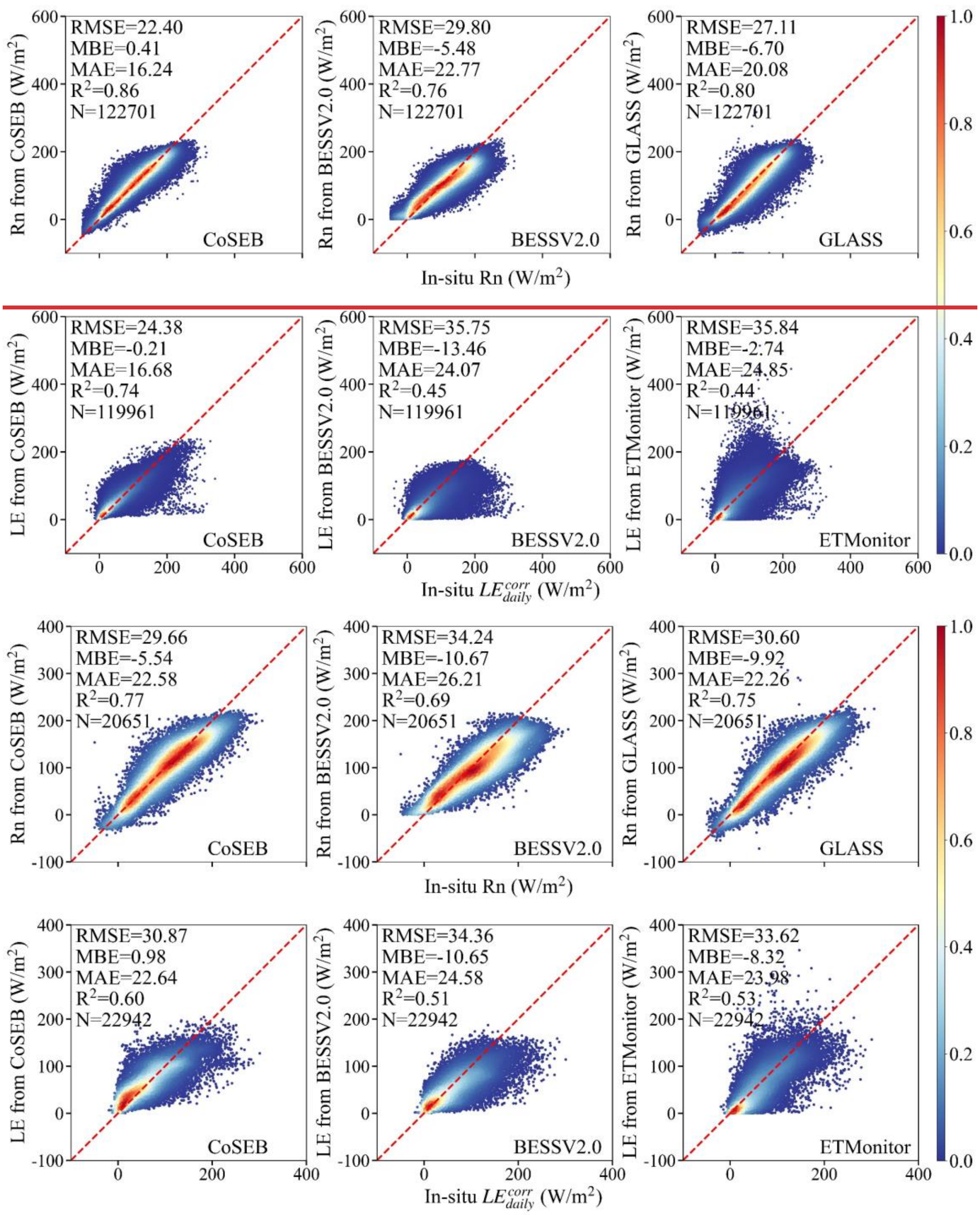

Fig. 7 Comparison of the daily net radiation (Rn, the upper row) and latent heat flux (LE, the lower row) from the CoSEB-based datasets, BESSV2.0, GLASS and ETMonitor with the in situ observed Rn, and energy imbalance-corrected LE (LE_{daily}^{corr}) at ~~134~~ 44 ~~eddy covariance~~test sites. The colorbar represents the normalized density of data points.

Figs. 8, 9 and 10 compare the 8-day SW_{IN}, LW_{IN} and LW_{OUT}, Rn and LE, as well as H from the CoSEB-based datasets and mainstream products, with in situ observations at 44 test~~134 EC~~ sites, respectively. Overall, the CoSEB-based datasets outperformed the mainstream products/datasets for all surface radiation and heat fluxes, where the CoSEB-based datasets reduced the RMSE by ~~4.62~~0.24 W/m^2 to 1~~4.64~~0.48 W/m^2 and increased the R^2 by 0.~~04~~ 01 to 0.~~41~~ 38 compared to mainstream products. Specifically, for SW_{IN}, LW_{IN} and LW_{OUT}, the RMSE increased from 1~~2.81~~8.54 W/m^2, ~~9.22~~18.50 W/m^2 and ~~8.34~~9.41 W/m^2 in the CoSEB-based datasets to 21.~~23~~ 35 W/m^2, ~~15.37~~20.39 W/m^2 and 14.~~70~~ 48 W/m^2 in the GLASS, respectively, and for SW_{IN} from ~~12.81~~18.54 W/m^2 in the CoSEB-based datasets to ~~17.43~~18.78 W/m^2 in the BESS-Rad. For Rn, the RMSE increased from 1~~3.38~~9.12 W/m^2 in the CoSEB-based datasets to ~23 W/m^2 in the FLUXCOM and GLASS and to >27 W/m^2 in the BESSV2.0~~18.64 W/m² in the GLASS and to >23 W/m² in the FLUXCOM and BESSV2.0~~, while the R^2 decreased from 0.~~91~~ 82 in the CoSEB-based datasets to 0.75 in the FLUXCOM and GLASS and to 0.~~82~~ 62 in the ~~GLASS~~ BESSV2.0~~and to <0.72 in the FLUXCOM and BESSV2.0~~. Likewise, for LE, the RMSE increased from ~~19.99~~22.31 W/m^2 in the CoSEB-based datasets to ~~~26.16~~25 W/m^2 in the FLUXCOM, PML_V2, BESSV2.0 and ETMonitor, and to >~~28.17~~32 W/m^2 in ~~BESSV2.0,~~ MOD16A2~~, PML_V2 and ETMonitor~~, while the R^2 decreased from 0.~~8~~ 67 in the CoSEB-based datasets to ~0.~~65~~ 60 in the FLUXCOM, PML_V2, BESSV2.0 and ETMonitor~~FLUXCOM~~, and to <0.~~6~~ 3 in the ~~remaining products~~MOD16A1. For H, the RMSE increased from ~~17.44~~21.63 W/m^2 in the CoSEB-based datasets to 2~~3.96~~2.64 W/m^2 in the FLUXCOM.

The differences between the estimates from the CoSEB-based datasets and mainstream datasets are likely multifactorial, arising from the simplification and parameterization uncertainties in physics-based models, as well as the lack of physical constraints, limited training samples, and incomplete consideration of influencing factors in other machine-learning-based models.

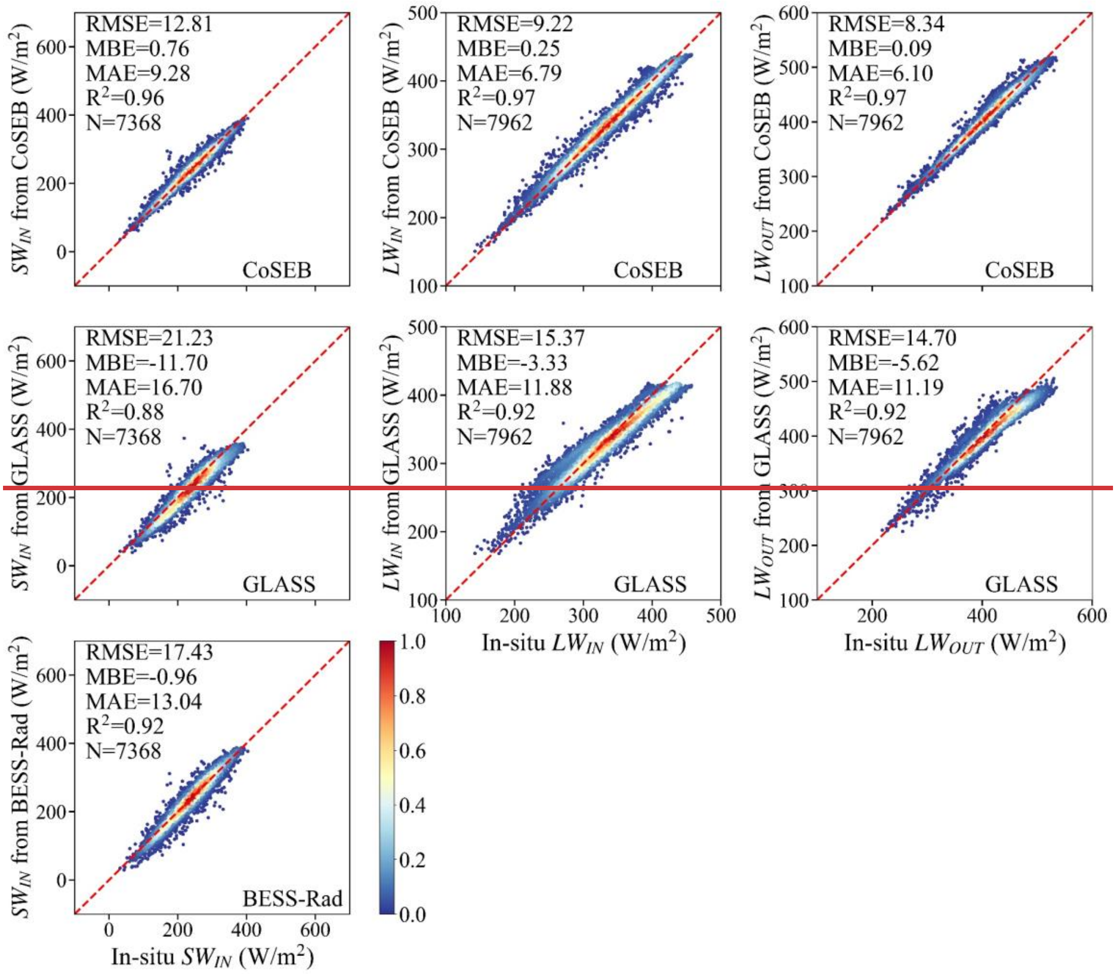
RMSE=12.81
MBE=0.76
MAE=9.28
R2=0.96
N=7368
SWIN from CoSEB (W/m2)
CoSEB
RMSE=9.22
MBE=0.25
MAE=6.79
R2=0.97
N=7962
LWIN from CoSEB (W/m2)
CoSEB
RMSE=8.34
MBE=0.09
MAE=6.10
R2=0.97
N=7962
LWOUT from CoSEB (W/m2)
CoSEB
RMSE=21.23
MBE=-11.70
MAE=16.70
R2=0.88
N=7368
SWIN from GLASS (W/m2)
GLASS
RMSE=15.37
MBE=-3.33
MAE=11.88
R2=0.92
N=7962
LWIN from GLASS (W/m2)
GLASS
In-situ LWIN (W/m2)
RMSE=14.70
MBE=-5.62
MAE=11.19
R2=0.92
N=7962
LWOUT from GLASS (W/m2)
GLASS
In-situ LWOUT (W/m2)
RMSE=17.43
MBE=-0.96
MAE=13.04
R2=0.92
N=7368
SWIN from BESS-Rad (W/m2)
BESS-Rad
In-situ SWIN (W/m2)

501

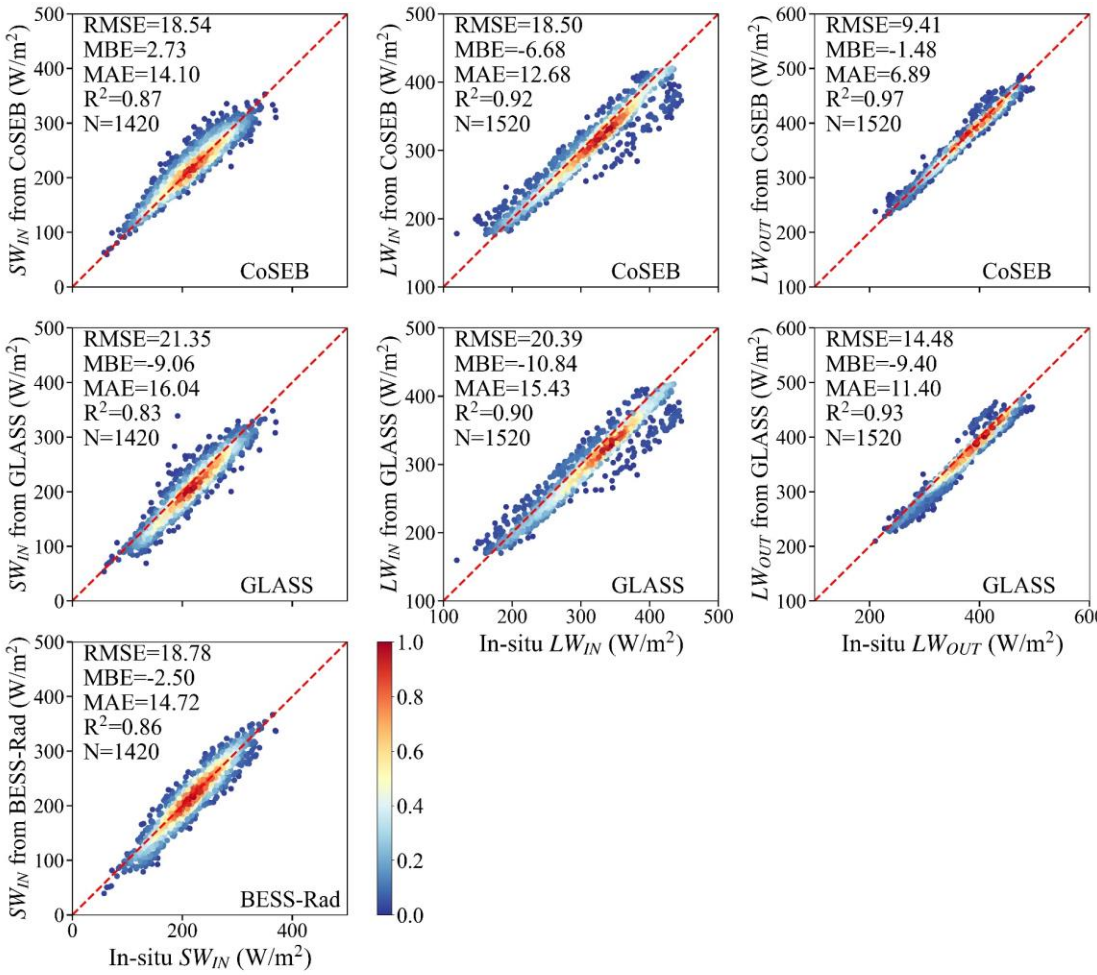

502

503 **Fig. 8 Same as Fig. 6, but for the comparison at 8-day scale.**

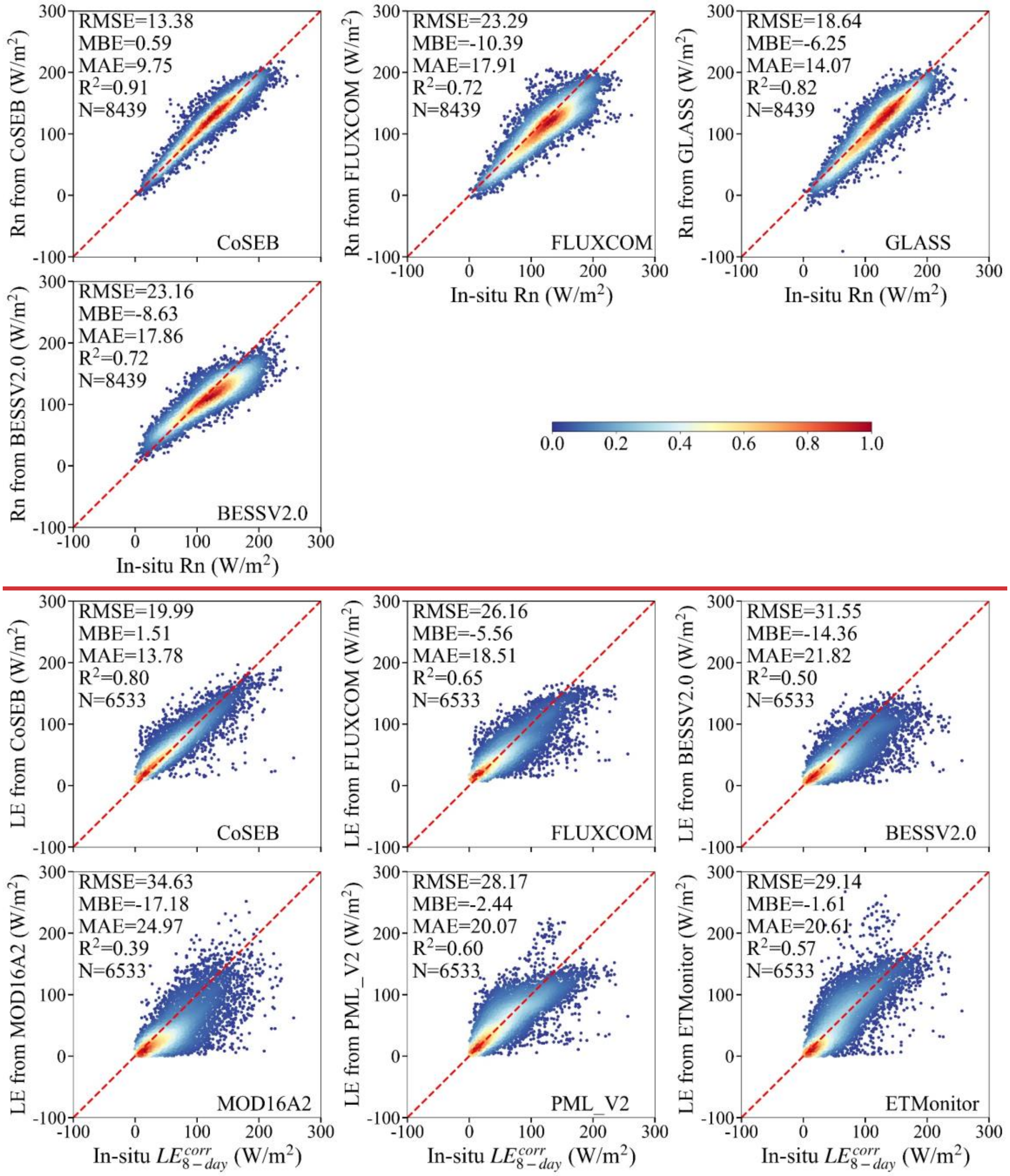
RMSE=13.38
MBE=0.59
MAE=9.75
R2=0.91
N=8439
CoSEB
Rn from CoSEB (W/m2)
RMSE=23.29
MBE=-10.39
MAE=17.91
R2=0.72
N=8439
FLUXCOM
Rn from FLUXCOM (W/m2)
RMSE=18.64
MBE=-6.25
MAE=14.07
R2=0.82
N=8439
GLASS
Rn from GLASS (W/m2)
RMSE=23.16
MBE=-8.63
MAE=17.86
R2=0.72
N=8439
BESSV2.0
Rn from BESSV2.0 (W/m2)
In-situ Rn (W/m2)
0.0 0.2 0.4 0.6 0.8 1.0
RMSE=19.99
MBE=1.51
MAE=13.78
R2=0.80
N=6533
CoSEB
LE from CoSEB (W/m2)
RMSE=26.16
MBE=-5.56
MAE=18.51
R2=0.65
N=6533
FLUXCOM
LE from FLUXCOM (W/m2)
RMSE=31.55
MBE=-14.36
MAE=21.82
R2=0.50
N=6533
BESSV2.0
LE from BESSV2.0 (W/m2)
RMSE=34.63
MBE=-17.18
MAE=24.97
R2=0.39
N=6533
MOD16A2
LE from MOD16A2 (W/m2)
RMSE=28.17
MBE=-2.44
MAE=20.07
R2=0.60
N=6533
PML_V2
LE from PML_V2 (W/m2)
RMSE=29.14
MBE=-1.61
MAE=20.61
R2=0.57
N=6533
ETMonitor
LE from ETMonitor (W/m2)
In-situ LE corr 8-day (W/m2)

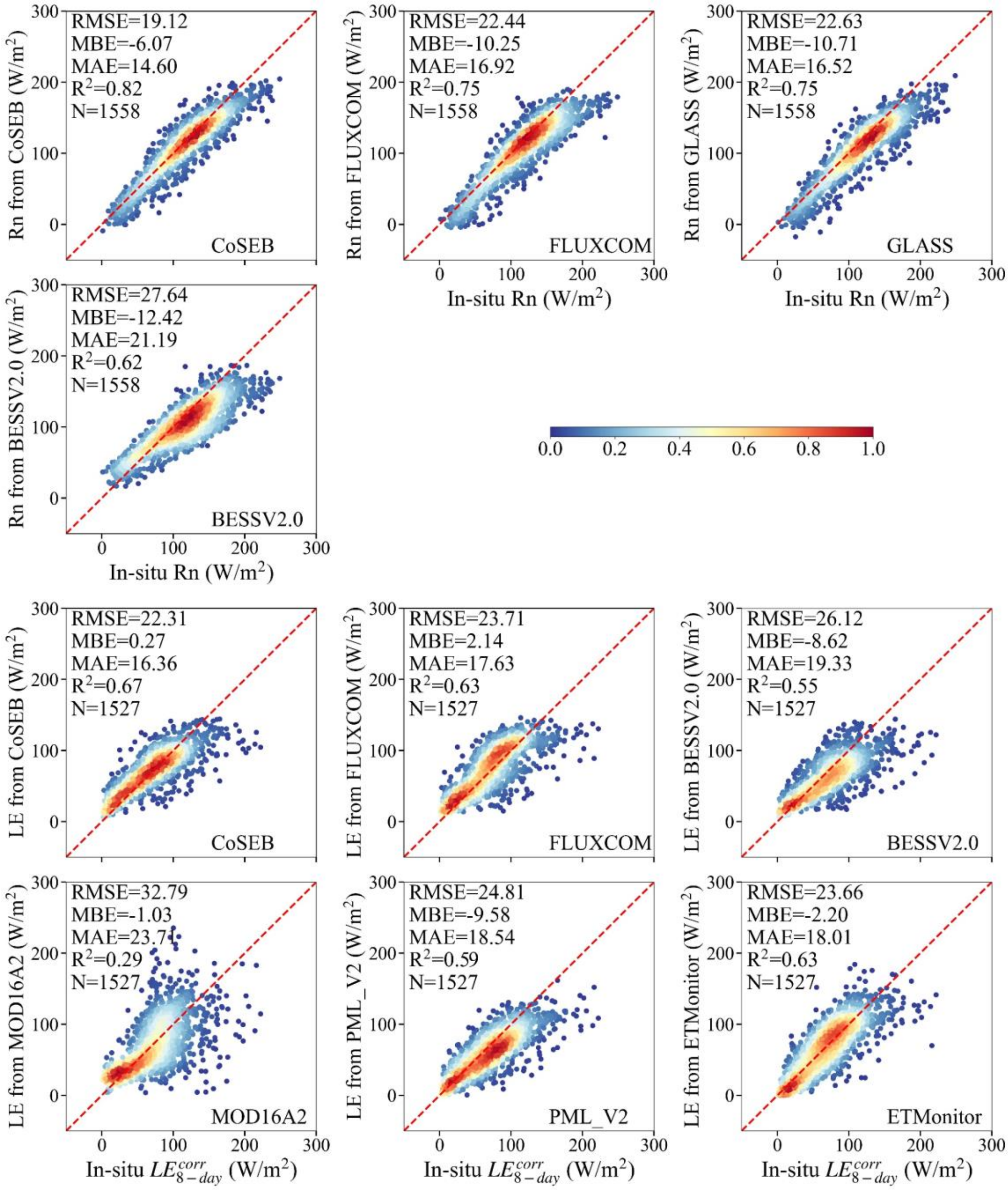

Fig. 9 Comparison of the 8-day net radiation (Rn, the upper two rows) and latent heat flux (LE, the lower three rows) from the CoSEB-based datasets, FLUXCOM, BESSV2.0, GLASS, MOD16A2, PML_V2 and ETMonitor with in situ observed Rn, and energy imbalance-corrected LE (LE_{8-day}^{corr}) at ~~134~~ 44 test~~eddy covariance~~ sites. The colorbar represents the normalized density of data points.

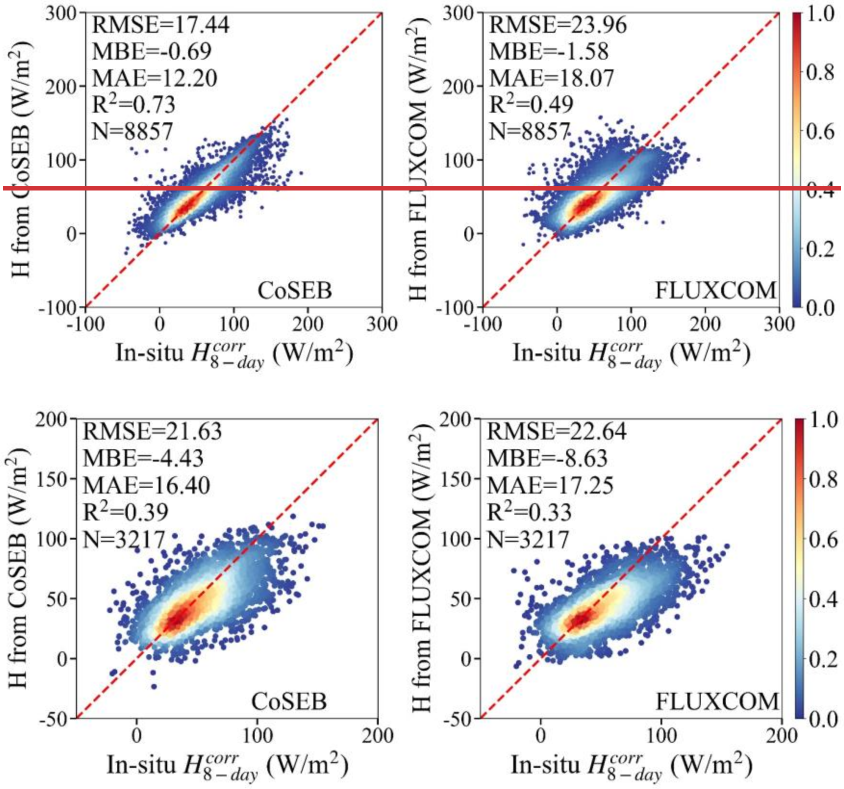

Fig. 10 Comparison of the 8-day sensible heat flux (H) from the CoSEB-based datasets and the FLUXCOM with the in situ energy imbalance-corrected H (H_{8-day}^{corr}) at ~~134~~ 44 ~~eddy covariance~~test sites. The colorbar represents the normalized density of data points.

4.3 Spatial-temporal patterns of global land surface radiation and heat fluxes

In addition to the validation and inter-comparison of the CoSEB-based datasets at the ~~global~~ site scale~~s~~, we further inter-compared the estimates of land surface radiation and heat fluxes from the CoSEB-based datasets and the mainstream products/datasets, in terms of their global spatial and temporal patterns.

Figs. 11, 12 and 13 show the spatial distributions (excluding Greenland, Antarctic continent, deserts, water bodies and permanent snow) and latitudinal profiles of the global 0.05° mean annual SW_{IN}, LW_{IN} and LW_{OUT}, Rn and LE, as well as H from 2001 to 2018, respectively, as derived from the CoSEB-based datasets and mainstream products/datasets [i.e. GLASS, BESS-Rad, BESSV2.0, FLUXCOM, MOD16A2, PML_V2 and ETMonitor, resampled to 0.05° using arithmetic averaging method or cubic convolutional method if necessary]. Overall, the spatial patterns of the estimates from the CoSEB-based datasets aligned well with those observed in these mainstream products/datasets, though regional discrepancies were present. Specifically, the mean annual LW_{IN}, LW_{OUT}, Rn, and LE generally exhibited decreasing trends from the equator towards higher latitudes, peaking in regions such as the Amazon Rainforest, Congo Rainforest, and the Malay Archipelago. In contrast, the higher mean annual SW_{IN} and H were mainly found in the Tibetan Plateau, southwestern U.S., mid-west Australia, Sahel and Southern Africa, while the lower values were found in high-latitude regions of >50°N. In the region with ~~of~~ high values, the mean annual estimates of SW_{IN} from the CoSEB-based datasets were higher than those from GLASS but lower than those from BESS-Rad, the estimates of LW_{IN} and LW_{OUT} from the CoSEB-based datasets were both higher than those from GLASS, the estimates of Rn from the CoSEB-based datasets were significantly higher than those from BESSV2.0, and comparable to or slightly higher than those from FLUXCOM and GLASS, the estimates of LE from the CoSEB-based datasets were close to those from BESSV2.0 and PML_V2, but slightly lower than those from FLUXCOM, MOD16A2 and ETMonitor. Besides, the estimates of H from the CoSEB-based datasets were higher than those from FLUXCOM in regions with high values, while lower than those from FLUXCOM in regions with low values.

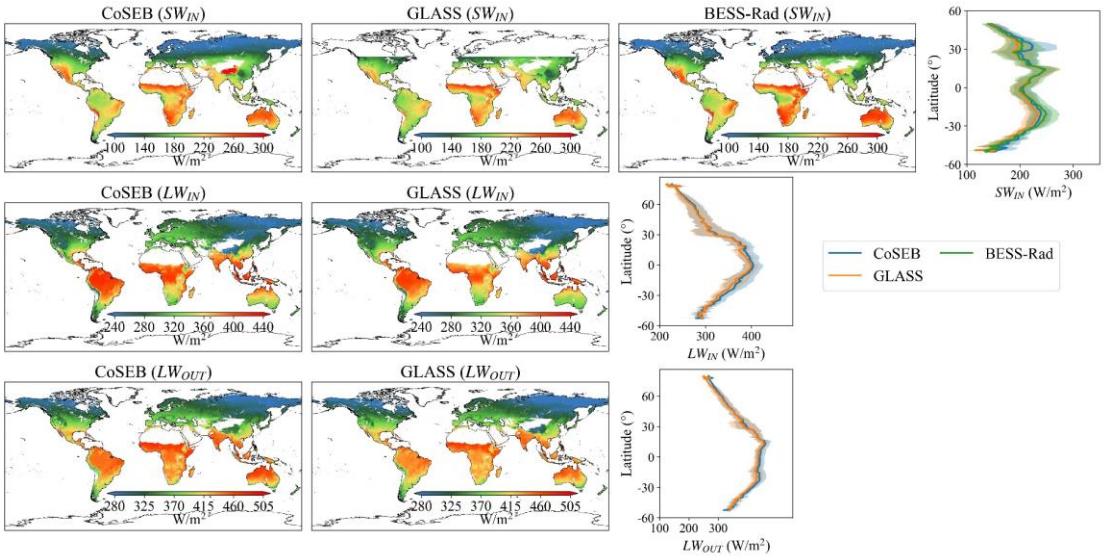

Fig.11 Spatial patterns of global mean annual downward shortwave radiation (SW_{IN}, the first row), downward longwave radiation (LW_{IN}, the second row) and upward longwave radiation (LW_{OUT}, the third row) from 2001 to 2018 by CoSEB-based datasets, GLASS and BESS-Rad. The rightmost subfigure of each row represents the latitudinal profiles of mean annual SW_{IN}, LW_{IN} and LW_{OUT} from CoSEB-based datasets, GLASS and BESS-Rad, where the shaded area represents the variation of standard deviation for each product.

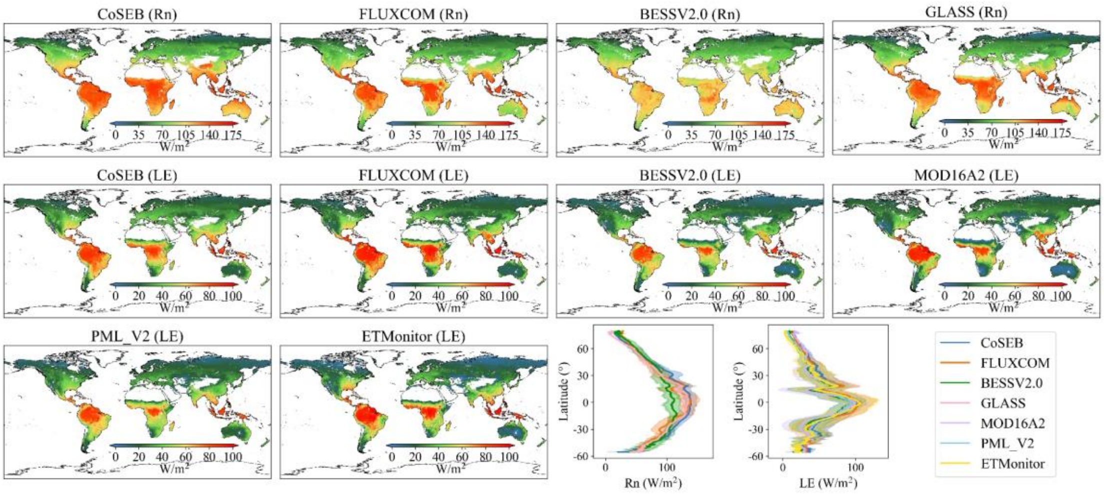

Fig.12 Spatial patterns of global mean annual net radiation (*Rn*, the first row) and latent heat flux (*LE*, the second and third rows) from 2001 to 2018 by CoSEB-based datasets, FLUXCOM, BESSV2.0, MOD16A2, PML_V2, ETMonitor and GLASS. The last two subfigures of the third row represent the latitudinal profiles of mean annual Rn and LE from CoSEB-based datasets and these mainstream products/datasets, where the shaded area represents the variation of standard deviation for each product.

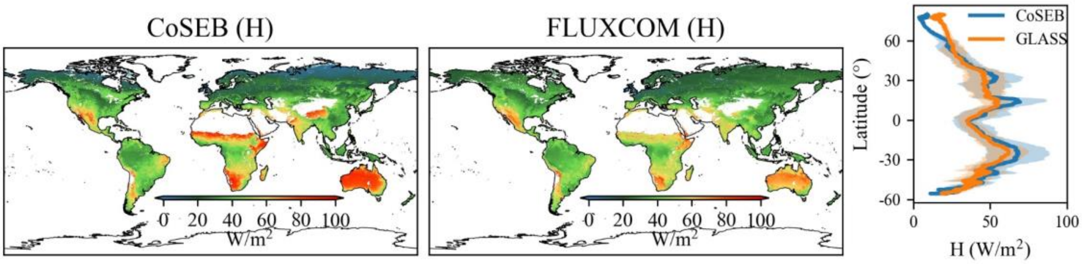

Fig.13 Spatial patterns of global mean annual sensible heat flux (*H*) from 2001 to 2018 by CoSEB-based datasets and FLUXCOM. The rightmost subfigure represents the latitudinal profiles of mean annual H from CoSEB-based datasets and FLUXCOM, where the shaded area represents the variation of standard deviation for each product.

The temporal evolutions of the global (excluding Greenland, Antarctic continent, deserts, water bodies and permanent snow) land surface radiation and heat fluxes derived from the CoSEB-based datasets and mainstream products/datasets from 2001 to 2018 were also investigated, as shown in Fig. 14. The results indicated that the temporal variation of each flux from the CoSEB-based datasets generally agreed well with those from mainstream products/datasets, exhibiting relatively stable trends. The global annual mean estimates using area weighting average by the CoSEB-based datasets from 2001 to 2018 varied between ~185.22 and ~189.50 W/m^2 with the mean of ~187.23 W/m^2 for SW_{IN}, between ~32.67 and ~33.20 W/m^2 with the mean of ~32.96 W/m^2 for SW_{OUT}, between ~330.24 and ~334.14 W/m^2 with the mean of ~331.50 W/m^2 for LW_{IN}, between ~387.25 and ~390.82 W/m^2 with the mean of ~388.81 W/m^2 for LW_{OUT}, between ~95.41 and ~99.39 W/m^2 with the mean of 97.11 W/m^2 for Rn, between ~53.24 and ~56.37 W/m^2 with the mean of ~54.53 W/m^2 for LE, between ~40.44 and ~41.96 W/m^2 with the mean of ~41.29 W/m^2 for H, and between ~1.22 and ~1.52 W/m^2 with the mean of ~1.33 W/m^2 for G. For each radiation or heat flux, the annual mean estimates from the CoSEB-based datasets were overall higher than those from the mainstream products/datasets. In particular, the annual mean Rn estimates from the CoSEB-based datasets were higher than those from FLUXCOM, GLASS and BESSV2.0 sequentially, and the annual mean LE estimates from the CoSEB-based datasets were marginally higher than those from FLUXCOM, but substantially exceeded those from ETMonitor, PML_V2, MOD16A2 and BESSV2.0 sequentially.

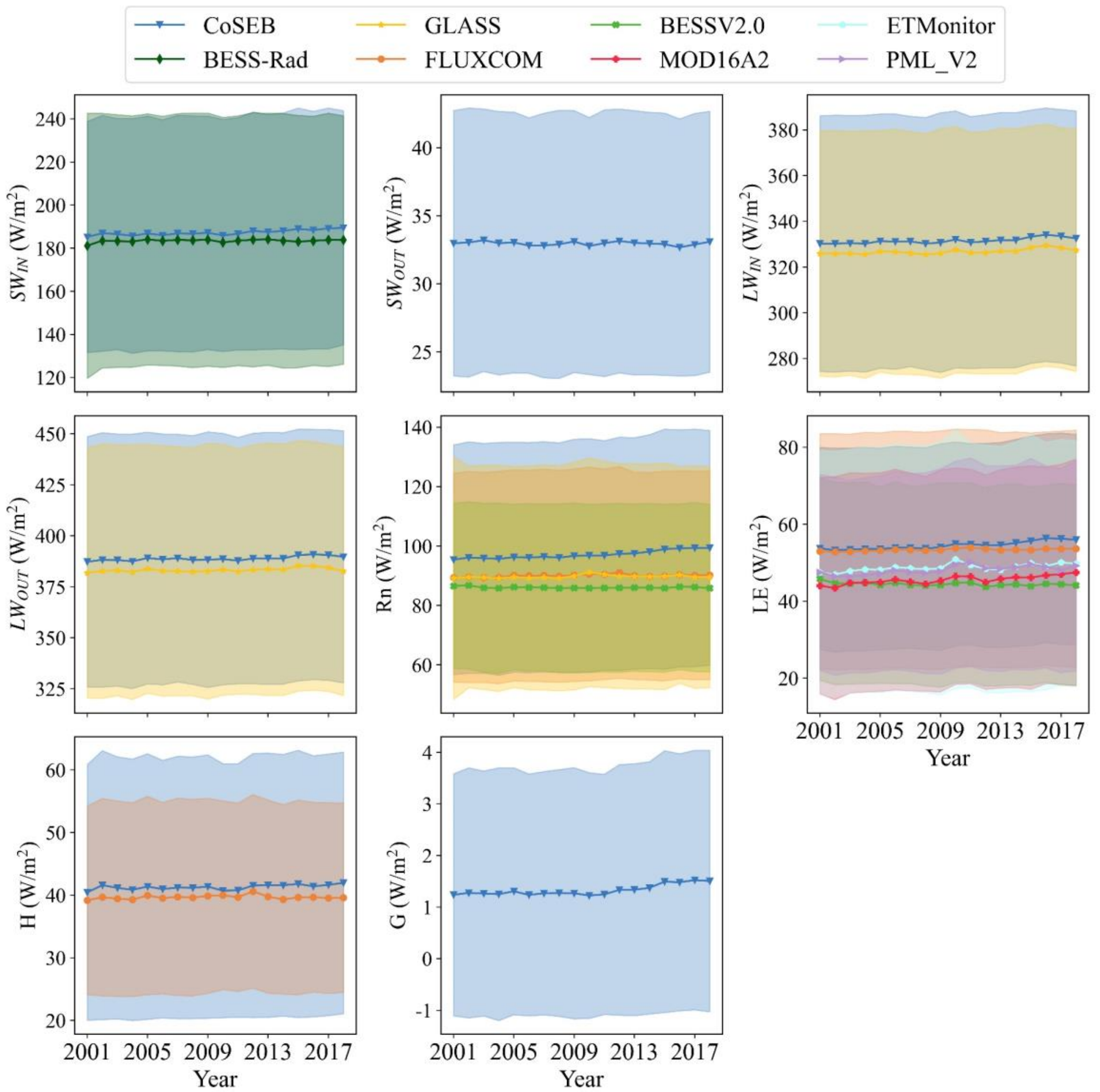

Fig. 14 Temporal variation of annual mean downward shortwave radiation (SW_{IN}), upward shortwave radiation (SW_{OUT}), downward longwave radiation (LW_{IN}), upward longwave radiation (LW_{OUT}), net radiation (Rn), latent heat flux (LE), sensible heat flux (H) and soil heat flux (G) from 2001 to 2018 from the CoSEB-based datasets, BESS-Rad, GLASS, FLUXCOM, BESSV2.0, PML_V2, MOD16A2 and ETMonitor. The shaded area represents the variation of standard deviation for each product.

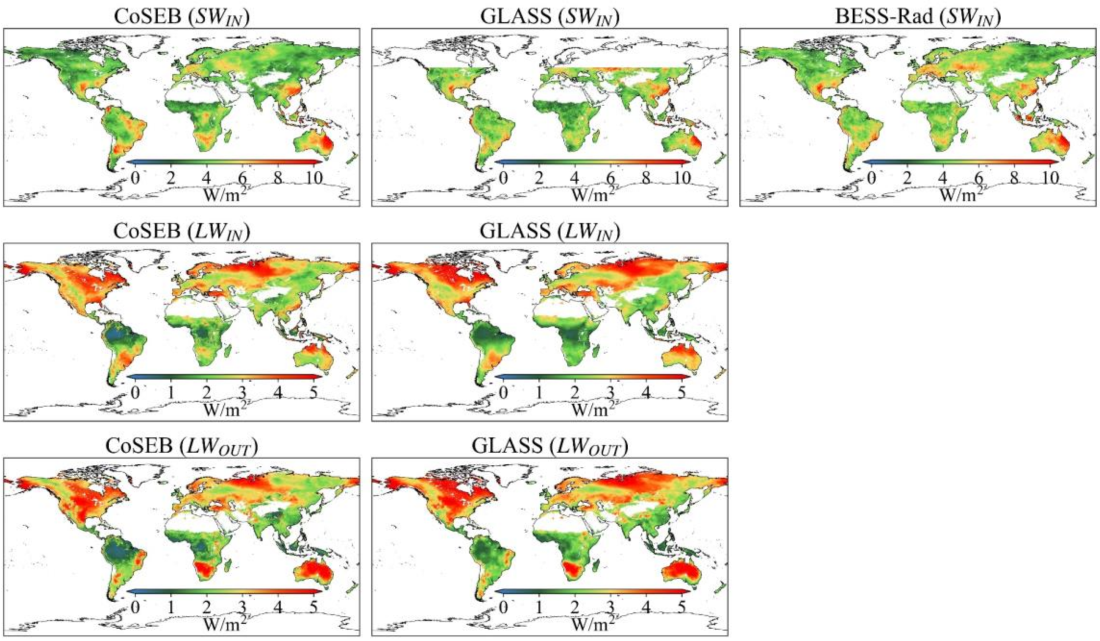

Fig. 15 Spatial distribution of interannual variability (standard deviation) of downward shortwave radiation (*SW_{IN}*, the first row), downward longwave radiation (*LW_{IN}*, the second row) and upward longwave radiation (*LW_{OUT}*, the third row) from 2001 to 2018 by the CoSEB-based datasets, GLASS and BESS-Rad.

Figs. 15, 16 and 17 show the spatial patterns (excluding Greenland, Antarctic continent, deserts, water bodies and permanent snow) of interannual variability of SW_{IN}, LW_{IN} and LW_{OUT}, Rn and LE, as well as H from 2001 to 2018, respectively, derived from the CoSEB-based datasets and mainstream products/datasets. In general, the estimates from the CoSEB-based datasets displayed similar interannual variability in space with those from the mainstream products/datasets. Specially, the estimates of SW_{IN} from the CoSEB-based datasets, BESS-Rad, and GLASS exhibited a significant interannual variability mainly in northeastern Australia, eastern South America, Southeast China, and Southwest North America. The interannual variability of LW_{IN} and LW_{OUT} by the CoSEB-based datasets and GLASS displayed high values primarily at middle-to-high latitudes of the Northern Hemisphere and parts of Africa and Australia. The interannual variability of Rn observed by the CoSEB-based datasets was generally lower than that of GLASS, but higher than that of BESSV2.0 and FLUXCOM. The CoSEB-based datasets missed the strong interannual variability of LE as observed in MOD16A2, PML_V2 and ETMonitor in parts of Africa, Australia and eastern South

America. Furthermore, FLUXCOM exhibited the weakest interannual variability of LE in almost all regions. The interannual variability of H derived from the CoSEB-based datasets was higher than ~~those~~ that from FLUXCOM, with stronger interannual variabilities mainly observed in parts of eastern South America, southern Africa, and northeastern Australia.

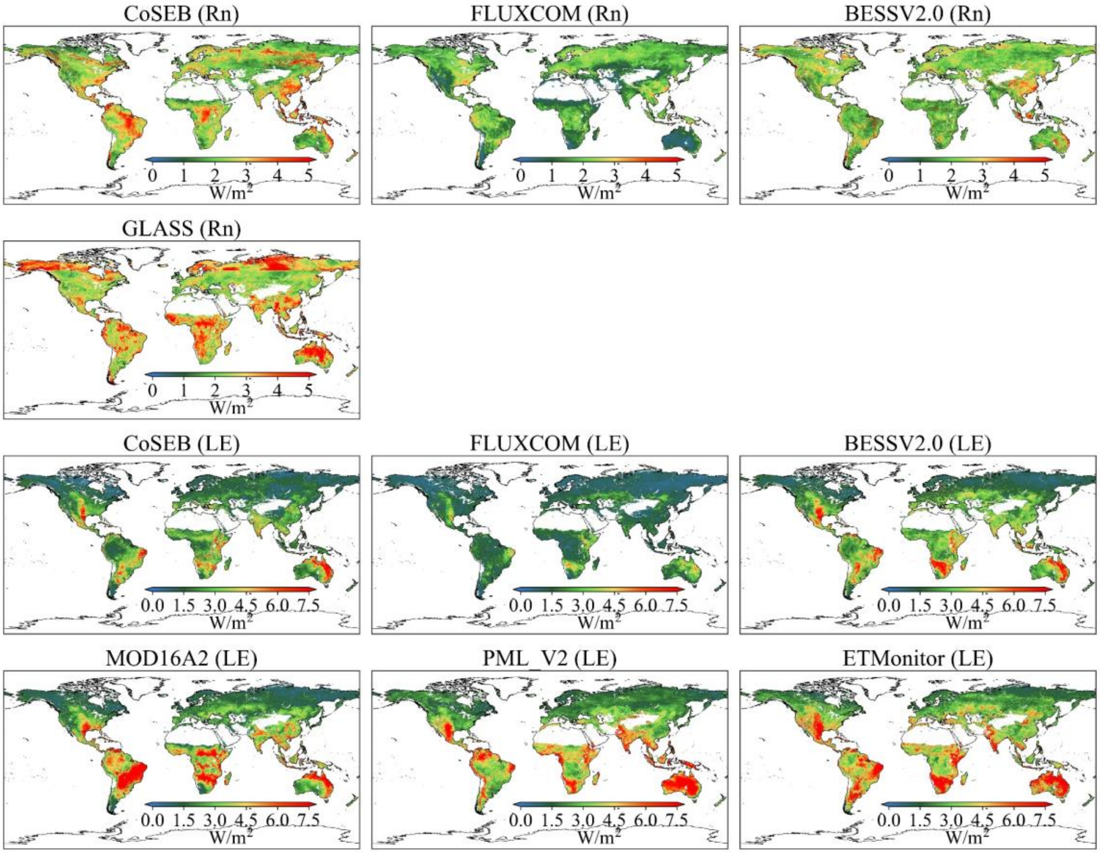

Fig. 16 Spatial distribution of interannual variability (standard deviation) of net radiation (Rn, the first and second rows) and latent heat flux (LE, the third and fourth row) from 2001 to 2018 by the CoSEB-based datasets, FLUXCOM, BESSV2.0, MOD16A2, PML_V2, ETMonitor and GLASS.

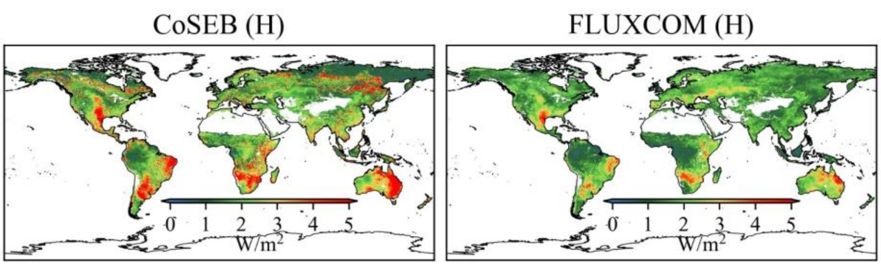

Fig. 17 Spatial distribution of interannual variability (standard deviation) of sensible heat flux (H) from 2001 to 2018 by the CoSEB-based datasets and FLUXCOM.

5 Discussion

Accurately monitoring the spatial and temporal variations of global land surface radiation and heat fluxes is crucial for quantifying the exchange of radiation, heat and water between the land and atmosphere under global climate change (Chen et al., 2020; Du et al., 2024; Kim et al., 2023; Liang et al., 2006; Wang et al., 2020). However, although numerous global RS-based products/datasets of land surface radiation and heat fluxes have been developed using physical and/or statistical methods, they typically provide either merely a single flux or multiple fluxes (see Table 1) that are estimated separately from uncoordinated models (Huang et al., 2024; Jung et al., 2019; Sun et al., 2023; Tang et al., 2019), leading to noticeable radiation imbalance and/or heat imbalance when these products are combined for practical applications. To address these limitations, we generated high-accuracy global datasets of land surface radiation and heat fluxes from 2000 to 2020 that adhere to both radiation and heat conservation laws, using our proposed CoSEB model (Wang et al., 2025).

Our CoSEB model, integrating underlying physical principles of training datasets into machine learning technique to effectively learn the interrelations among multiple targeted outputs, was originally designed for coordinating estimates of global land surface energy balance components (Rn, LE, H and G) to satisfy the energy conservation (Wang et al., 2025). Inspired by the idea of constructing the original CoSEB model, we further incorporated land surface radiation fluxes into our model to simultaneously consider the physical constraints of both surface radiation and heat conservation principles, by renewing the CoSEB using multiple remote sensing ~~products~~and~~,~~ reanalysis datasets, as well as in-situ observations of SW_{IN}, SW_{OUT}, LW_{IN}, LW_{OUT}, Rn, LE, H and G. In selecting the 19 input variables to accommodate the additional target variables, prior knowledge derived from previous studies was employed to identify factors that exert significant influence on surface radiation and heat flux while maintaining relative inter-independence as much as possible (Jung et al., 2019; Mohan et al., 2020; Wang et al., 2021; Xian et al., 2024). This practice is commonly adopted in data-driven models for estimating land surface water, energy, and carbon fluxes (Bai et al., 2024; Elghawi et al., 2023; Han et al., 2023; O. & Orth, 2021). The importance scores of the 19 different feature variables are exhibited in Table S4 in the Supplementary Material, and downward solar radiation, the primary source of the energy at the earth surface, is the most important input variable, consistent with the results from our previous study (Wang et al., 2025). Although some of the selected variables may exhibit a certain degree of multi-collinearity, each contributes unique and physically meaningful information, supporting the inclusion of all variables in model construction. ~~To comprehensively account for the main factors influencing surface radiation and heat fluxes (Mohan et al., 2020; Wang et al., 2021; Xian et al., 2024)~~[JW1]~~, the renewed CoSEB model utilized 19 easily accessible parameters/variables from ERA5-Land reanalysis datasets, GLASS products, MODIS products, GMTED2010 and NOAA/GML as input, which were readily available to generate datasets of global land surface radiation and heat fluxes in a practical and operational manner.(Wang et al., 2025)~~Note that the variable importance, derived from the built-in method of the random forests and potentially affected by multicollinearity among the input variables, is presented only as a reference. Retaining all 19 feature variables ensures the model's flexibility and generalization capability, enabling future incorporation of additional representative ground-based observations for further training and improvement. Besides, to investigate the impact of lagged effects of input variables on model performance, experiments were also conducted by adding lagged variables (e.g., the air temperature of the previous day) to the 19 input features. The results (Fig. S4 in the Supplementary Material) showed almost no improvement in model accuracy, suggesting that lagged effects on model performance were negligible within the CoSEB framework for estimates of daily surface radiation and heat fluxes. Furthermore, to better illustrate the effect of including additional radiation components (SW_{IN}, SW_{OUT}, LW_{IN} and LW_{OUT}) in the renewed CoSEB model compared with the original version by Wang et al. (2025), we have tested the performance of a reconstructed model that estimated only Rn, LE, H and G using the same independent variables and samples as those in the renewed CoSEB model. The results (Fig. S5 in the supplementary material) showed no significant differences in accuracy compared with those of the renewed CoSEB model, indicating the expansion of radiation components did not compromise model performance.

The main advantages of our CoSEB-based datasets of land surface radiation and heat fluxes lie in that [1] they are the first ~~RS-based~~data-driven global datasets that satisfy both surface radiation balance (SWI_{IN} - SW_{OUT} + LW_{IN} - LW_{OUT} = Rn $\cancel{SW_{IN} - SW_{OUT} + LW_{IN} - LW_{OUT} = Rn}$) and heat balance (LE + H + G = Rn $\cancel{LE + H + G = Rn}$) among the eight fluxes, as demonstrated by both the RIR and EIR of 0, [2] the radiation and heat fluxes are characterized by high accuracies when validated against in~~-~~situ measurements at ~~134 "homogeneous"~~44 independent test sites (see the ~~first~~ second paragraph in Section ~~4.2~~2.1), where (1) the RMSEs for daily estimates of SW_{IN}, SW_{OUT}, LW_{IN}, LW_{OUT}, Rn, LE, H and G from the CoSEB-based datasets were ~~28.51~~37.52 W/m^2, 1~~0.39~~4.20 W/m^2, ~~14.29~~22.47 W/m^2, 1~~0.62~~3.78 W/m^2, 2~~2.40~~9.66 W/m^2, ~~24.38~~30.87 W/m^2, 2~~2.67~~9.75 W/m^2 and ~~6.77~~5.69 W/m^2, respectively, as well as for 8-day estimates were 1~~2.81~~8.54 W/m^2, ~~7.08~~12.19 W/m^2, ~~9.22~~18.50 W/m^2, ~~8.34~~9.41 W/m^2, 1~~3.38~~9.12 W/m^2, ~~19.99~~22.31 W/m^2, ~~17.44~~21.63 W/m^2 and ~~4.25~~4.60 W/m^2, respectively, (2) the CoSEB-based datasets, in comparison to the mainstream RS-based products/datasets (i.e. GLASS, BESS-Rad, FLUXCOM, BESSV2.0, MOD16A2, PML_V2 and ETMonitor), better agreed with the in situ observations at ~~134 EC~~the 44 test sites, showing the RMSE reductions ranging from ~~4.35~~0.01 W/m^2 to ~~11.46~~4.58 W/m^2 for SW_{IN}, LW_{IN}, LW_{OUT}, Rn and LE at daily scale, and ~~4.62~~0.24 W/m^2 to 1~~4.64~~0.48 W/m^2 for SW_{IN}, LW_{IN}, LW_{OUT}, Rn, LE and H at 8-day scale. Furthermore, the CoSEB-based datasets outperformed the ERA5-Land reanalysis datasets in estimating surface energy fluxes (where SW_{OUT}, LW_{OUT}, Rn and G for the ERA-Land were inferred from surface radiation balance and heat balance), particularly for SW_{OUT}, H and G, with RMSE reductions of 0.13-8.15 W/m^2 when validated against in situ observations at the 44 test sites (Figs. S6 and S7 in the Supplementary Material). Preliminary analysis indicates that the CoSEB-based datasets exhibit spatial patterns consistent with those of mainstream RS-based datasets and Earth system model outputs (see Fig. S8 in the supplementary material). More detailed analysis about their similarities and differences can be further conducted in future work.

Our developed datasets could be potentially applied in many fields, including but not limited to (1) exploring the spatial-temporal patterns of global land surface radiation and heat flux (es) and their driving mechanisms over the past decades under global change (e.g., rising CO_2 concentration, greening land surface and increasing air temperature), (2) investigating the variability of land surface radiation and heat fluxes caused by extreme events and human activities, e.g. afforestation or deforestation, wildfire, air pollution, weather extremes and urbanization, (3) assessing the resources of solar energy, geothermal energy, surface and ground water at regional and global scales, (4) monitoring natural hazards, e.g. drought in agriculture and forestry.

The uncertainties of our datasets are relevant to (1) the data preprocessing, and (2) the application of the CoSEB ~~at~~ model across different spatial scales. Specifically, ~~the~~ daily averages of surface radiation and heat fluxes for each day were~~as~~ obtained for analysis from good-quality half-hourly observations when the fraction of these good-quality half-hourly observations was greater than 80% in a day, due to the lack of consensus on the method for aggregating gapped half-hourly observations to daily data (Tang et al., 2024a; Yao et al., 2017; Zheng et al., 2022). Simple temporal interpolation of half-hourly in situ observations, which could therefore introduce substantial uncertainties, was not applied, because surface radiation and heat fluxes are sensitive to short-term variations in meteorological conditions and their intraday dynamics are often complex. Likewise, since there was no agreement on how to correct for the energy imbalance of turbulent heat fluxes, we adopted the most widely applied Bowen ratio method to enforce energy closure between $Rn-G$ and $LE+H$ (Castelli et al., 2018; Twine et al., 2000; Zhang et al., 2021). Another potential source of uncertainty arises from differences in meteorological reanalysis data caused by spatial downscaling, which, as demonstrated in our previous study (Wang et al., 2025, the last paragraph of Section 5.1), has a relatively small impact on model estimates by the machine-learning-based CoSEB model combined with finer-resolution surface-related variables that partially compensate for the spatial heterogeneity and localized variations not captured by the coarse-resolution datasets.~~(Wang et al., 2025, the last paragraph of Section 5.1)~~ ~~(Wang et al., 2025, the last paragraph of Section 5.1)~~These data preprocessing had an effect on the construction of the renewed CoSEB model, which may further affect the global datasets. Moreover, the renewed CoSEB model was constructed at the spatial scale of 500 m to match the footprints of the in situ EC observations, but applied at the spatial resolution of 0.05° to generate global datasets, mainly limited by the computing and storage capabilities ~~in~~ of our personal computers. However, the CoSEB-based datasets have also been validated and inter-compared at ~~134 EC~~44 independent test sites to demonstrate that the difference in spatial scale would not much affect the performance of the datasets. Despite these uncertainties, it is worth emphasizing that our work was the first attempt to innovatively develop data-driven energy-conservation datasets of global land surface radiation and heat fluxes with high accuracies.

6 Data availability

The energy-conservation datasets of global land surface radiation and heat fluxes generated by the CoSEB model with spatial-temporal resolutions of daily and 0.05° from Feb.26, 2000 to Dec.31, 2020 are freely available through the National Tibetan Plateau Data Center at https://doi.org/10.11888/Terre.tpdc.302559 (Tang et al., 2025a) and through the Science Data Bank (ScienceDB) at https://doi.org/10.57760/sciencedb.27228 (Tang et al., 2025b).

7 Summary and Conclusion

This study for the first time developed data-driven energy-conservation datasets of global land surface radiation and heat fluxes using our CoSEB model renewed based on GLASS and MODIS products, ERA5-Land reanalysis datasets, topographic data, CO_2 concentration data, and observations at 258 EC sites worldwide~~ from the FLUXNET, AmeriFlux, EuroFlux, OzFlux, ChinaFLUX and TPDC~~.

The CoSEB-based datasets of land surface radiation and heat fluxes are the first ~~RS-based~~data-driven global datasets that satisfy both surface radiation balance (SWI_N - SW_{OUT} + LW_{IN} - LW_{OUT} = Rn~~$SW_{IN} - SW_{OUT} + LW_{IN} - LW_{OUT} = Rn$~~) and heat balance (LE + H + G = Rn~~$LE + H + G = Rn$~~) among the eight fluxes. Meanwhile, the CoSEB-based datasets outperformed the mainstream products/datasets in accuracy. Specifically, at ~~134 ~~44~~EC ~~ independent test sites, the RMSEs (R^2) for daily estimates of SW_{IN}, SW_{OUT}, LW_{IN}, LW_{OUT}, Rn, LE, H and G from the CoSEB-based datasets were 37.52 W/m^2 (0.81), 14.20 W/m^2 (0.42), 22.47 W/m^2 (0.90), 13.78 W/m^2 (0.95), 29.66 W/m^2 (0.77), 30.87 W/m^2 (0.60), 29.75 W/m^2 (0.44) and 5.69 W/m^2 (0.44), respectively~~the RMSEs for daily estimates of SW_{IN}, SW_{IN}, LW_{IN}, LW_{OUT}, Rn, LE, H and G from the CoSEB-based datasets were 28.51 W/m^2, 10.39 W/m^2, 14.29 W/m^2, 10.62 W/m^2, 22.40 W/m^2, 24.38 W/m^2, 22.67 W/m^2 and 6.77 W/m^2, respectively~~, as well as for 8-day estimates were ~~12.81~~18.54 W/m^2 (0.87), ~~7.08~~12.19 W/m^2 (0.39), ~~9.22~~18.50 W/m^2 (0.92), ~~8.34~~9.41 W/m^2 (0.97), 1~~3.38~~9.12 W/m^2 (0.82), ~~19.99~~22.31 W/m^2 (0.67), ~~17.44~~21.63 W/m^2 (0.39) and ~~4.25~~4.60 W/m^2 (0.47), respectively. Moreover, the estimates from the CoSEB-based datasets in comparison to those from the mainstream products/datasets reduced the RMSE by ~~4.35~~0.01 W/m^2 to ~~11.46~~4.58 W/m^2 and increased the R^2 by 0.~~04 ~~01 to 0.~~3~~09 for SW_{IN}, LW_{IN}, LW_{OUT}, Rn and LE at daily scale, and reduced the RMSE by ~~4.62~~0.24 W/m^2 to 1~~4.64~~0.48 W/m^2 and increased the R^2 by 0.~~04 ~~01 to 0.~~41 ~~38 for SW_{IN}, LW_{IN}, LW_{OUT}, Rn, LE and H at 8-day scale, when these estimates were validated against in situ observations at ~~134 ~~44 ~~EC ~~independent test sites. Furthermore, the CoSEB-based datasets effectively captured the spatial-temporal variability of global land surface radiation and heat fluxes, aligning well with those from the mainstream products.

Our developed datasets hold significant potential for application across diverse fields such as agriculture, forestry, hydrology, meteorology, ecology, and environmental science. They can facilitate comprehensive studies on the variability, impacts, responses, adaptation strategies, and mitigation measures of global and regional land surface radiation and heat fluxes under the influences of climate change and human activities. These datasets will provide valuable insights and data support for scientific research, policy-making, and environmental management, advancing global solutions to address climate change.

Author contribution

JW: Writing – original draft, Visualization, Software, Formal analysis, Data curation. RT: Writing – original draft, Validation, Supervision, Methodology, Funding acquisition, Formal analysis, Conceptualization. ML: Writing – review & editing, Validation. ZL: Writing – review & editing.

Competing interests

The authors declare that they have no conflict of interest.

Acknowledgment

We thank the work from the AmeriFlux, FLUXNET, EuroFlux, OzFlux, ChinaFLUX, the National Tibetan Plateau/Third Pole Environment Data Center and SURFRAD for providing in situ measurements. We would also like to thank Dr. Martin Jung and Dr. Ulrich Weber for providing the FLUXCOM Bowen ratio-corrected products. This work is supported by the National Natural Science Foundation of China [42271378], and the Strategic Priority Research Program of the Chinese Academy of Sciences (Grant No. XDB0740202).

References

Bai, Y., Mallick, K., Hu, T., Zhang, S., Yang, S. and Ahmadi, A.: Integrating machine learning with thermal-driven analytical energy balance model improved terrestrial evapotranspiration estimation through enhanced surface conductance, Remote Sens. Environ., 311, 114308. 10.1016/j.rse.2024.114308, 2024.

Bartkowiak, P., Ventura, B., Jacob, A. and Castelli, M.: A Copernicus-based evapotranspiration dataset at 100 m spatial resolution over four Mediterranean basins, Earth Syst. Sci. Data, 16, 4709-4734. 10.5194/essd-16-4709-2024, 2024.

Berbery, E. H., Mitchell, K. E., Benjamin, S., Smirnova, T., Ritchie, H., Hogue, R. and Radeva, E.: Assessment of land‐surface energy budgets from regional and global models, J. Geophys. Res.-Atmos., 104, 19329-19348. 10.1029/1999jd900128, 1999.

Betts, A. K., Ball, J. H., Beljaars, A. C. M., Miller, M. J. and Viterbo, P. A.: The land surface‐atmosphere interaction: A review based on observational and global modeling perspectives, J. Geophys. Res.-Atmos., 101, 7209-7225. 10.1029/95jd02135, 1996.

Castelli, M., Anderson, M. C., Yang, Y., Wohlfahrt, G., Bertoldi, G., Niedrist, G., Hammerle, A., Zhao, P., Zebisch, M. and Notarnicola, C.: Two-source energy balance modeling of evapotranspiration in Alpine grasslands, Remote Sens. Environ., 209, 327-342. 10.1016/j.rse.2018.02.062, 2018.

Chen, J., He, T., Jiang, B. and Liang, S.: Estimation of all-sky all-wave daily net radiation at high latitudes from MODIS data, Remote Sens. Environ., 245, 111842. 10.1016/j.rse.2020.111842, 2020.

de Wit, A. J. W., Boogaard, H. L. and van Diepen, C. A.: Spatial resolution of precipitation and radiation: The effect on regional crop yield forecasts, Agric. For. Meteorol., 135, 156-168. 10.1016/j.agrformet.2005.11.012, 2005.

Du, Y., Wang, T., Zhou, Y., Letu, H., Li, D. and Xian, Y.: Towards user-friendly all-sky surface longwave downward radiation from space: General scheme and product, Bull. Amer. Meteorol. Soc., 105, E1303–E1319. 10.1175/bams-d-23-0126.1, 2024.

ElGhawi, R., Kraft, B., Reimers, C., Reichstein, M., Körner, M., Gentine, P. and Winkler, A. J.: Hybrid modeling of evapotranspiration: inferring stomatal and aerodynamic resistances using combined physics-based and machine learning, Environ. Res. Lett., 18, 034039. 10.1088/1748-9326/acbbe0, 2023.

Ersi, C., Sudu, B., Song, Z., Bao, Y., Wei, S., Zhang, J., Tong, Z., Liu, X., Le, W. and Rina, S.: The potential of NIRvP in estimating evapotranspiration, Remote Sens. Environ., 315, 114405. 10.1016/j.rse.2024.114405, 2024.

Han, Q., Zeng, Y., Zhang, L., Wang, C., Prikaziuk, E., Niu, Z. and Su, B.: Global long term daily 1 km surface soil moisture dataset with physics informed machine learning, Sci. Data, 10, 101. 10.1038/s41597-023-02011-7, 2023.

Huang, J., Yu, H., Guan, X., Wang, G. and Guo, R.: Accelerated dryland expansion under climate change, Nat. Clim. Chang., 6, 166-171. 10.1038/nclimate2837, 2015.

Huang, L., Luo, Y., Chen, J. M., Tang, Q., Steenhuis, T., Cheng, W. and Shi, W.: Satellite-based near-real-time global daily terrestrial evapotranspiration estimates, Earth Syst. Sci. Data, 16, 3993-4019. 10.5194/essd-16-3993-2024, 2024.

Jia, B., Xie, Z., Dai, A., Shi, C. and Chen, F.: Evaluation of satellite and reanalysis products of downward surface solar radiation over East Asia: Spatial and seasonal variations, J. Geophys. Res.-Atmos., 118, 3431-3446. 10.1002/jgrd.50353, 2013.

Jiang, B., Zhang, Y., Liang, S., Wohlfahrt, G., Arain, A., Cescatti, A., Georgiadis, T., Jia, K., Kiely, G., Lund, M., Montagnani, L., Magliulo, V., Ortiz, P. S., Oechel, W., Vaccari, F. P., Yao, Y. and Zhang, X.: Empirical estimation of daytime net radiation from shortwave radiation and ancillary information, Agric. For. Meteorol., 211-212, 23-36. 10.1016/j.agrformet.2015.05.003, 2015.

Jiao, B., Su, Y., Li, Q., Manara, V. and Wild, M.: An integrated and homogenized global surface solar radiation dataset and its reconstruction based on a convolutional neural network approach, Earth Syst. Sci. Data, 15, 4519-4535. 10.5194/essd-15-4519-2023, 2023.

Jung, M., Koirala, S., Weber, U., Ichii, K., Gans, F., Camps-Valls, G., Papale, D., Schwalm, C., Tramontana, G. and Reichstein, M.: The FLUXCOM ensemble of global land-atmosphere energy fluxes, Sci. Data, 6, 74. 10.1038/s41597-019-0076-8, 2019.

Kim, Y., Park, H., Kimball, J. S., Colliander, A. and McCabe, M. F.: Global estimates of daily evapotranspiration using SMAP surface and root-zone soil moisture, Remote Sens. Environ., 298, 113803. 10.1016/j.rse.2023.113803, 2023.

Li, B., Ryu, Y., Jiang, C., Dechant, B., Liu, J., Yan, Y. and Li, X.: BESSv2.0: A satellite-based and coupled-process model for quantifying long-term global land–atmosphere fluxes, Remote Sens. Environ., 295, 113696. 10.1016/j.rse.2023.113696, 2023.

Liang, S., Wang, D., He, T. and Yu, Y.: Remote sensing of earth's energy budget: synthesis and review, Int. J. Digit. Earth, 12, 737-780. 10.1080/17538947.2019.1597189, 2019.

Liang, S., Zheng, T., Liu, R., Fang, H., Tsay, S. C. and Running, S.: Estimation of incident photosynthetically active radiation from Moderate Resolution Imaging Spectrometer data, J. Geophys. Res.-Atmos., 111. 10.1029/2005jd006730, 2006.

Liu, S., Xu, Z., Song, L., Zhao, Q., Ge, Y., Xu, T., Ma, Y., Zhu, Z., Jia, Z. and Zhang, F.: Upscaling evapotranspiration measurements from multi-site to the satellite pixel scale over heterogeneous land surfaces, Agric. For. Meteorol., 230, 97-113. 10.1016/j.agrformet.2016.04.008, 2016.

Mohan, M. M. P., Kanchirapuzha, R. and Varma, M. R. R.: Review of approaches for the estimation of sensible heat flux in remote sensing-based evapotranspiration models, J. Appl. Remote Sens., 14, 041501-041501. 10.1117/1.Jrs.14.041501, 2020.

Mu, Q., Zhao, M. and Running, S. W.: Improvements to a MODIS global terrestrial evapotranspiration algorithm, Remote Sens. Environ., 115, 1781-1800. 10.1016/j.rse.2011.02.019, 2011.

Mueller, R. W., Matsoukas, C., Gratzki, A., Behr, H. D. and Hollmann, R.: The CM-SAF operational scheme for the satellite based retrieval of solar surface irradiance — A LUT based eigenvector hybrid approach, Remote Sens. Environ., 113, 1012-1024. 10.1016/j.rse.2009.01.012, 2009.

Muñoz-Sabater, J., Dutra, E., Agustí-Panareda, A., Albergel, C., Arduini, G., Balsamo, G., Boussetta, S., Choulga, M., Harrigan, S., Hersbach, H., Martens, B., Miralles, D. G., Piles, M., Rodríguez-Fernández, N. J., Zsoter, E., Buontempo, C. and Thépaut, J.-N.: ERA5-Land: a state-of-the-art global reanalysis dataset for land applications, Earth Syst. Sci. Data, 13, 4349-4383. 10.5194/essd-13-4349-2021, 2021.

Nemani, R. R., Keeling, C. D., Hashimoto, H., Jolly, W. M., Piper, S. C., Tucker, C. J., Myneni, R. B. and Running, S. W.: Climate-driven increases in global terrestrial net primary production from 1982 to 1999, Science, 300, 1560-1563. 10.1126/science.1082750, 2003.

O., S. and Orth, R.: Global soil moisture data derived through machine learning trained with in-situ measurements, Sci. Data, 8. 10.1038/s41597-021-00964-1, 2021.

Peng, Z., Letu, H., Wang, T., Shi, C., Zhao, C., Tana, G., Zhao, N., Dai, T., Tang, R., Shang, H., Shi, J. and Chen, L.: Estimation of shortwave solar radiation using the artificial neural network from Himawari-8 satellite imagery over China, Journal of Quantitative Spectroscopy and Radiative Transfer, 240, 106672. 10.1016/j.jqsrt.2019.106672, 2020.

Rios, G. and Ramamurthy, P.: A novel model to estimate sensible heat fluxes in urban areas using satellite-derived data, Remote Sens. Environ., 270, 112880. 10.1016/j.rse.2021.112880, 2022.

Ryu, Y., Jiang, C., Kobayashi, H. and Detto, M.: MODIS-derived global land products of shortwave radiation and diffuse and total photosynthetically active radiation at 5 km resolution from 2000, Remote Sens. Environ., 204, 812-825. 10.1016/j.rse.2017.09.021, 2018.

Sellers, P. J., Dickinson, R. E., Randall, D. A., Betts, A. K., Hall, F. G., Berry, J. A., Collatz, G. J., Denning, A. S., Mooney, H. A., Nobre, C. A., Sato, N., Field, C. B. and Henderson-Sellers, A.: Modeling the Exchanges of Energy, Water, and Carbon Between Continents and the Atmosphere, Science, 275, 502-509. 10.1126/science.275.5299.502, 1997.

Sun, S., Bi, Z., Xiao, J., Liu, Y., Sun, G., Ju, W., Liu, C., Mu, M., Li, J., Zhou, Y., Li, X., Liu, Y. and Chen, H.: A global 5 km monthly potential evapotranspiration dataset (1982–2015) estimated by the Shuttleworth–Wallace model, Earth Syst. Sci. Data, 15, 4849-4876. 10.5194/essd-15-4849-2023, 2023.

Tang, R., Peng, Z., Liu, M., Li, Z.-L., Jiang, Y., Hu, Y., Huang, L., Wang, Y., Wang, J., Jia, L., Zheng, C., Zhang, Y., Zhang, K., Yao, Y., Chen, X., Xiong, Y., Zeng, Z. and Fisher, J. B.: Spatial-temporal patterns of land surface evapotranspiration from global products, Remote Sens. Environ., 304, 114066. 10.1016/j.rse.2024.114066, 2024a.

Tang, R., Wang, J., Liu, M. and Li, Z.-L.: Energy-conservation datasets of global land surface radiation and heat fluxes from 2000-2020 generated by CoSEB, National Tibetan Plateau / Third Pole Environment Data Center. [data set], https://doi.org/10.11888/Terre.tpdc.302559, 2025a.

Tang, R., Wang, J., Liu, M. and Li, Z.-L.: Energy-conservation datasets of global land surface radiation and heat fluxes from 2000-2020 generated by CoSEB, Science Data Bank: Science Data Bank. [data set], https://doi.org/10.57760/sciencedb.27228, 2025b.

Tang, W., He, J., Qi, J. and Yang, K.: A dense station-based, long-term and high-accuracy dataset of daily surface solar radiation in China, Earth Syst. Sci. Data, 15, 4537-4551. 10.5194/essd-15-4537-2023, 2023.

Tang, W., He, J., Shao, C., Song, J., Yuan, Z. and Yan, B.: Constructing a long-term global dataset of direct and diffuse radiation (10 km, 3 h, 1983–2018) separating from the satellite-based estimates of global radiation, Remote Sens. Environ., 311, 114292. 10.1016/j.rse.2024.114292, 2024b.

Tang, W., Yang, K., Qin, J., Li, X. and Niu, X.: A 16-year dataset (2000–2015) of high-resolution (3 h, 10 km) global surface solar radiation, Earth Syst. Sci. Data, 11, 1905-1915. 10.5194/essd-11-1905-2019, 2019.

Twine, T. E., Kustas, W. P., Norman, J. M., Cook, D. R., Houser, P. R., Meyers, T. P., Prueger, J. H., Starks, P. J. and Wesely, M. L.: Correcting eddy-covariance flux underestimates over a grassland, Agric. For. Meteorol., 103, 279-300. 10.1016/S0168-1923(00)00123-4, 2000.

van der Tol, C.: Validation of remote sensing of bare soil ground heat flux, Remote Sens. Environ., 121, 275-286. 10.1016/j.rse.2012.02.009, 2012.

Wang, D., Liang, S., He, T. and Shi, Q.: Estimation of Daily Surface Shortwave Net Radiation From the Combined MODIS Data, IEEE Trans. Geosci. Remote Sensing, 53, 5519-5529. 10.1109/tgrs.2015.2424716, 2015.

Wang, D., Liang, S., Li, R. and Jia, A.: A synergic study on estimating surface downward shortwave radiation from satellite data, Remote Sens. Environ., 264, 112639. 10.1016/j.rse.2021.112639, 2021.

Wang, J., Tang, R., Liu, M., Jiang, Y., Huang, L. and Li, Z.-L.: Coordinated estimates of 4-day 500 m global land surface energy balance components, Remote Sens. Environ., 326, 114795. 10.1016/j.rse.2025.114795, 2025.

Wang, K. C., Dickinson, R. E., Wild, M. and Liang, S.: Atmospheric impacts on climatic variability of surface incident solar radiation, Atmos. Chem. Phys., 12, 9581-9592. 10.5194/acp-12-9581-2012, 2012.

Wang, T., Shi, J., Ma, Y., Letu, H. and Li, X.: All-sky longwave downward radiation from satellite measurements: General parameterizations based on LST, column water vapor and cloud top temperature, ISPRS-J. Photogramm. Remote Sens., 161, 52-60. 10.1016/j.isprsjprs.2020.01.011, 2020.

Wang, Y., Hu, J., Li, R., Song, B. and Hailemariam, M.: Remote sensing of daily evapotranspiration and gross primary productivity of four forest ecosystems in East Asia using satellite multi-channel passive microwave measurements, Agric. For. Meteorol., 339, 109595. 10.1016/j.agrformet.2023.109595, 2023.

Wild, M.: Global dimming and brightening: A review, J. Geophys. Res.-Atmos., 114, D00D16. 10.1029/2008jd011470, 2009.

Wild, M., Folini, D., Schär, C., Loeb, N., Dutton, E. G. and König-Langlo, G.: The global energy balance from a surface perspective, Clim. Dyn., 40, 3107-3134. 10.1007/s00382-012-1569-8, 2012.

Wild, M. and Liepert, B.: The Earth radiation balance as driver of the global hydrological cycle, Environ. Res. Lett., 0, 025203. 10.1088/1748-9326/5/2/025003, 2010.

Xia, X. A., Wang, P. C., Chen, H. B. and Liang, F.: Analysis of downwelling surface solar radiation in China from National Centers for Environmental Prediction reanalysis, satellite estimates, and surface observations, J. Geophys. Res.-Atmos., 111, D09103. 10.1029/2005jd006405, 2006.

Xian, Y., Wang, T., Leng, W., Letu, H., Shi, J., Wang, G., Yan, X. and Yuan, H.: Can Topographic Effects on Solar Radiation Be Ignored: Evidence From the Tibetan Plateau, Geophys. Res. Lett., 51, e2024GL108653. 10.1029/2024gl108653, 2024.

Xu, J., Liang, S. and Jiang, B.: A global long-term (1981–2019) daily land surface radiation budget product from AVHRR satellite data using a residual convolutional neural network, Earth Syst. Sci. Data, 14, 2315-2341. 10.5194/essd-14-2315-2022, 2022a.

Xu, J., Liang, S., Ma, H. and He, T.: Generating 5 km resolution 1981–2018 daily global land surface longwave radiation products from AVHRR shortwave and longwave observations using densely connected convolutional neural networks, Remote Sens. Environ., 280, 113223. 10.1016/j.rse.2022.113223, 2022b.

Yao, Y., Liang, S., Li, X., Chen, J., Liu, S., Jia, K., Zhang, X., Xiao, Z., Fisher, J. B., Mu, Q., Pan, M., Liu, M., Cheng, J., Jiang, B., Xie, X., Grünwald, T., Bernhofer, C. and Roupsard, O.: Improving global terrestrial evapotranspiration estimation using support vector machine by integrating three process-based algorithms, Agric. For. Meteorol., 242, 55-74. 10.1016/j.agrformet.2017.04.011, 2017.

Yu, L., Qiu, G. Y., Yan, C., Zhao, W., Zou, Z., Ding, J., Qin, L. and Xiong, Y.: A global terrestrial evapotranspiration product based on the three-temperature model with fewer input parameters and no calibration requirement, Earth Syst. Sci. Data, 14, 3673-3693. 10.5194/essd-14-3673-2022, 2022.

Zhang, C., Long, D., Zhang, Y., Anderson, M. C., Kustas, W. P. and Yang, Y.: A decadal (2008–2017) daily evapotranspiration data set of 1 km spatial resolution and spatial completeness across the North China Plain using TSEB and data fusion, Remote Sens. Environ., 262, 112519. 10.1016/j.rse.2021.112519, 2021.

Zhang, J., Zhao, L., Deng, S., Xu, W. and Zhang, Y.: A critical review of the models used to estimate solar radiation, Renew. Sust. Energ. Rev., 70, 314-329. 10.1016/j.rser.2016.11.124, 2017.

Zhang, K., Kimball, J. S., Nemani, R. R. and Running, S. W.: A continuous satellite-derived global record of land surface evapotranspiration from 1983 to 2006, Water Resour. Res., 46, W09522. 10.1029/2009wr008800, 2010.

Zhang, X., Liang, S., Zhou, G., Wu, H. and Zhao, X.: Generating Global LAnd Surface Satellite incident shortwave radiation and photosynthetically active radiation products from multiple satellite data, Remote Sens. Environ., 152, 318-332. 10.1016/j.rse.2014.07.003, 2014.

Zhang, Y., Kong, D., Gan, R., Chiew, F. H. S., McVicar, T. R., Zhang, Q. and Yang, Y.: Coupled estimation of 500 m and 8-day resolution global evapotranspiration and gross primary production in 2002–2017, Remote Sens. Environ., 222, 165-182. 10.1016/j.rse.2018.12.031, 2019.

Zheng, C., Jia, L. and Hu, G.: Global land surface evapotranspiration monitoring by ETMonitor model driven by multi-source satellite earth observations, J. Hydrol., 613, 128444. 10.1016/j.jhydrol.2022.128444, 2022.